ESTIMATION OF INHALATION RISK DUE TO THORON AND DECAY PRODUCTS IN THORIUM FUEL HANDLING FACILITIES

By

SANDEEP DATTATRAYA KANSE

PHYS01201304016

Bhabha Atomic Research Centre, Mumbai

A thesis submitted to the

Board of Studies in Physical Sciences

in partial fulfilment of requirements

for the Degree of

DOCTOR OF PHILOSOPHY

of

HOMI BHABHA NATIONAL INSTITUTE

March, 2021

Homi Bhabha National Institute

Recommendations of the Viva Voce Committee

As members of the Viva Voce Committee, we certify that we have read the dissertation prepared by Mr. Sandeep Dattatraya Kanse entitled "Estimation of Inhalation Risk Due to Thoron and Decay Products in Thorium Fuel Handling Facilities" and recommend that it may be accepted as fulfilling the thesis requirement for the award of Degree of Doctor of Philosophy.

Chairman - Prof. C. P. Kaushik		Date: 21.9.21
Guide / Convener - Prof. B. K. Sapra		Date: 21.9.2021
Examiner - Prof. N. Karunakara	Attended through VC, email consent attached.	Date:
Member 1- Prof. T. Palani Selvam		Date: 21/09/2021
Member 2- Prof. Vandana Pulhani		Date: 21/09/2021
Member 3- Dr. B. K. Sahoo		Date: 21. 9. 2021

Final approval and acceptance of this thesis is contingent upon the candidate's submission of the final copies of the thesis to HBNI.

I hereby certify that I have read this thesis prepared under my direction and recommend that it may be accepted as fulfilling the thesis requirement.

Date:

Place:

Signature of Guide 21.9.2021

STATEMENT BY AUTHOR

This dissertation has been submitted in partial fulfilment of requirements for an advanced degree at Homi Bhabha National Institute (HBNI) and is deposited in the Library to be made available to borrowers under rules of the HBNI.

Brief quotations from this dissertation are allowable without special permission, provided that accurate acknowledgement of source is made. Requests for permission for extended quotation from or reproduction of this manuscript in whole or in part may be granted by the Competent Authority of HBNI when in his or her judgment the proposed use of the material is in the interests of scholarship. In all other instances, however, permission must be obtained from the author.

Sandeep D. Kanse

DECLARATION

I, hereby declare that the investigation presented in the thesis has been carried out by me. The work is original and has not been submitted earlier as a whole or in part for a degree / diploma at this or any other Institution / University.

Sandeep D. Kanse

List of Publications arising from the thesis

Journal

1. "A novel method based on ^{220}Rn (thoron) exhalation rate of indoor surfaces for robust estimates of ^{220}Rn concentration and equilibrium factor to compute inhalation dose," **Kanse, S. D.**, Sahoo, B. K., Gaware, J. J. & Sapra, B. K., *Chemosphere*, **2021**, *267*, 128908.
2. "A study of thoron exhalation from monazite-rich beach sands of High Background Radiation Areas of Kerala and Odisha, India," **Kanse, S. D.**, Sahoo, B. K., Gaware, J. J., Prajith, R. & Sapra, B. K., *Environ. Earth Sci.*, **2016**, *75,* 1–10.
3. "Effect of ^{220}Rn gas concentration distribution on its transmission from a delay chamber: evolving a CFD-based uniformity index," Agarwal, T. K., Joshi, M., Sahoo, B. K., **Kanse, S. D.** & Sapra, B. K., *Radiat. Prot. Dosimetry,* **2016**, *168,* 546–552.
4. "Estimation of attached and unattached progeny of ^{222}Rn and ^{220}Rn concentration using deposition based progeny sensors," Mehra, R., Bangotra, P., Kaur, K., **Kanse, S.** & Mishra, R., *Radiat. Prot. Dosimetry*, **2015**, *167,* 92–96.
5. "A new pin-hole discriminated ^{222}Rn/^{220}Rn passive measurement device with single entry face," Sahoo, B. K., Sapra, B. K., **Kanse, S. D.**, Gaware, J. J. & Mayya, Y. S., *Radiat. Meas.*, **2013**, *58,* 52–60.
6. "Powder sandwich technique: A novel method for determining the thoron emanation potential of powders bearing high ^{224}Ra content," **Kanse, S. D.**, Sahoo, B. K., Sapra, B. K., Gaware, J. J. & Mayya, Y. S., *Radiat. Meas.*, **2013**, *48,* 82–87.

Conferences

1. "A Methodology to Predict Thoron (^{220}Rn) Source Term from Thorium-bearing Powders Stored in Containers," **S.D. Kanse**, B.K. Sahoo, J.J. Gaware, T.K. Agarwal and B.K. Sapra. **2014** CD of Proceedings of National Conference on

Power from Thorium: Present Status and Future Directions, Mumbai, paper: NCPth-2014/30

2. "Measurement of radon concentration in ground water samples of Hanumangarh district, Rajasthan," Kansal Sandeep, Singla Amit Kumar, **Kanse Sandeep**, Sahoo Bijay and Mehra, Rohit **2017**. Proceedings of the twentieth national conference on solid state nuclear track detectors and their applications.

3. "Estimation of unattached fraction and annual effective dose from EEC in Doaba region of Punjab," P Bangotra, R Mehra, R Jakhu, M Arrora, P Pandit, **S Kanse,2017** Proceedings of the thirteenth DAE-BRNS nuclear and radiochemistry symposium

4. "Mapping of thoron emission from monazite bearing beach sands at high background radiation areas of Kerala and Orissa," **SD Kanse**, BK Sahoo, JJ Gaware, BK Sapra, YS Mayya,**2013,** Proceedings of the thirtieth IARP conference on radiological protection and safety in nuclear reactors and radiation installations.

Sandeep D. Kanse

ACKNOWLEDGEMENTS

At the outset I would like to thank my guide Dr B. K. Sapra for the encouragement, support and guidance she has lent me for this work and beyond. The thoughtful inputs, trust and freedom she gave was instrumental in completion of this work.

I am thankful to Dr Y.S. Mayya, Adjunct professor, IIT Bombay and former Head, RP&AD BARC for encouraging me to take up this work and being a constant inspiration in my life. I acknowledge members of my doctoral committee, Dr C.P. Kaushik (Chairman), Dr T. Palani Selvam and Dr Vandana Pulhani; as well as ex-members Dr R. M. Tripathi, Dr R. Baskaran and Sh V. Shivakumar for their critical comments and invaluable guidance during the reviews of this work.

I would like to express my special thanks and appreciation for my colleagues and friends Sh Arshad Khan, Dr B.K. Sahoo, Sh J.J. Gaware, Sh. T.K. Agarwal, Dr Rosaline Mishra, Smt Rama Prajith, Smt Rajeswari Pradhan, Sh Dinesh Kumbhar and Sh S. Jalaluddin, for their constant support and help in office. I acknowledge the efforts of Dr B.K. Sahoo and Dr Rosaline Mishra in reviewing the thesis. I thank Piyali Banerjee and her colleagues at HP Unit, PREFRE, Tarapur for their help in experiments done at Tarapur.

I express my gratitude and indebtedness to all the teachers who have enriched my knowledge and my life.

My friends have always been an important part in my life and I am happy to acknowledge their role in my success.

I dedicate this thesis to my beloved family. I am grateful and indebted to my parents Smt Latika and Sh Dattatraya Kanse for their endless love and blessings. The values they inculcated in me have made me the person I am today. I am thankful to my parents-in-law Smt Urmila and Sh Laxman Gaikwad for their encouragement. I am infinitely thankful to my wife Prachi Kanse for making my dreams her own and being the perfect partner in my life. Without her unconditional love, encouragement and conviction I would have never completed this work. Our sweet daughter Swara is a source of unlimited joy and happiness and has given a new perspective to our life.

I am also thankful to all other family members who have supported and encouraged me throughout my life.

I express my gratitude to everyone who supported and helped me in one way or other, throughout the course of this work.

Sandeep D. Kanse

CONTENTS

CHAPTER 4 MODELING OF THORON AND ITS DECAY PRODUCTS IN CLOSED ENVIRONMENTS 86

SUMMARY

India has planned to use thorium based nuclear reactors for generation of nuclear power on commercial scale. The setting up and operation of these reactors will require establishing of a number of thorium handling facilities as a part of thorium fuel cycle. These facilities will have a high potential of thoron exposure and risk to the personnel working there, due to the handling of large quantities of thorium enriched materials.

The work presented in this thesis was taken up considering the need to have the readiness to deal with the issue of radiological risk due to thoron and its decay products in occupational environments of thorium processing facilities. The topic has been addressed by developing tools and methods to estimate the thoron source term in the facilities, to predict the properties of thoron and its decay products in the occupational environments and to estimate the radiological dose and risk due to them.

The thoron emission model for porous source matrix was developed and validated for thorium powders and monazite rich sand. The effect of moisture on diffusion coefficient and emanation fraction of powders was studied in detail. Geometry based emanation models were developed for three new shapes of sand grains. Experimental study for thoron emission during bubbling was carried out and compared with theoretical model.

The thoron concentration profile around a source was modelled and validated for two different environments. A model was developed to predict properties of thoron decay products in occupational environment using parameters such as aerosol size averaged attachment rates and deposition velocities, room dimensions and ventilation rate as

input parameters. It was validated through multi-parametric measurements in a thorium processing facility for occupational environment, and through measurements in twenty five houses for dwellings environment. The model was applied to study the effect of various factors on thoron decay products properties in a typical thorium facility.

The study of radiation dose due to inhalation of thoron and its decay products was carried out using a program written for implementation of latest ICRP bio-kinetic and dosimetric model. The comparison for thoron dose to an Indian worker and ICRP standard worker was done. The effect of parameters like attached decay product size distribution and unattached fraction on the dose to thoron and its decay products was studied.

The work presented in the thesis provides necessary tools for estimation of risk in upcoming facilities catering to thorium based reactors proposed to be built in India. These will be very useful to make predictions for thoron right from its source term to its concentration in workplaces and finally to the radiation dose and risk. This information will be of immense help in planning for the radiation protection measures and systems at the stage of designing of the facilities.

LIST OF FIGURES

LIST OF TABLES

Chapter 1

INTRODUCTION

1.1. Background

Radon (^{222}Rn) and thoron (^{220}Rn) gases occur naturally in the environment as part of the ^{238}U and ^{232}Th decay series. Being noble gases they tend to come out of the source materials into open environment, where they decay to their radioactive decay products [1], [2]. The exposure of humans to air bearing radon, thoron and their decay products can result in considerable radiation dose, especially the internal dose resulting from inhalation. The radiological significance of this has been established through numerous studies and it is well known that exposure to high concentrations of these gases and their decay products increases risk of lung cancer in exposed individuals [2]–[4].

Of the two gaseous radioisotopes, thoron has been considered to be less potent because most of the thoron formed in the source materials is unable to come out to environment in the short time before undergoing radioactive decay owing to its short half-life (55.6s). This results in generally low concentrations of thoron in most indoor environments [2]. However thoron concentrations in the environment can reach considerably high levels when the source activity strength is very high, like in the environments of naturally occurring High Natural Background Radiation Areas (HNBRAs) with high thorium content in soils or in places where Technologically Enhanced Naturally Occurring Radioactive Materials (TENORMs) are handled [5]–[7]. The thorium processing facilities is one such setting where materials with high thorium activity and thoron source potential are handled. India has planned to use thorium based reactors for commercial nuclear power generation in the third stage of its Nuclear power programme, due to the various advantages it has with use of thorium as nuclear fuel [8]–[11]. Some thorium based reactors like Advanced Heavy Water Reactor (AHWR) and Indian Molten Salt Breeder Reactors (IMSBR) are currently under development [12], [13]. The operation of these reactors will require designing and development of facilities handling thorium in very large quantities as a part of the thorium fuel cycle. Due to the large quantity of thorium planned to be handled, the radiological risk due to thoron and its decay products will be high in these facilities. To deal with this risk it is necessary to have proper methodology to predict thoron emission potentials, probable concentrations and resultant doses and risk in the upcoming facilities.

However, research on thoron in context of occupational environments is seriously lacking, as most of the thoron studies have been carried out for natural materials and for residential environments. Not much information is available for thoron emission characteristics for materials handled in thorium fuel cycle, the concentration profiles and behaviour of thoron and its decay products in industrial environment of thorium facilities or the factors that affect the radiation doses and risk to exposed occupational personnel. The purpose of this work is to attempt to fill this knowledge gap by systematically studying and modeling thoron emission from materials handled in thorium fuel cycle, the behaviour of thoron and its decay products in the industrial environments and identifying factors which are most influential in deciding radiation dose and risk after exposure. The study aims to put in place a methodological framework to estimate/predict the inhalation dose due to thoron and its decay products based on use of source term, dispersion parameters and dosimetry models.

The present chapter describes the radiological significance of thoron, the importance of thorium fuel cycle for India, typical facilities associated with thorium fuel cycles and need of study of thoron in these facilities. It also highlights the specific aspects of thoron in thorium processing facilities where more work is required to be done.

1.2. Radiological Significance of thoron

As described above, thoron is a naturally occurring radioactive noble gas which tends to come out of the source matrices because of its mobile nature. On being released to environment it decays to various decay products which are atoms of solid and also radioactive (Figure 1.1).

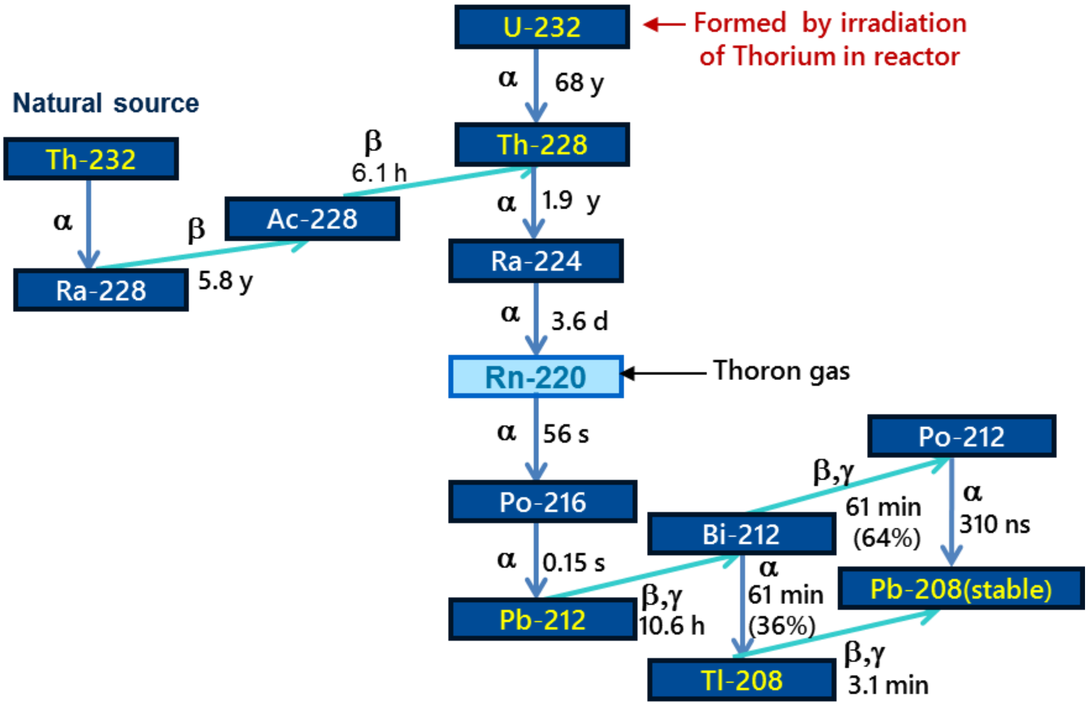

Figure 1.1: Radioactive decay series of ^{232}Th

The main pathway for exposure of humans to thoron and its air-borne decay products is by inhalation. When an individual breathes the air containing them, the decay products are deposited in the respiratory tract. A large fraction of the deposited decay products undergoes radioactive transformation before being cleared out from the body. Most of these transformations result in emission of alpha and beta particles which impart their energies to the surrounding tissues, predominantly of the respiratory tract. This causes significant biological damage to cells and can subsequently lead to cell mutation and cancer. This process is schematically presented in Figure 1.2.

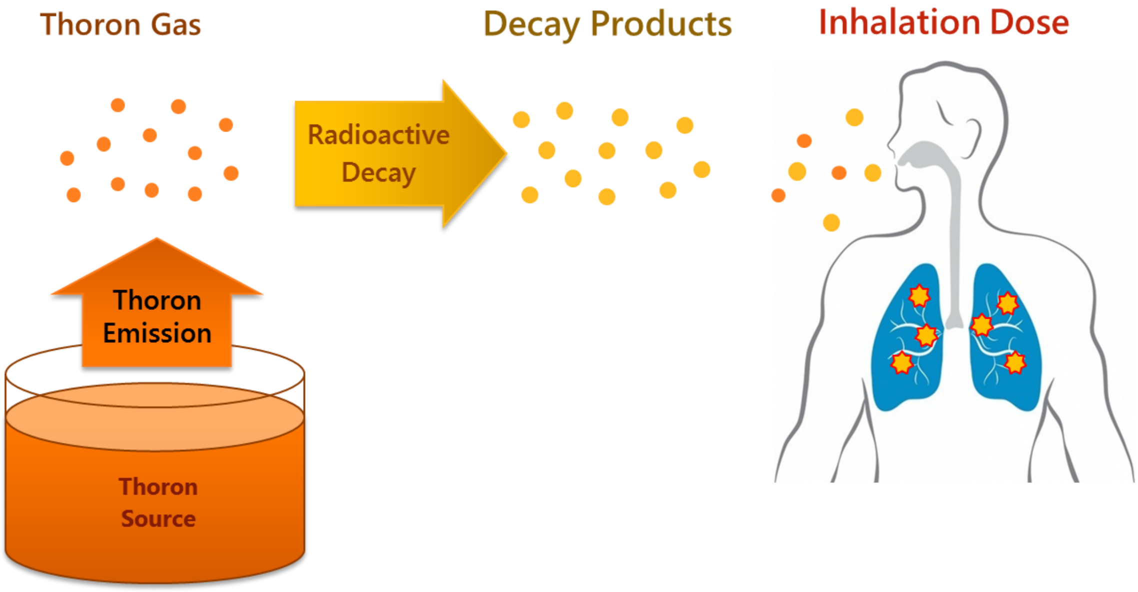

Figure 1.2: Schematic diagram of processes leading up to thoron exposure and radiation dose

However, the concentration of thoron in normal environments is usually quite low, making it difficult to determine the risk due to thoron through actual measurements [2]. On the other hand, the risk of lung cancer due to radon (which demonstrates same behaviour) has been studied in great detail. In fact, radon remains the only source, other than atomic bomb radiation, where the risk of radiation has been obtained from epidemiological studies with reliable confidence [14]–[16]. The radiological risk estimates for thoron are obtained by comparison with radon. Considering the potential of the decay products to impart inhalation radiation dose, the risk from thoron decay products is about four times that of radon decay products for an equal concentration [2]. Moreover, thoron decay products tend to remain in air for longer time due to comparatively longer life than radon decay products and results in a higher concentration. This makes thoron a greater health risk in cases where sufficient amount of thoron may be released to the environment.

1.3. Importance of Thorium Fuel Cycle

India has a unique position in the world in terms of availability of nuclear fuel resource, with modest availability of uranium, but large thorium reserves. It plans to utilize the vast thorium resource through a 'three-stage nuclear power programme' [17]. This sequential program is based on a closed fuel cycle, where the spent fuel of one stage is reprocessed to produce fuel for the next stage. The closed fuel cycle thus multiplies manifold the energy potential of the fuel and greatly reduces the quantity of radioactive waste generated. The first stage comprises of Pressurized Heavy Water Reactors (PHWRs) fuelled by natural uranium. Natural uranium contains only 0.7% of ^{235}U, which undergoes fission to release energy. The remaining 99.3% comprises ^{238}U which is not fissile. However, it is converted to fissile ^{239}Pu during irradiation in PHWRs in a small quantity. The second stage will comprise of Fast Breeder Reactors (FBRs) fuelled by ^{239}Pu recovered from reprocessing of the first stage spent fuel. In FBRs ^{239}Pu will undergo fission producing energy and breeding ^{238}U in blanket to ^{239}Pu.

^{232}Th is not fissile and needs to be converted to a fissile ^{233}U for obtaining energy through nuclear fission. This is planned to be achieved by introducing it in FBRs at an optimal time. The third stage of the Indian nuclear power program will use this generated ^{233}U in advanced self-sustaining thorium-based reactors. New ^{232}Th will be converted to ^{233}U setting up cycle for complete utilization of thorium as nuclear fuel.

India is also developing a few thorium based reactors like AHWR and IMSBR to demonstrate use of thorium on an industrial scale as nuclear energy source and in process, develop the technologies for the third stage. Many facilities will need to be established in order to support the closed fuel cycle of the thorium based reactors.

1.4. Thoron emission potential in thorium facilities

The various facilities envisaged to cater to thorium fuel cycle range from the *front end* facilities where thorium will be extracted from natural materials to the *back end* facilities which will separate ^{233}U from the thorium fuel bundles utilized in the reactor. Currently, there exist some facilities related to the front end of the cycle. The main source of thorium in case of India is the monazite rich sands that are present in placer deposits on beaches in various parts of India [10]. These sands are mined by dredging and subjected to processes like size and gravity based segregation and magnetic and electrostatic separation to isolate monazite [18]. Monazite usually has a thorium activity content of around 100 Bq g^{-1}[19]. The monazite is then subjected to chemical processes like caustic digestion and solvent extraction to obtain thorium in form of powders like thorium oxalate and thorium oxide. The thorium activity in these powders is of order of few thousand Bq g^{-1}.

When thorium is separated chemically, it has ^{232}Th and ^{228}Th in equilibrium with each other. The formation of thoron is governed by the activity of ^{228}Th since ^{224}Ra is in equilibrium with it (Figure 1.1). ^{228}Th decay rate follows its comparatively short half-life of 1.9 years, while the rate of its formation from ^{232}Th is governed by the half-life of ^{228}Ra (5.8 y). This results in a behaviour of ^{228}Th activity (and in turn the thoron generation rate) where there is initially a decrease in the activity following thorium separation and then an increasing trend after a period of five years. The thoron generation rate in 1kg of thorium as a function of time since separation is shown in

Figure 1.3. The thoron generation reaches a minimum value which is about 45 per cent of initial value in about 5 years.

The obtained thorium powders are then treated to processes like calcination and sintering to convert them to *fuel pellets* [9]. The fuel pellets are then integrated to form fuel bundles to be used in reactor. The thorium fuel in reactor undergoes various nuclear reactions involving neutrons. This results in formation of the fissile ^{233}U which actually undergoes nuclear fission to give energy [8]. During irradiation in nuclear reactor, various other competing nuclear reactions also take place leading to the formation of other different radio-nuclides in different proportions.

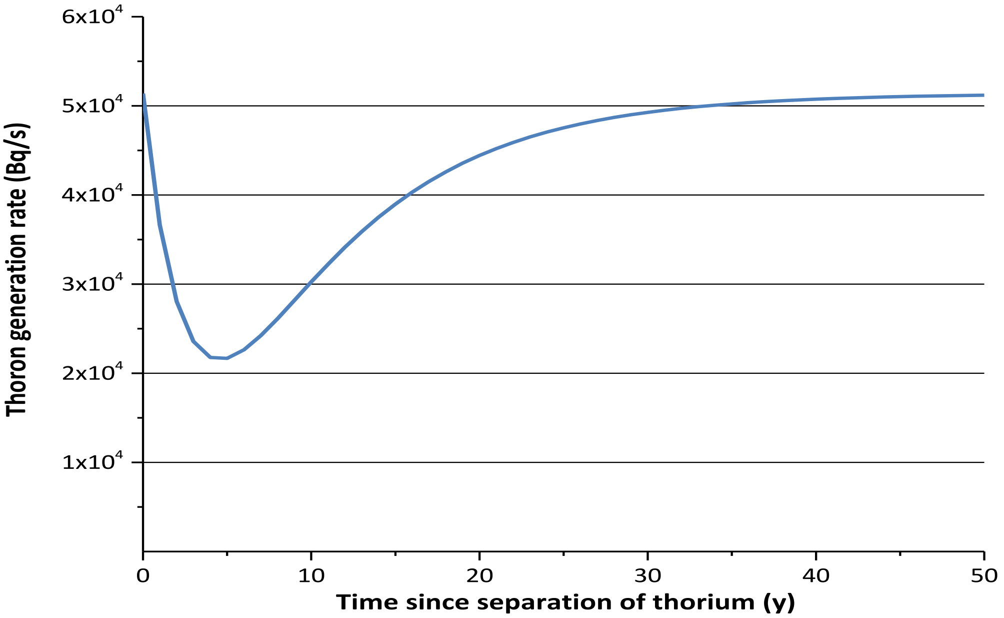

Figure 1.3: Plot of thoron generation rate in 1kg of thorium against time since separation

As a part of the closed fuel cycle the ^{233}U formed needs to be separated. However, conversion of ^{232}Th to ^{233}U is inherently accompanied by formation of radioisotope ^{232}U in the reactor [20]. The ^{232}U decays directly to ^{228}Th with a half-life of 68 y and results in formation of thoron and its decay product. It is expected that the concentration of ^{232}U in ^{233}U will be about 500 parts per million (ppm) [21], [22]. The thoron generation rate for 1 kg of ^{233}U containing 500 ppm of ^{232}U is shown in Figure 1.4.

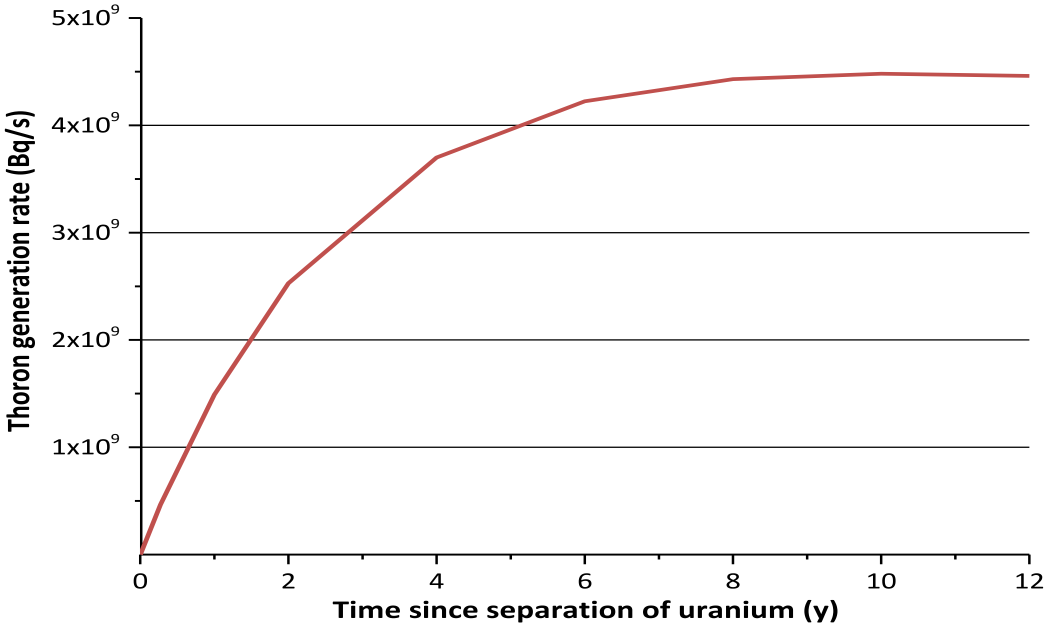

Figure 1.4: Thoron generation rate in 1kg uranium-233 fuel containing 500ppm of ^{232}U

It can be seen that the thoron generation rate in uranium fuel separated from thorium irradiated in a reactor builds up at a high rate initially and follows the growth curve of ^{228}Th. It can also be seen that the thoron generation rate at maximum level is higher than the maximum thoron generation rate in thorium by 10^5 times. Thus, the radiological issues due to thoron and its decay products will be magnified manifold in the backend of thorium fuel cycle and in further processing of uranium-233 fuel.

Table 1.1: Approximate ^{228}Th content in materials handled in the thorium fuel

Material	^{228}Th content (Bq kg^{-1})
Monazite sand	4×10^4
Thorium	4×10^6
Uranium-233 (with 500 ppm ^{232}U)	4×10^{11}

The comparative thoron generation potential can be understood by the approximate ^{228}Th content in different materials handled in the thorium fuel cycle shown in Table 1.1. The magnitude of radiological concern due to thoron will be proportional to ^{228}Th content, as this will govern thoron production.

1.5. Research Framework

The problem of radiological risk due to thoron and its decay products can be represented by conceptual framework shown in Figure 1.5.

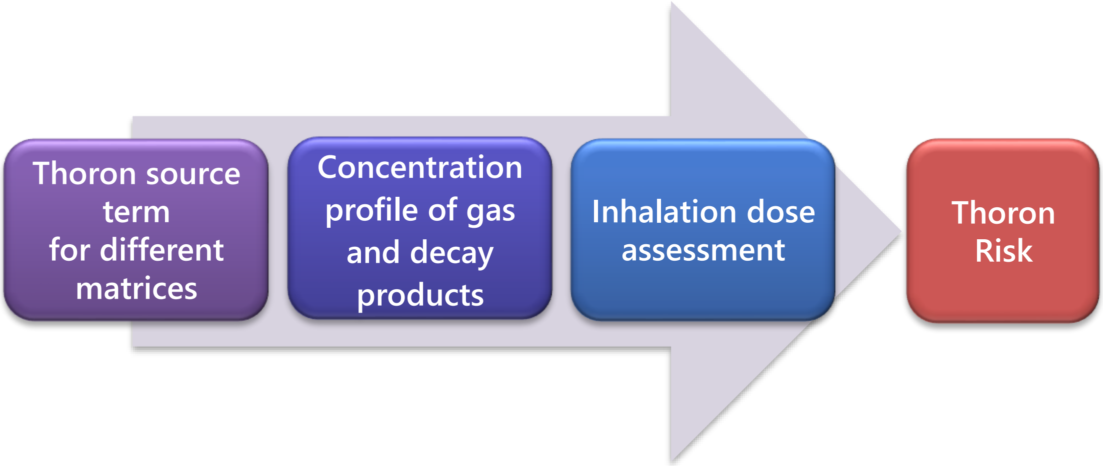

Figure 1.5: Conceptual framework for problem of thoron radiological risk in thorium facilities

In order to be able to deal with the problem successfully, it is necessary that we have a proper knowledge of three components: 1) Thoron Source term, 2) Concentration profile of gas and decay products in environment and 3) Inhalation dose estimation. The research on thoron in occupational environments with respect to these is still lacking. The thorium fuel cycle is being predominantly pursued by India and hence the onus is on the Indian researchers to carry out in-depth studies on these aspects. Each of the components of the above framework is discussed in detail below.

1.5.1. Thoron source term estimation

The quantity of thoron released to the working environment will fundamentally decide the overall radioactivity concentration levels and radiation exposure. As discussed in section 1.4, the ^{228}Th content is one factor which controls this. Since thoron is short-lived, only a fraction of all the thoron atoms generated is actually able to travel out of the source to the environment before undergoing radioactive decay [23]. Studies in natural environment show that in case of dense solids, only a small portion of thoron generated in a thin layer below the surface comes out to the environment [24]. But in case of materials like soil which are porous in nature, thoron from deeper volume can also come out by travelling through the pores, resulting in an increased thoron emission. General models for thoron transport and emission have been studied for soil [25]–[28], but not many studies are available for thoron emission from materials handled in thorium fuel cycle. The prediction of thoron source term in thorium fuel handling facilities requires suitable modifications and validation of these models for different thorium bearing materials. Processes like sparging require experimentation for selection of models describing thoron transfer from liquid to air. A proper methodology aided with correct models and suitable tools for determining relevant parameters is required for an accurate estimation of thoron source term, which is a basic necessity for estimating risk due to thoron.

1.5.2. Thoron and decay product behaviour in environment

Following the release of thoron from source, the next component which decides the risk due to thoron and its decay products is the behaviour of thoron and its decay products in the working environment. Most of the thoron decays out immediately after being exhaled and its concentration in the environment is generally very low. However, when thoron release is significant, thoron gas concentration is found to demonstrate a non-uniform profile with very high concentration near the source, which decreases rapidly with increasing distance from it [29]–[33]. The decay products formed from thoron are considerably long lived and remain in the environment after their formation. The properties of the decay products are instrumental in deciding the actual delivered radiation dose. These in turn are mainly dependent on the characteristics of ambient aerosols present in the environment. The concentration and properties of decay product aerosols also depend upon factors like ventilation rates, room dimensions, turbulence in air etc. [1]. Basic models to predict properties of thoron and decay products in residential environments have been proposed [34], [35]. However, they need to be suitably modified and validated for occupational environments of thorium processing facilities. The validated models can then be applied to explore the effect different parameters have on thoron decay product properties.

1.5.3. Inhalation dosimetry for thoron

The last component of the framework to address thoron risk is dosimetry. The pathway of exposure to thoron and its decay products in occupational environment is by inhalation [36], [37]. The dose to an exposed occupational worker following an exposure to thoron will depend upon the decay product related parameters like concentration and activity size distribution, and person-specific parameters like breathing rate and physiology of the exposed person. The most commonly used method for estimating thoron dose is to measure the thoron and decay product concentrations and use standard dose conversion factors provided by UNSCEAR [2] or ICRP [38]. However, these dose conversion factors do not account for the different nature of aerosols and hence the thoron decay products, which is expected in thorium processing facilities. Moreover, these dose conversion factors have been calculated using the properties of thoron decay products in normal residential environments. Hence, it is necessary to analyse the exact nature of variation in thoron dose conversion factor that can arise for different types of thorium processing facilities and understand which factors have significant effect on it, so that these are given special attention while determining thoron dose.

1.6. Objectives and Scope of the present work

The work presented in this thesis aims to fill the knowledge gap in different aspects related to thoron risk estimation in thorium fuel cycles, described above. Adapting the models for thoron transport and emission for porous matrices and liquids for the case of thoron emission from materials handled in thorium fuel cycle forms the first objective. Validation of the models through laboratory experiments and in-situ measurements in existing facilities follows. Development of standard methodology for thoron source term estimation along with simple methods for fast in-situ measurement of different thoron emission parameters to be used as input in models emerge as outcome of the study. The second objective is development of models to predict thoron concentration profile and adapt the decay product model for thoron decay products in houses to the case of occupational environments. The models are validated by laboratory experiments and multi-parametric measurements in a thorium processing facility. Post validation the decay product model is used to obtain insight on the effect of various parameters on the decay products acting in presence of each other. The models form an important part of thoron risk estimation methodology by linking thoron source term to individual exposure. The third objective is to have a dose estimation method to study and accurately predict radiation dose due to thoron and its decay products using the exposure values. A software program based on the latest ICRP biokinetic and dosimetric models is written and validated. The same is applied to study how factors like physiology, breathing rate and thoron decay product properties affect the actual thoron dose and resulting risk, and identify which of them are most influential.

Chapter 2

BASIC THEORY, METHODS AND TECHNIQUES

2.1. Background

This chapter presents information on basic theory, measurement methods and techniques for study of thoron and its decay products which have been used in the course of work presented in the dissertation. The general significance of thoron and its decay product and the various terminologies and units used in field of radon and thoron is discussed. The physics of thoron emission from porous matrices, the general characteristics and properties of thoron and its decay products in indoor environment and the processes which affect these are explained. The various instruments, methods and techniques used for the study of thoron and its decay products in the work presented in the thesis are described.

2.2. An introduction to thoron (^{220}Rn) and its progeny

Thoron is a noble gas produced by decay of ^{224}Ra which occurs in the natural decay series of the primordial radionuclide ^{232}Th. It undergoes radioactive nuclear transformation by alpha decay with a half-life of 55.6 s. Owing to its gaseous nature, thoron tends to move out of the source matrix and come out to the environment. However, due to its short half-life, much of the gas decays out before it is able to travel sufficient distance to be exhaled from the source. Thus thoron emission is significantly less as compared to radon [39]. The decay products of thoron are mostly short lived radioactive solids which emit alpha or beta particles. The half-lives and the modes of decay for thoron decay products are shown in Table 2.1. Thoron decays to ^{216}Po which has very short half-life and is always considered to be in equilibrium with the gas. The next decay product is ^{212}Pb which is a beta emitter. Though the beta emission of ^{212}Pb itself is responsible for only a tiny part of dose to human respiratory tract, the concentration of ^{212}Pb is responsible for more than 90 per cent of the overall dose due to thoron decay products (equation 2.2) [34]. This is due to the fact that the longer half-life of ^{212}Pb results in its concentration in air being higher than other decay products. Moreover, after ^{212}Pb is deposited in human respiratory tract, it decays to other alpha-emitting radionuclides in its decay chain which impart significant dose. The next decay product ^{212}Bi has two modes of decay, resulting in branching of decay chain with 64 % decaying by beta emission and 36 % decaying by alpha emission. Each branch has a radioisotope of importance from radiological standpoint. The ^{212}Po radionuclide decays by emission of alpha with a very high energy of 8.4 MeV and in the other branch ^{208}Tl decays by emitting one of the strongest gammas of energy 2.62 MeV.

Table 2.1: The decay modes and energies of radiation for ^{220}Rn and its decay products

Decay Product	**Elemental Name**	**Half life**	**Principal radiation & energies (MeV)**
^{220}Rn	Radon - 220	55.6 s	α 6.29 (100 %)
^{216}Po	Polonium - 216	0.15 s	α 6.78 (100 %)
^{212}Pb	Lead - 212	10.6 h	β 0.35 (81 %)
^{212}Bi	Bismuth - 212 (64%)	60.6 min	β 2.27 (54 %)
^{212}Po	Polonium - 212	0.305 μs	α 8.78 (100 %)
^{208}Pb	Lead - 208	Stable	None
^{212}Bi	Bismuth - 212 (36%)	60.6 min	α 6.05 (24 %), 6.09 (12 %)
^{208}Tl	Thallium - 208	3.07 min	β1.8 (50 %)
^{208}Pb	Lead - 208	Stable	None

2.3. Basic Theory

2.3.1. Special quantities and units

Some terminologies and special quantities are used in literature for radon (including thoron) and its decay products to describe the concentrations and inhalation exposure. These are explained, primarily in context of thoron below.

2.3.1.1. Potential Alpha Energy (PAE)

The potential alpha energy E_{Pi} (MeV) of an atom i in the decay chain of thoron is the total alpha energy emitted during decay of this atom through the decay chain to the stable radionuclide ^{208}Pb. PAE per activity (J Bq^{-1}) of a radionuclide i, is E_{Pi} / λ_i with λ_i (s^{-1}) being the radioactive decay constant of the radionuclide.

2.3.1.2. Potential Alpha Energy Concentration in Air (PAEC)

The "potential alpha energy concentration" is a legacy quantity used to describe the radiation dose potential for thoron (and radon). It is the sum of the potential alpha energy of all decay product atoms present per unit volume of the air. The potential alpha energy per unit activity of thoron decay products is presented in Table 2.2. The potential alpha energy concentration (C_P) for a mixture of thoron decay products in air will is given as:

$$C_P = \sum_i C_i \frac{E_{Pi}}{\lambda_i} \qquad \textbf{2.1}$$

where C_i (Bq m^{-3}) is the concentration of decay product i in air.

The SI unit of PAEC is J m^{-3}. The PAEC describes the dose potential associated with the decay products in a better way than other quantities and is useful to understand the comparative risk associated with radon and thoron decay products.

Table 2.2: Potential alpha energy per unit activity for thoron decay products [40]

Nuclide	**Half-life**	**Potential alpha energy per unit activity**	
		MeV Bq^{-1}	**10^{-10}J Bq^{-1}**
^{216}Po	0.15 s	3.16	5.1×10^{-3}
^{212}Pb	10.64 h	4.312×10^{5}	691
^{212}Bi	60.6 min	4.090×10^{4}	65.5
^{212}Po	304 ns	3.85×10^{-6}	6.2×10^{-9}
Total at equilibrium, per Bq of^{220}Rn		4.721×10^{5}	756

2.3.1.3. Working Level

The working level (WL) is an old unit of PAEC defined as the concentration of thoron decay products in any combination which would potentially produce 1.30×10^{8} MeV of PAE per m^3 of air [38].

2.3.1.4. Equilibrium equivalent thoron concentration

The equilibrium equivalent thoron concentration (EETC) (Bq m^{-3}) is defined as that activity concentration of thoron gas, in equilibrium with its short-lived progeny, which would have the same PAEC as the existing non-equilibrium mixture[38]. A thoron concentration of 275 Bq m^{-3} in equilibrium with its decay product corresponds to 1 WL. The EETC for any combination of concentration C_i of individual decay product i can be calculated as [1]:

$$EETC = 7\times10^{-6} C_{Po-216} + 0.913\times C_{Pb-212} + 0.087\times C_{Bi-212} + 8\times10^{-10} C_{Po-212} \qquad \textbf{2.2}$$

2.3.1.5. Equilibrium factor, F

The equilibrium factor (F) is defined as the ratio of EETC to the measured thoron gas concentration.

$$F = \frac{EETC}{C_{Tn}} \tag{2.3}$$

where C_{Tn} is the concentration of thoron. Depending upon the context of application, the thoron concentration value can be an average value for an environment, or a localised measurement value.

2.3.1.6. Unattached fraction

The unattached fraction (f) is defined as the fraction of thoron decay products that are not attached to the ambient environmental aerosols.

2.3.1.7. Exposure

The exposure (E) (Bq m^{-3} h) is defined as the time-integral over decay product activity concentration. The same can be expressed in terms of PAEC. It is expressed in SI units as J m^{-3} h, or the historical unit of working level month (WLM). 1 WLM is defined as the exposure to a concentration of 1 WL for a working month of 170 h. For thoron 1WLM corresponds to 1.32×10^{7} Bq m^{-3}h of EETC.

2.3.2. Emission and transport of thoron in porous matrix

2.3.2.1. Generation of radon/thoron

Thoron is produced from ^{232}Th present in soil or any other matrix. The thoron generation rate is proportional to ^{232}Th content and it is increased much more by the technological enhancement of natural materials in cases like mining of thorium ores and industries processing these ores. The theory for radon emission from porous matrix is well established and the primary physics remains the same for thoron too [41]–[43]. The amount of thoron that is transported through the matrix and is exhaled to indoor environment depends on the properties of the matrix, such as porosity, tortuosity, permeability, presence of cracks and the conditions such as moisture content, rate of saturation and pressure gradients. The amount of thoron exhaled to the environment can cover a range over several orders of magnitude due to a large variation in magnitude of these parameters.

2.3.2.2. Emanation of radon/thoron

Of all the thoron atoms generated by the decay of ^{224}Ra contained in the grain of matrix, only a fraction is released into pore spaces and mobilized. One of the three possibilities is valid when a radon/thoron atom is formed by decay of a radium atom:

1) It may travel a short distance and remain embedded in the same grain

2) It can travel across a pore space and become embedded in an adjacent grain or

3) It is released into a pore space.

The process where a radon/thoron atom formed in a radium-bearing grain is released into pore space is termed as emanation and the fraction of the radon/thoron atoms formed in the grains that is emanated, is called ‘emanation coefficient’.

2.3.2.3. Thoron transport in porous media

There are primarily two mechanisms responsible for transport of radon in porous media after its emanation. These are as described below:

1) Thoron can be transported due to differences in concentration (see Figure 1.1), called as diffusive transport or diffusion. Diffusive transport is considered to be one of the

main processes for exhalation of thoron from building materials, soils and other porous media sources.

2) Thoron can also be transported by the flow of air, known as advective transport or advection.

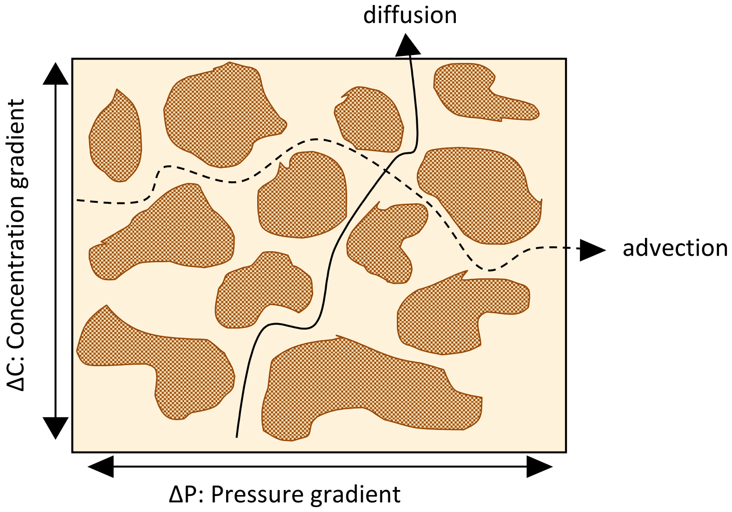

Figure 2.1: Schematic representation of advective and diffusive transport of radon due to pressure and concentration gradients, respectively

2.3.3. Behaviour of thoron in indoor environment

Thoron atom being short lived decays before it can travel a long distance in air after its exhalation. As a result, thoron gas is never uniformly distributed in indoor environment. Its concentration is generally highest near the source and decreases in near exponential pattern with increasing distance from it. It has a very short molecular diffusion length of 3 cm in undisturbed air at room temperature [44]. However, the diffusion length can increase due to role of turbulence in transport of thoron atoms. Studies have been carried out to observe thoron distribution in closed spaces and comparing with concentration profile predicted by diffusion mechanism and an effective diffusion coefficient (or turbulent diffusion coefficient) assumed to be homogeneous for a room.

The model calculations using this approach provided the values for turbulent diffusion length of thoron ranging from 50-60 cm. [29]–[31], [33]. A typical graph for thoron distribution considering thoron emanation from a wall is shown in figure 1.2.

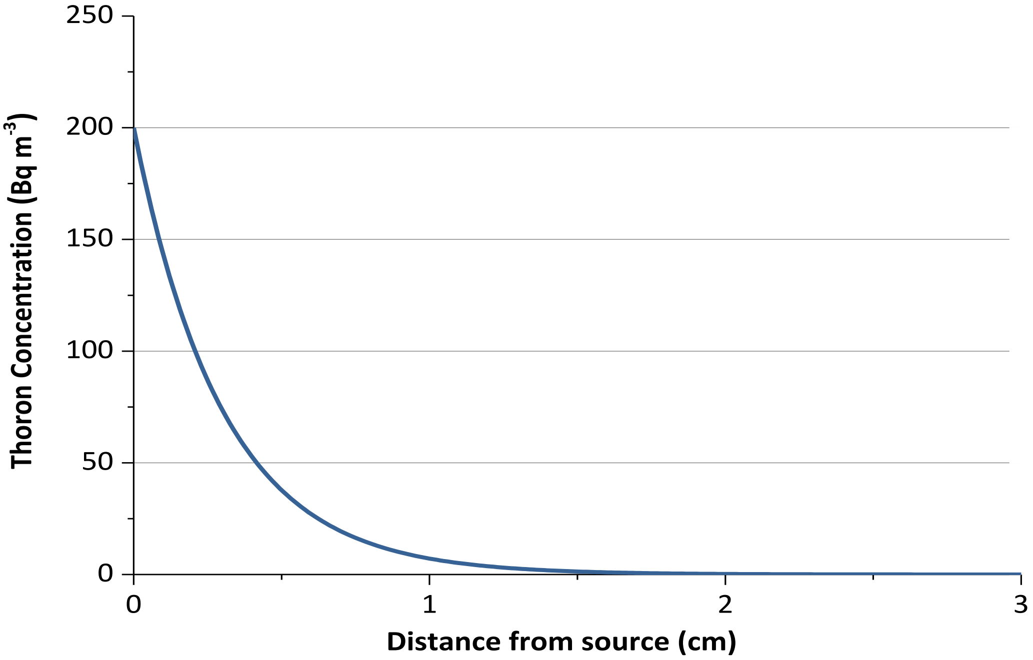

Figure 2.2: Thoron concentration profile with the distance from the source wall

1.5 Indoor radon thoron decay products dynamics

Radon/thoron decays by a series of several alpha and beta particle emitters. After the alpha-decay of a nucleus, the produced atom is positively charged due to the sustained recoil. However, within a few milliseconds, they neutralize by recombination with negative air ions and by charge transfer processes on reaction with trace atmospheric gases like NO, NO_2, H_2O vapours and other impurities, to form clusters or “unattached” or “fine” particles with diameters typically between 0.5-5 nm. These radionuclides may also attach to the ambient aerosol particles within a time frame of 1-100s forming the “attached or coarse” radioactive decay product species. The attachment of the decay products to the existing atmospheric aerosol particles is a function of size (d) of the aerosol particles. For $d > 0.1$ µm, the attachment process is determined by pure diffusion laws. On the other hand, for $d < 0.1$ μm, the attachment is controlled by pure kinetic theory of gases and is proportional to the particle surface area.

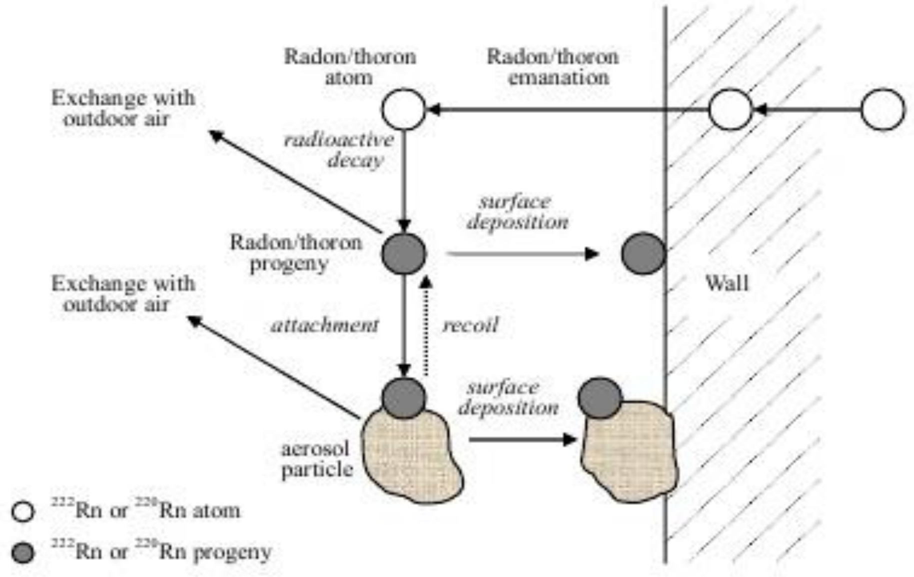

Figure 2.3: Representation of formation, transport and removal processes for Radon/Thoron Progeny in an Enclosed Space.

The decay products present in the form of aerosols are removed from the environment by radioactive decay, removal by ventilation and deposition on the available surfaces. Hence the total concentration of decay products in the room is governed by parameters like ventilation rate, the sizes of the decay products which governs the deposition rate, and turbulence in the air which also affects the deposition.

2.3.4. Thoron Radiological significance and Dosimetry

2.3.4.1. Radiological significance of thoron

Inhalation of high cumulative levels of ^{222}Rn and, in particular, its α-particle-emitting decay products has been linked to an increased risk of lung cancer among underground miners [15]. Similarly, the epidemiological studies for residential environments have also linked greater risk of lung cancer to radon [45]–[48]. In contrast to radon, thoron concentration is mostly negligible in all types of environment and a very few studies in the past were dedicated to measurement of thoron and its decay products and its epidemiology. However thoron and its decay products have received an increased attention in recent times [49]–[52]. It has been observed that thoron can be an issue of radiological concern in some types of indoor environments.

2.3.4.2. Role of thoron decay products in overall thoron dose

The radiation dose due to thoron is primarily imparted to respiratory tract following inhalation of the air containing thoron and its decay products. Thoron gas being inert is exhaled completely after inhalation. But the decay products being solid particles get deposited in the pathways of human respiratory tract. The radioactive half-life of thoron decay products are such that following their inhalation a major fraction decays in lungs, before they are cleared either by absorption into blood or by particle transport to alimentary tract [40]. Hence, the decay products of thoron impart a much higher fraction of the dose as compared to thoron gas. For practical radiological protection, Dose Conversion Factor (DCF) which relates the exposure of thoron and its decay products in the environment to the resultant dose is used.

2.3.4.3. A review of Dose estimation methods and dose coefficient for thoron

The low concentrations of thoron found in general, and the difficulty in measurement due to its short half-life have affected the studies of thoron dose estimation over the years. Historically, the recommended methods for thoron dose estimation have been primarily based on those for radon. The evolution of dose estimation for radon in itself is a unique story. Because of the early recognition of the radioactive potential of radon it received keen attention in mining environments and later in residential environments as well. Epidemiological studies of occupational exposures of miners and domestic exposures of the public have provided strong and complementary evidence of the risks of lung cancer following inhalation of radon and its progeny [15], [45]–[47], [53], [54]. Radon is one of the very few radiation sources for which the epidemiologically established risk value is available. The International Commission on Radiological Protection (ICRP) (which is the primary body providing recommendations and guidance on protection against the risks associated with ionising radiation from various sources including radon) recommended the *Dose conversion convention* in its Publication 65 [38]. In this method, the detriment (lung cancer) associated with unit exposure is divided by the detriment per unit effective dose to obtain radon dose conversion factor. But in case of thoron there is no epidemiological data available. Hence, the dose conversion factor for thoron (in terms of EETC) has been obtained by comparing the dose per unit exposure obtained by dosimetric models with radon and using the dose conversion convention in analogy with radon. ICRP, in its latest publication (ICRP publication 137), has recommended that doses from radon and radon progeny should be calculated using biokinetic and dosimetric models[40]. The publication has also provided the dose coefficients for thoron for the environments of indoor workplaces and mines. The dose coefficient for indoor workplaces has been obtained using aerosol characteristics for indoor offices and other similar environments [34], [55]. However, for the exposure situations where aerosol properties are considerably different the calculation of site-specific dose coefficients using dosimetric models is advised.

2.4. Measurement Methods and Techniques:

2.4.1. Measurement of thoron gas

The active measurement and sampling of thoron gas is a challenging task given the complex behaviour due to its very short half-life. The techniques and instruments used for measurement of thoron gas are described in short below.

2.4.1.1. RnDuo radon and thoron monitor

The thoron gas concentration measurement in most of the cases has been done using SMART RnDuo (AQTEK System, India) radon and thoron monitor. It is a ZnS:Ag scintillation cell based portable continuous monitor for detection of radon, thoron and gross alpha in sampled air [56]. The basic detector is a cylindrical cell with an active volume of 153 cm^3 with the coating of a thin layer of ZnS:Ag scintillator on the internal surface. It has an alpha detection efficiency of 0.75 and an overall sensitivity of 1.2 cph/Bq m^{-3}. For measurement of thoron, air is sampled through a filter paper to remove the aerosol particles. In a 15 minutes measuring interval, the air sampling and alpha measurement is carried out for first 5 minutes followed by stopping of flow and a delay of 5 minutes. In the next 5 minutes the alpha counting is done without flow to obtain background count rate. The thoron concentration is calculated using the counts for sampled air and background counts and displayed at the end of interval. The monitor's minimum detection limit for thoron is 12 Bqm^{-3} at 1 sigma and 1 h counting cycle and the upper detection limit is 10 MBq m^{-3}. Equipment has an in-built micro pump of flow capacity 0.7 l/min for air sampling and has no effect of humidity and trace gases variation on measurement of radon. A photograph of the monitor is shown in Figure 2.4.

Figure 2.4: Photograph of Smart RnDuo radon and thoron Monitor

2.4.1.2. Precautions in active measurement of thoron

Certain precautions have to be taken during the active sampling and measurement of thoron gas. The detector reads out the concentration of thoron in the detector volume. Hence for long sampling paths, a correction for thoron decay during its transit from sampling point to the detector volume has to be accounted for. For the use of the detector in close loop setups, like during the measurements of thoron mass emanation rate and exhalation rate, the derivation of correction factor is more complex and can be obtained in line with the procedure used by Kanse et al.(2013) [57].

In case of measurements for determination of concentration profile of thoron, the direct sampling by pump (which is integral for thoron measurement) disturbs the existing concentration profile. Hence, a diffusion cup attachment was used to carry out this measurement. The schematic of the same is shown in Figure 2.5. The diffusion cup is an impermeable cup of dimensions 6 cm diameter and 5 cm height with a provision to attach a filter paper at its open face. The thoron entering the cup by diffusion was sampled by internal pump of the thoron monitor. The flow of air was limited inside the closed loop measurement setup, thus minimizing the disturbance to prevalent thoron concentration profile.

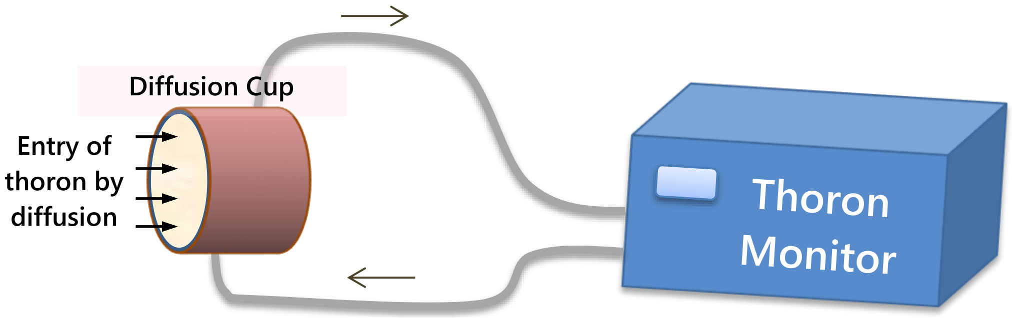

Figure 2.5: Schematic for diffusion cup sampler for measurement of thoron

2.4.1.3. Pinhole dosimeter

The Pinhole dosimeter is a passive Solid State Nuclear Track Detector (SSNTD) based device which can give a time integrated concentration of radon and thoron gas for the duration of exposure [58]. The schematic diagram of the pinhole dosimeter is shown in Figure 2.6. The dosimeter consists of two cylindrical chambers called ‘radon+thoron’ chamber and “radon” chamber, each having a diameter of 6 cm and height of 4 cm. The two are connected to each other in such a way that the gas first enters radon+thoron chamber through the single entry face by diffusion and then passes to radon chamber through pinholes made in central disc separating the two chambers. The pin-holes are optimised in such a way that they cut off thoron flux and allow only radon to get accumulated in the radon chamber. For detecting the gas concentration, a LR-115 SSNTD film is placed inside each chamber. The alpha particles emitted by radon and thoron gas, and their decay products register tracks on the films. At the end of exposure, these tracks are etched and counted according to the procedure described in section (2.4.1.4).

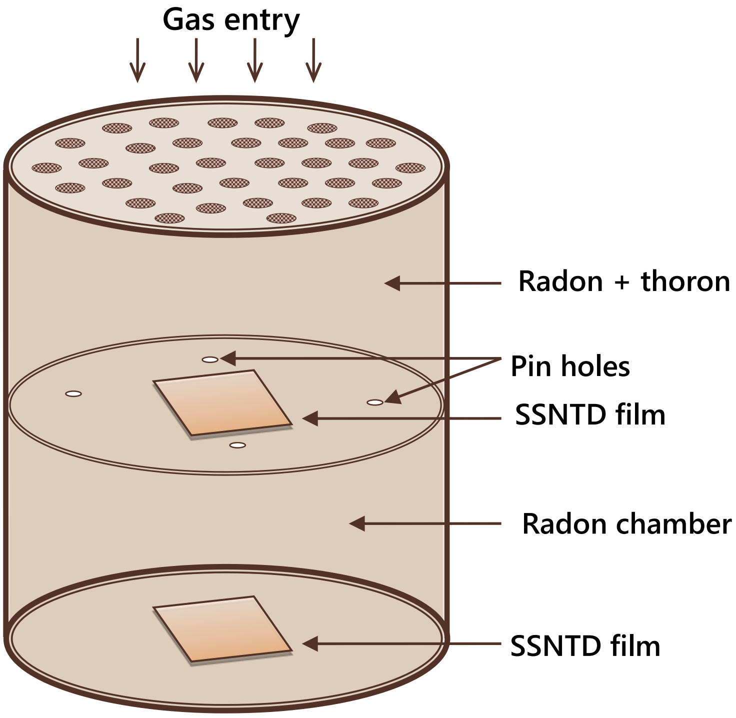

Figure 2.6: Schematic diagram of Pinhole dosimeter

Finally, the radon and thoron gas concentrations are determined using following equations:

$$C_R = (T_1 - B)/(d.k_R) \tag{2.4}$$

$$C_T = (T_2 - d.C_R k_R' - B)/(d.k_T) \tag{2.5}$$

where, T_1 is the track density observed in ‘radon’ chamber, k_R is the calibration factor of radon in ‘radon’ chamber for radon, d is the number of days of exposure, T_2 is the track density observed in the ‘radon+thoron’ chamber, k_R' and k_T are the calibration factors of radon and thoron in ‘radon+thoron’ chamber and B is the background tracks.

2.4.1.4. Etching of LR115 films and counting of tracks using spark counter

In order to determine the track density of the exposed LR115 films in pinhole dosimeter and other detectors, they are needed to be processed by chemical etching to enlarge the tracks, which can be counted using a spark counter [59], [60]. In the process of chemical etching, the LR115 films are immersed in an aqueous solution of 10% NaOH at a temperature of 60°C for 60 minutes (with stirring) and 90 minutes (without stirring). The damaged trails in the films get preferentially dissolved in the etching solution, compared to the bulk material. This results in enlargement of the tracks, making them easier to be counted.

In the spark counter, the thin etched track detector (about 8 - 10 µm thick) is placed between two electrodes forming a capacitor. The bottom electrode is a thick conductive electrode, commonly made of brass. The thin LR-115 detector is placed on the thick electrode. The aluminized mylar is placed on the detector such that the aluminized surface faces the detector as well as the thin electrode. A weight is placed on the top to ensure good contact between the electrodes, the detector and the aluminized film. When electric field is applied, the air in the track/hole starts discharging and produces a spark. As soon as a spark occurs, the capacitor discharge and corresponding number is counted in scalar through proper algorithms. The process is repeated multiple times till all the holes/tracks present on exposed area of detectors get sparked. The operating voltage of the spark counter is optimized at 500V.The programmable spark counter directly gives the track density value as read out.

2.4.2. Measurement of thoron decay products

2.4.2.1. Filter paper sampling and counting

The Filter paper grab sampling method is an active technique used to determine the thoron decay product activity concentration. In this method, a known volume of air is sampled through a filter paper using a pump. The decay products present in the sampled air are deposited on the filter paper. The alpha activity deposited on the filter paper is counted using a ZnS:Ag based counter. The counting of alpha activity is performed after a delay of about 5 hours so that the decay products of radon, if any, decay completely. Using the measured alpha counts X, the flux of atoms deposited per unit time φ_T (s^{-1}) can be obtained using equation[61]:

$$\varphi_T = \frac{X}{\eta Z_T} \tag{2.6}$$

where, η is the efficiency of alpha-counter, Z_T is the counting factor which is function of sampling interval and delay for alpha counting. The details for calculation of counting factor for thoron are provided by Mishra et al. [61]. The concentration of ^{212}Pb activity in the room C_{Pb212} and the EETC can then be calculated as:

$$C_{Pb212} = \frac{\varphi_T \lambda_{Pb212}}{q} \tag{2.7}$$

where, q(m^3 s^{-1})is the flow rate for sampling, and λ_{Pb212}(s^{-1}) is the decay constant of ^{212}Pb.

2.4.2.2. Direct thoron progeny sensor (DTPS)technique

Deposition based Direct Radon and Thoron progeny sensors (DTPS) are passive detectors for measurement of thoron decay products. They consist of LR-115 SSNTD film mounted with suitable absorber of appropriate thickness. A photograph of the DTPS detector is shown in Figure 2.7.

Figure 2.7: Photograph of Direct thoron progeny sensor (DTPS) detector

The detector works on the principal of selectively registering tracks for alpha originating from the desired radionuclide (^{212}Po) deposited on the detector, achieved by optimising the absorber thickness. The absorber used in DTPS is 50 μm thick aluminized mylar which results in selective detection of 8.78 MeV alpha particle emitted by ^{212}Po. The schematic diagram of the detector system is shown in Figure 2.8.

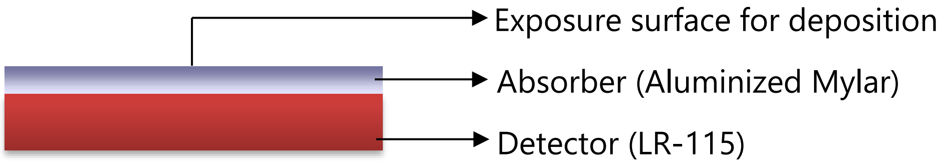

Figure 2.8: Schematic diagram of DTPS detector for thoron decay products

The DTPS detector primarily measures time integrated flux for decay product deposition. The number of tracks per unit area per unit time *T* can be correlated to the thoron decay product concentration (*EETC*) in air using the Sensitivity factor *S* applicable for the particular environment as:

$$EETC(Bqm^{-3}) = \frac{T(Tracks\ cm^{-2}\ d^{-1})}{S(Tracks\ cm^{-2}\ d^{-1} / EETC(Bq\ m^{-3}))} \qquad \mathbf{2.8}$$

2.4.2.3. Wire-mesh capped DTPS

Wire-mesh capped DTPS is a detector used to detect only those thoron decay products that are attached to aerosols i.e. attached fraction or coarse fraction. It is basically a DTPS capped with a 200 mesh type wire screen which acts as a fine fraction separator. The unattached fraction of the thoron decay products is trapped on the wire mesh through diffusion process, but the attached decay product particles are able to pass through it and are deposited on the DTPS. The tracks registered on the detector are a measure of the attached thoron decay product concentration. A photograph of the wire mesh capped detector is shown in Figure 2.9.

Figure 2.9: Photograph of wire mesh capped DTPS detector

2.4.2.4. Integrated Sampler

Integrated Sampler is a DTPS based thoron decay product detector with active mode of sampling [62]. The air is sampled through a sampling head consisting of a wire mesh followed by a filter paper, using a pump. A DTPS film is placed before the wire mesh and the filter paper each to detect alpha particles emitted from thoron decay product deposited on them. The schematic diagram of the arrangement is shown in Figure 2.10.

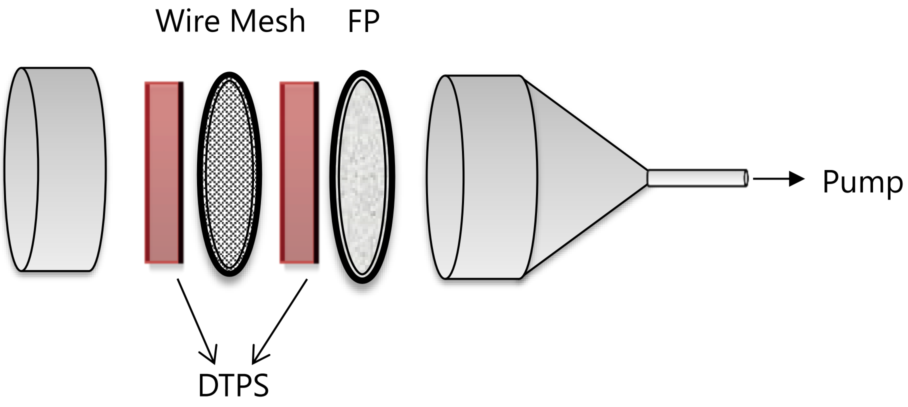

Figure 2.10: Schematic diagram of integrated sampler based on DTPS

During the sampling the unattached fraction of thoron decay product is first deposited on the wire mesh and the attached decay products which pass through are then deposited on the filter paper.

The SSNTD films from set of exposed DTPS are then removed, processed and the track density, T (tracks cm^{-2}) is determined. The thoron decay product concentration (EETC) corresponding to the two fractions is estimated using the relation [62]:

$$EETC_{unatt} = \frac{T_{WM}}{tS_{WM}} \qquad \textbf{2.9a}$$

$$EETC_{att} = \frac{T_{FP}}{tS_{FP}} \qquad \textbf{2.9b}$$

where, T_{WM} and T_{FP} are the track density obtained for DTPS corresponding to wire mesh and filter paper respectively. t is the sampling time and S_{WM} and S_{FP} are the sensitivity factors for wire mesh and filter paper respectively for converting the track density into EETC. A photograph of the sampler is shown in Figure 2.11.

Figure 2.11: Photograph of integrated sampler

2.4.2.5. Particle size separation using impactor technique

The activity size distribution of thoron decay products is an important parameter useful to predict different behaviours like attachment and depositions. In the present work, the activity size distribution of ^{220}Rn decay product was carried out using Cascade (Anderson) Impactor.

A cascade impactor separates the aerosols sampled using a pump into different particle size ranges which get deposited on the various stages using the different impaction properties for them. The sampled air is passed through multiple nozzles at each stage, which direct the airborne particles towards an impaction surface in front. The schematic diagram for the process is shown in Figure 2.12.The different stages in the impactor collect particles of different sizes. The first stage of the impactor is a pre-separator stage. The last stage of the impactor is an absolute filter stage; it collects the particles which are too small to be deposited by impaction in the previous stages. The cut off diameter for an impactor stage is defined as the size of particles collected with 50% efficiency. The Anderson impactor classifies the particles from 0.4 µm to 10 µm in 8 size classes and operates at 28.3 lpm flow.

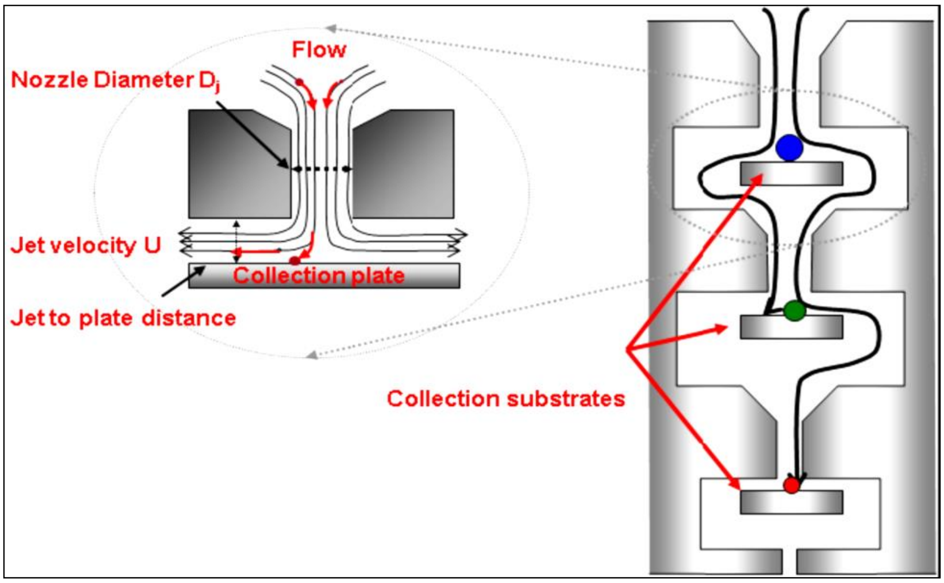

Figure 2.12: Schematic diagram for process of particle impaction and its application in cascade impactor

Ideally, the collection efficiency would be a step function so that all particles bigger than certain cut-point are collected on the impactor stage whereas all particles smaller than certain size continue with the flow to lower stages. However, due to bounce and blow-off, some of the bigger particles will go to lower stages than they should, and due to diffusion, some of the smaller particles will stay on upper stages although not desired.

The activity of thoron decay products deposited on each stage was determined using the alpha counting method. To obtain the Activity Median Aerodynamic Diameter (AMAD) and Geometric Standard Deviation (GSD) for the thoron decay product activity, a plot of cumulative activity depositions less than the stated size against the aerodynamic diameters was plotted. The cumulative fractional deposition is plotted on probability scale and aerodynamic diameter on a logarithmic scale. A straight line fitting was done on this graph and the AMAD and GSD values were calculated using the fitting parameters [63].

2.4.3. Powder sandwich technique for measurement of thoron mass emanation rate

The mass emanation rate of thoron is an important parameter required to determine thoron source term in various context. However, the short lived nature of thoron presents many challenges such as losses during its diffusion from pore space of the matrix to the external environment, termed as matrix absorption. There can also be a loss of thoron in its transit path between the sampling point and detector during sampling and measurement. Considering the need to address all these factors, two different setups were developed for measurement of thoron mass emanation rate. The first setup called ‘Powder Sandwich Technique’ was developed for measurement of thoron mass emanation rate from a matrix with very high ^{224}Ra content such as thorium powders. The other setup was for matrices with slightly lower ^{224}Ra content where a higher quantity of matrix is necessary for accurate thoron measurement. Besides these issues, additional consideration in case of thorium bearing powders is considerably high radioactivity content which can lead to issues such as radioactive contamination of detector and other instruments in experimental setup and possibility of radiation exposure during handling.

The technique for determination of thoron mass emanation rate requires accurate measurement of all the thoron released from the matrix. Such techniques available for the correct determination of thoron emanation rate are still few. In the method used by Greeman and Rose [64], the measurement system needs to be calibrated with a standard sample of known exhalation rate. On the other hand, the method used by Iimoto et al. [65] does not account for the loss of thoron in the powder matrix due to its decay during the transit in thick layer (matrix absorption); and hence does not give an exact value of emanation co-efficient. The method proposed by Ujic et.al. [66] requires determination of thoron diffusion coefficient in the sample in order to determine the mass emanation rate. To overcome these drawbacks a new and relatively simple method for measuring thoron mass emanation rate for powders with considerably high ^{224}Ra content was developed.

In this method the thorium bearing powder is sandwiched between two filter papers. This arrangement is sealed at the circular edge using adhesive, to avoid any spillage or loss of the powder. This arrangement ensures that the thickness of powder sample is much less than the thoron diffusion length, avoiding any loss of thoron due to matrix absorption and supports complete removal of thoron gas emanated from the powder.

The technique utilizes a closed loop setup in which thoron emanated from the powder sandwich is removed using flow through arrangement and is measured using suitable thoron detector. The thoron mass emanation rate J_M (Bq kg^{-1}s^{-1}) for the powder is estimated using a mass balance model from the measured equilibrium thoron concentration C_{eq} (Bq m^{-3}) as [67]:

$$J_M = \frac{C_{eq} V \lambda}{M} \tag{2.10}$$

where, V (m^3) is the total volume of the experimental setup and M (kg) is the mass of thoron emitting sample.

2.4.4. Measurement of thoron exhalation rate

The measurement of thoron exhalation rate (Bq m^{-2} s^{-1}) from the surfaces of different sources was carried out using accumulator technique [28], [68]–[70]. The technique basically involves the measurement of thoron gas accumulated in an inverted cup called *accumulator* with open face placed on the surface of source. A schematic diagram for the accumulation of thoron in an accumulator is shown in Fig.2.1.

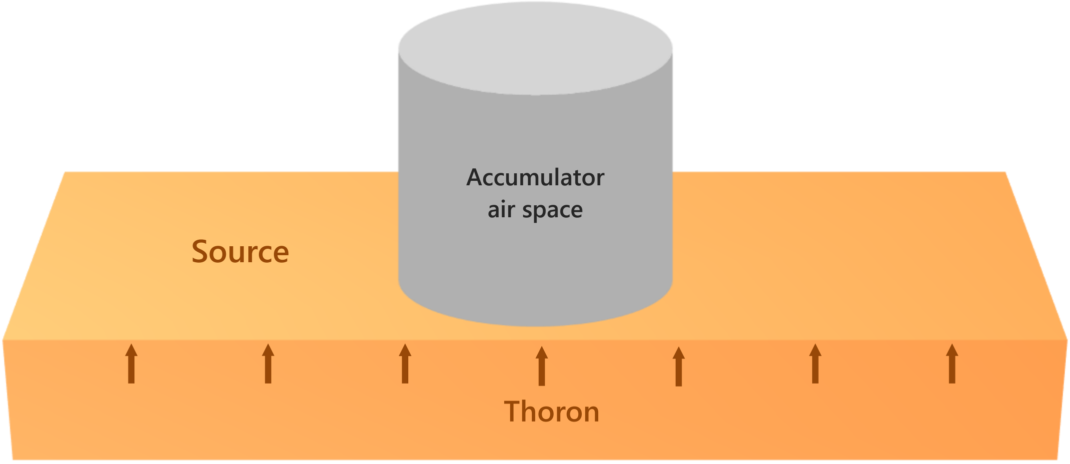

Figure 2.13: Schematic diagram of an accumulator placed on a source surface

Accumulators are placed in an inverted position on the surface of the source, or partially buried in source. To measure the concentration of thoron accumulated in the accumulator, it is connected to thoron monitor and a pump in a closed loop setup. Once the thoron concentration reaches an equilibrium value, C_{eq}, the thoron flux, J_S (Bq $m^{-2}s^{-1}$) is calculated using its value as [69]–[71]:

$$J_S = \frac{C_{eq} V \lambda}{A} \qquad \textbf{2.11}$$

where, λ is the thoron decay constant (0.0126 s^{-1}), V is the total volume of measurement setup including that of accumulator, detector and tubing (m^3) and A is the surface area (m^2) of the source covered by the accumulator.

The technique requires some modification for the case of shorter lived thoron, which tends to have concentration gradients in confined spaces and undergoes loss due to radioactive decay during sampling. To address this problem, an in-house developed accumulator set up with a relatively small accumulator (5 cm diameter and 7 cm height) was used so that the assumption of uniform concentration in the accumulator was valid. Shorter sampling tubes were used to avoid loss of thoron due to radioactive decay.

2.4.5. Determination of specific ^{224}Ra content

The specific ^{224}Ra content, R_a (Bq kg^{-1}) is required as an input parameter in determination of thoron emanation coefficient using. The same was measured using gamma spectrometry. For this, the samples were dried and put into a polypropylene container of standard dimension. The container was sealed and left undisturbed for a period of five days, in order to achieve a secular equilibrium between ^{224}Ra and its daughter products up to ^{208}Tl. The samples were then analysed using NaI (Tl) detector (GSpec, Electronics Enterprises Ltd., India). The calibration of the detector was done using standard thorium source (RGTh-1, IAEA). The activity of ^{224}Ra was estimated using the photopeaks of ^{212}Pb (239 keV), ^{212}Bi (727 keV) and ^{208}Tl (2614 keV). The spectrum was acquired for sufficiently long time so as to obtain good counting statistics resulting in a variable counting times depending on the activity of the various analysed samples.

Chapter 3

STUDY OF THORON SOURCE TERM FOR VARIOUS PROCESSES OF THORIUM FUEL CYCLE

3.1. Background

In thorium fuel cycle various materials with varying range of thorium content (more specifically ^{228}Th in context of thoron) are handled. These materials have different chemical and physical forms depending upon the processes associated with their formation. The thorium fuel cycle primarily consists of processes for separation of thorium from monazite bearing sands from beaches and subjecting it to various chemical and physical treatments to convert it to nuclear grade fuel for use in nuclear reactors. Monazite rich sands are the primary source for thorium and other rare earth minerals in India. These sands with thorium content of order of 1 to 100 Bq kg^{-1}[70], [72] are treated successively by processes such as centrifugal separation, electromagnetic separation, chemical leaching, solvent extraction etc. Thorium in various chemical forms is obtained as powder after these processes. These powders usually have thorium contents of the order of about a few hundreds to a few thousands of Bq kg^{-1}[57]. These powders are also subjected to treatments such as calcination and sintering [73]–[77]. Some processes also include handling of thorium in the form of liquids or solutions.

Thoron emission from these thorium bearing materials is a potent source of radiological exposure to occupational workers handling them. The very first step towards addressing the problem of radiological risk due to exposure to thoron and its decay products is prediction or evaluation of thoron source term during various processes of thorium fuel cycle. Almost all of the information currently available regarding the formation, mobilization, transport and emission of thoron is with respect to natural materials such as soils, rocks, minerals and building materials. A very limited literature is available for study of thoron emissions from materials handled during industrial processes and especially those associated with nuclear fuel cycle.

The two predominant modes through which thoron can be released to occupational environment in thorium processing facilities are: 1) by diffusion through porous substances such as powders, cakes, pellets etc. and 2) by bubbling of air or other gas through thorium bearing liquids during processes such as sparging, carried out in closed systems. Because of its short half-life, thoron diffusion length in most of the other materials is very small and it decays out before it can come out of it (also referred to as *matrix absorption* in some literature). Hence its emission from normal materials is restricted to superficial layer only.

3.2. Modeling of thoron exhalation from a porous matrix

The thoron transport in the porous matrices handled in thorium fuel cycles takes place primarily by diffusion. Hence in order to estimate the thoron emission from a porous matrix, a one-dimensional diffusion based model with specific thoron mass emanation rate and thoron diffusion length as input parameter was developed. The thoron mass emanation rate is a stable parameter and can be measured in a short time due to quick build up and saturation of thoron concentration during measurement. Suitable setups were developed for measuring specific thoron mass emanation rate and diffusion length of thoron. The whole methodology for prediction of thoron exhalation from porous matrices is described below.

3.2.1. Diffusion based model for thoron exhalation

The model for calculation of thoron exhalation rate from the surface of a porous matrix with finite thickness can be derived considering the analogy with similar model for radon [44]. Figure 3.1 is a schematic diagram for a porous material containing ^{224}Ra stored in a container. The model assumes that only one surface is available for thoron to be emitted out of the matrix. Thoron is continuously emanated from the grains to pore space of the matrix. Since thoron emission takes place from only one surface, a concentration gradient of thoron is created in a direction normal to the surface, i.e. along Z direction in case assumed in Figure 3.1. The ^{224}Ra distribution and other properties are assumed to be homogeneous for the matrix. The actual mobilisation of thoron gas takes place by diffusion in the pore volume of the matrix.

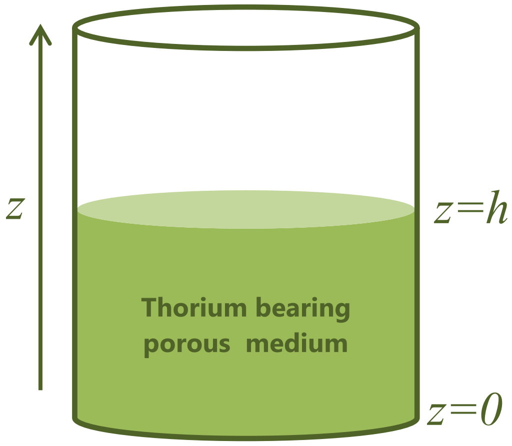

Figure 3.1: Schematic for thoron bearing porous medium

Hence the general equation for time rate of change of thoron activity in the pore volume C_p (Bq m^{-3}), can be written as

$$\frac{\partial C_p}{\partial t} = S_p - \frac{\partial J}{\partial z} - C_p \lambda \qquad \textbf{3.1}$$

where, S_p (Bq m^{-3} s^{-1}) is the thoron activity released into the unit pore space volume per unit time, J (Bq m^{-2} s^{-1}) is local flux of thoron crossing per unit pore area per unit time, λ (s^{-1}) is the radioactive decay constant of thoron.

If J_M (Bq kg^{-1}s^{-1}) is thoron mass emanation rate for the matrix and n_e is the porosity of the matrix, then thoron emanation rate per unit pore volume S_p will be given as:

$$S_p = \frac{J_M}{n_e} \qquad \mathbf{3.2}$$

The mass emanation rate can be expressed as:

$$J_M = R_a E \lambda \qquad \mathbf{3.3}$$

where, R_a (Bq kg^{-1}) is ^{224}Ra content in the matrix, E is radon emanation factor and λ (s^{-1}) is the decay constant of thoron.

The diffusion flux (J) in one dimension is given by Fick's first law of diffusion in terms of concentration gradient as:

$$J = -D_e \frac{\partial C_p}{\partial z} \qquad \mathbf{3.4}$$

where, D_e (m^2 s^{-1}) is the effective diffusion coefficient of thoron in the matrix which is the product of diffusion coefficient in porous matrix (D) and porosity of matrix (n_e).

Using equations 3.2, 3.3 and 3.4, equation 3.1 can now be written as:

$$\frac{\partial C_p}{\partial t} = \frac{R_a \rho_b E}{n_e} + D_e \frac{\partial C_p}{\partial z} - C_p \lambda \qquad \mathbf{3.5}$$

where, ρ_b (kg m^{-3}) is the bulk density of the matrix.

Under the condition of steady state, equation 3.5 is modified as:

$$D_e \frac{\partial^2 C_p}{\partial z^2} - C_p \lambda - \frac{R_a \rho_b E}{n_e} = 0 \quad \textbf{3.6}$$

The boundary conditions used to solve equation 3.6 are:

$J(0)=0$: flux is zero at the base due to impervious nature of container, and **3.7a**

$C(h) = C_{atm} \approx 0$: concentration is negligible at the matrix–air interface of matrix of thickness *h*. **3.7b**

Using the above boundary conditions and defining the diffusion length of thoron in the matrix as

$$l = \sqrt{\frac{D_e}{\lambda}} \quad \textbf{3.8}$$

Equation 3.6 is solved and the expression for thoron flux from the surface of the matrix J_s (Bq m^2 s^{-1}) is obtained as:

$$J_S = J_M \rho_b l \tanh \frac{h}{l} \quad \textbf{3.9}$$

The diffusion based thoron exhalation model represented by equation 3.9 can be used to calculate the thoron exhalation rate from any porous matrix by providing the input parameters viz. thoron mass emanation rate, thoron diffusion length in the matrix and the bulk density.

This model is similar to the model describing thoron emission from surface of a wall or porous slab, except for value of *h* which is equal to half the thickness of matrix in the latter model [41]. Since $\tanh \frac{h}{l}$ asymptotically approaches value of 1 with increasing value of *h*, the term can be neglected for matrix thickness sufficiently greater than the thoron diffusion length *l*. In this case, the model attains the form of well-known equation of radon flux from soil [2].

The thoron exhalation model was validated through measurements for two thorium bearing powders and two samples of monazite bearing sand. The experiments for the same are described below.

3.2.2. Validation of the thoron exhalation model: Thorium bearing powders

3.2.2.1. Measurement of thoron mass emanation rate

The thoron mass emanation rate for powders was measured using Powder sandwich technique described in section 2.4.3. For each of the studied powder, powder sandwiches containing different masses of the powder were prepared. These powder sandwiches were incorporated in the closed loop setup and the corresponding thoron concentration was measured. A plot of the equilibrium thoron concentration vs. the weight of the powder yielded a straight line. The mass emanation rate was then estimated using the slope of line as:

$$J_M = slope \times \lambda V \tag{3.10}$$

Table 3.1: Results for measurement of thoron mass emanation rate for powders

Powder Sample	**Mass emanation rate, J_M (Bq g^{-1} s^{-1})**
ADU	0.334 ± 0.003
Thorium oxide 1	0.314±0.007
Thorium oxide 2	3.57±0.03

The emanation rate of three powder samples: ammonium di-uranate (ADU) powder containing ^{232}U as the source of thoron, thorium oxide powder from a thorium facility an old thorium oxide powder stored in a container for 15yrs; was determined. The results for the same are presented in Table 3.1.

3.2.2.2. Measurement of thoron exhalation rate and comparison with model

A laboratory study was performed to measure the thoron exhalation rate corresponding to different heights for two powders: thorium oxide and ADU. Powder was filled up to varying height, in a glass beaker having diameter of 10 cm. The exhalation rate was measured using accumulator technique described in section 2.4.4. The accumulator was integrated in a closed loop setup with RnDuo thoron monitor having an in-built pump. The schematic diagram for the setup is shown in Figure 3.2.

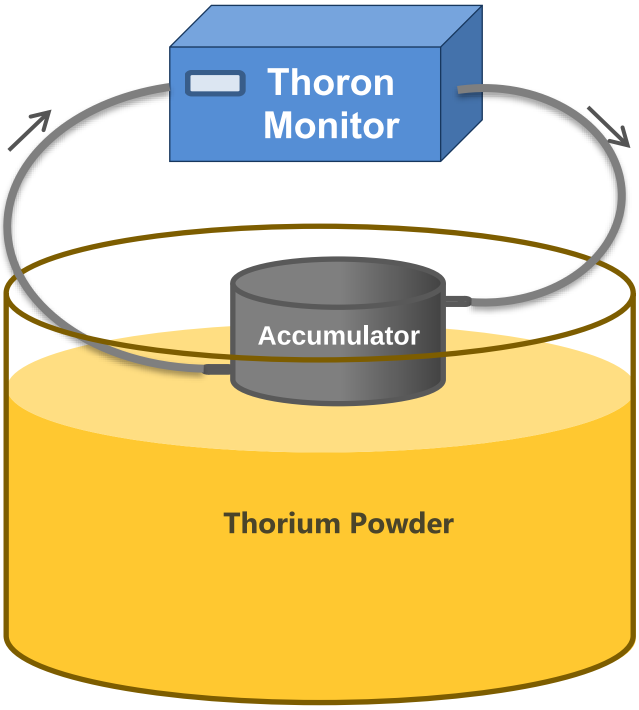

Figure 3.2: Schematic diagram of experimental setup for measurement of thoron exhalation from powders

The pump circulated the air inside the setup causing thoron to mix uniformly. The equilibrium thoron concentration C_{eq} (Bq m^{-3}) was measured using the thoron monitor and the same was used to obtain the thoron exhalation rate J_S (Bq m^{-2} s^{-1}) from powder using equation [69], [71]:

$$J_S = \frac{C_{eq} V \lambda}{A} \qquad \textbf{3.11}$$

where V(m^3) is the volume of the closed measurement setup and A (m^2) is the surface area covered by the accumulator.

The results for the measurements for thorium oxide and ADU are shown graphically in Figure 3.3 and Figure 3.4 respectively.

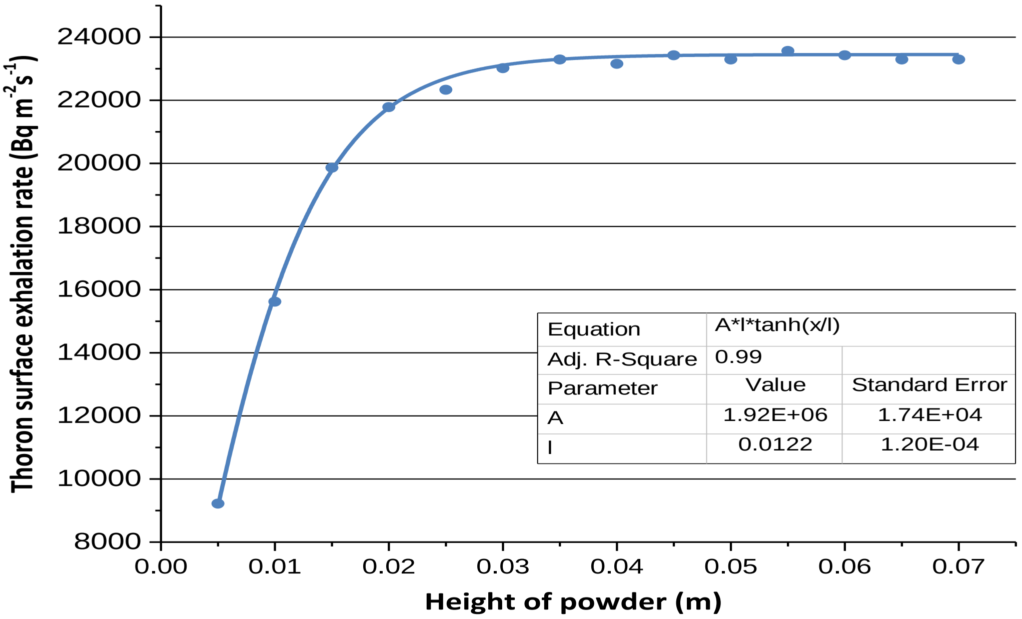

Equation	A*l*tanh(x/l)	
Adj. R-Square	0.99	
Parameter	Value	Standard Error
A	1.92E+06	1.74E+04
l	0.0122	1.20E-04

Figure 3.3: Plot of thoron surface exhalation rate against thorium oxide powder height, fitted with model to obtain diffusion length

The thoron exhalation model represented by equation 3.9 was fitted to the data in both the cases, with diffusion length as the variable parameter. For thorium oxide powder the model gave a very good fit with R^2 value of 0.997 and gave a value of 1.22±0.01 cm for the effective diffusion length. Similarly, for ADU powder the R^2 value for fitting of the model was 0.99 and it yielded the value for diffusion length as 1.75 ±0.03 cm. The very good fitting to the measured data thus validates the model.

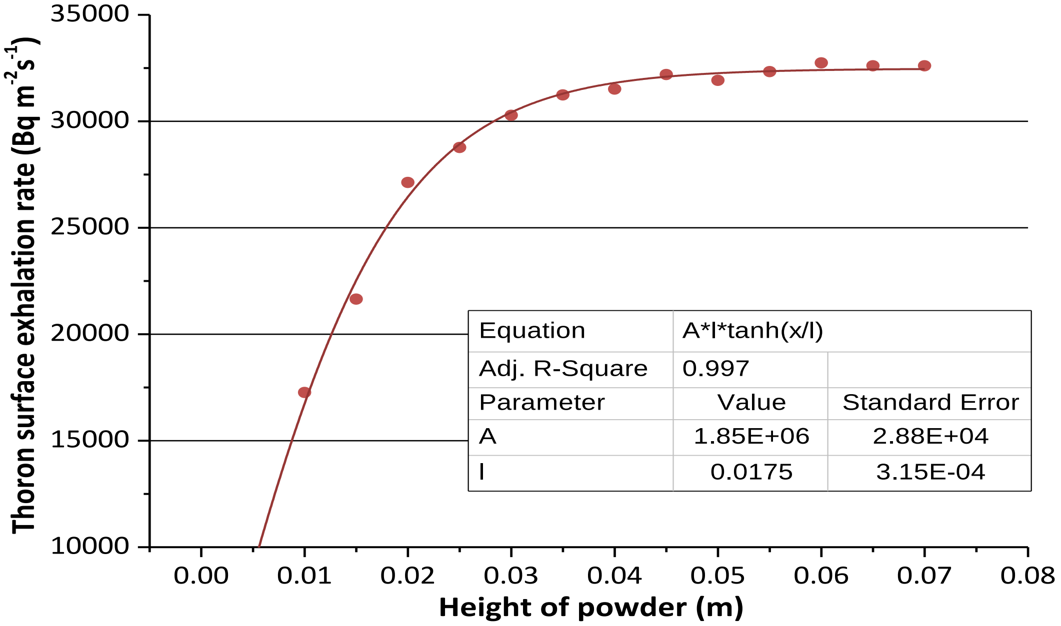

Figure 3.4: Plot of thoron surface exhalation rate against ADU powder height, fitted with model to obtain diffusion length

3.2.2.3. In-situ measurement in thorium facility for validation of model

a) ADU Powder

The performance of thoron exhalation model was checked in actual nuclear fuel processing facility. The processes carried out at the facility are separation of ADU precipitate by filtering, drying and calcination of the powder. For the prediction of thoron exhalation from the dry ADU powder, the mass emanation rate (J_M) measurement was done in-situ using Powder sandwich technique described in section2.4.3. The value for the same was used along with the diffusion length for thoron of 1.75 cm for ADU obtained in the laboratory measurement and the bulk density measured in-situ was used as input parameters in the thoron exhalation model. To compare how the prediction matched with the actual value, measurement of thoron exhalation rate from dry ADU in different areas of the facility was measured using the accumulator technique as described previously. The height of the powder was also measured for use in the model. The photograph for one such measurement is shown in Figure 3.5.

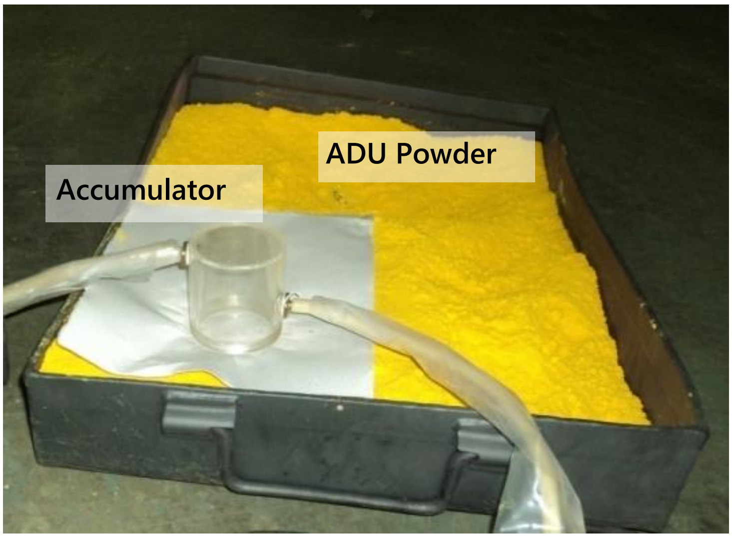

Figure 3.5: Photo of in-situ measurement of thoron flux from ADU in thorium facility

Measurements were done for three different cases with ADU powder heights of 3cm, 10cm and 35 cm. The comparison of the model predicted and in-situ measured values of thoron exhalation is shown in Table 3.2.

Table 3.2: Comparison of model predicted thoron exhalation rates for ADU powder with in-situ measured values

ADU powder height h (cm)	Model Predicted J_S (Bq m^{-2} s^{-1})	In-situ measured J_S (Bq m^{-2} s^{-1})
3	11510 ± 210	11340 ± 350
10	12395 ± 232	12290 ± 510
35	12395 ± 232	12580 ± 520

The values of thoron exhalation rate predicted by the model are in good agreement with the in-situ measured values considering the error bands. This shows the practical applicability of the diffusion based model and the associated methodology for thoron exhalation rate prediction in actual working environment.

b) Thorium Powders

In-situ measurements of thoron exhalation rate from three different powders (thorium nitrate, thorium oxalate and thorium oxide) stored in large drums at actual thorium processing facilities was carried out. The estimation of thoron mass emanation rate J_M and the bulk density of the powder was also done on-site. However, it was not possible to measure the diffusion length of thoron for the powders. Hence a diffusion length value of 2.5 cm was assumed as a conservative estimate based on the previous measurements for powders. The comparison of the in-situ measured thoron exhalation rate with the model predicted values for the three powders is shown in Table 3.3.

Table 3.3: Comparison of in-situ measured and model predicted values of thoron exhalation rate for three thorium bearing powders

Powder Sample	**Thoron exhalation rate (Bq m^{-2} s^{-1})**		
	By actual In-situ measurement	**Estimated using model**	**% Deviation**
Thorium Nitrate	49100 ± 835	62931 ± 1045	28
Thorium Oxalate	31460 ± 627	38740 ±815	23
Thorium Oxide	33250 ± 615	43708 ±874	31

The in-situ measured and model-predicted thoron exhalation rates are quite close to each other in case of all three powders. The deviation between them is of order of 20-

30 per cent. This can be attributed to the slightly high value of 2.5 cm assumed for thoron diffusion length, as the model prediction is over-estimating exhalation rates in all three cases. However, it is recommended to use this value in theoretical predictions to have a conservative estimate of thoron source term for use in purpose of radiation protection.

3.2.3. Validation of the thoron exhalation model: Monazite sand

The model for thoron exhalation rate was also tested in case of another thorium rich porous matrix, namely monazite rich sands. The High Level Natural Background Radiation Areas (HLNBRAs) of the coasts of Kerala and Odisha states of India have high contents of monazite (a mineral of thorium) in the beach sands because of placer deposits [19], [72], [78]–[80]. Due to the very high thorium content of these sands (1000-50000 Bq kg^{-1}) these regions provide a unique opportunity to study thoron in natural environment [81], [82].

3.2.3.1. Measurement of thoron mass emanation rate for sands

The Powder sandwich technique cannot be used for measurement of thoron mass emanation rate as the thoron emanation rate will be very small for a small quantity of sand. Hence a special experimental setup was developed to measure the thoron mass emanation rate from sand. It primarily consisted of a cylindrical sample holder with dimensions of 1.5cm diameter and 15cm height. The sample holder was hold in vertical orientation and had strong filters attached at both ends to hold against weight of the sand. The sample holder was incorporated in a closed loop setup consisting of thoron monitor with an internal pump, similar to that of powder sandwich technique. The schematic diagram of the setup is shown in Figure 3.6.

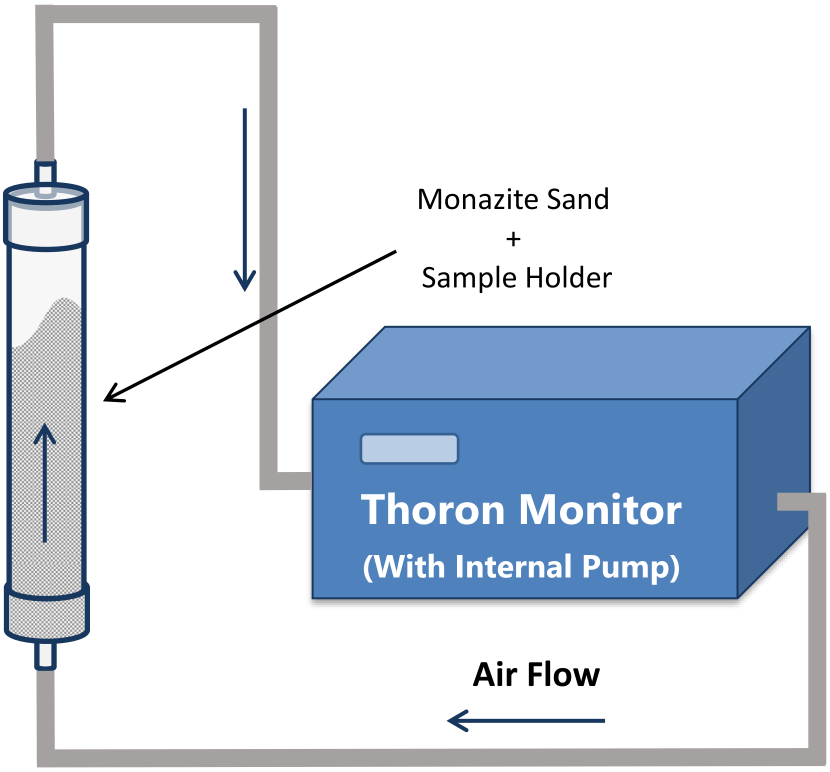

Figure 3.6: Setup or measurement of thoron mass emanation rate from sand and soil samples

After placing the sand sample in the holder, the air was circulated in the closed volume of the setup to remove all the thoron emanating from the sand. The direction of the flow in the sample holder was from bottom to top against the weight of the sand. Flow through the complete volume of the sample was ascertained so that all the emanated thoron was measured. The equilibrium thoron concentration, C_{eq} (Bq m^{-3}), was measured for different masses of samples, M (kg). The thoron mass emanation rate, J_M (Bq kg^{-1} s^{-1}) was then calculated using the equation:

$$J_M = \frac{C_{eq} V \lambda}{M} \qquad \textbf{3.12}$$

The slope for the least square linear fitting of the plot of C_{eq} versus M was used in equation 3.12 to determine the thoron mass emanation rate. The results for the measurements for the sand samples done in laboratory are presented in Table 3.4.

3.2.3.2. In-situ measurement of thoron exhalation from beaches of HNBRA

The performance of thoron exhalation model was tested by comparison with in-situ measurement of thoron exhalation rate from the surface of beach sand at 6 locations on the beaches of Chavara-Neendakara (CN) area in state of Kerala; and 4 locations on the beaches of Chhatrapur (CH) area of Odisha. The measurements were carried out using the accumulator technique described in detail in section 2.4.4. The accumulator was deployed on the beach with a 1 cm burial depth. The equilibrium thoron concentration C_{eq} was measured and used to calculate the thoron exhalation rate, J_S (Bq m^{-2} s^{-1}) using equation 3.11. The results for the measurement are shown in Table 3.4. The J_S values were then used along with the corresponding values of J_M and the bulk density ρ_b measured in laboratory, in the thoron diffusion model to determine thoron diffusion length which was the only unknown parameter. The results for the calculation are presented in Table 3.4. Since all measurements were carried out under similar conditions, the in-situ diffusion length was expected to be constant. The results obtained were in accordance with this as the diffusion length was found to be fairly constant with an average value of 2.27±0.34 cm for all measurements. Thus, this observation can be considered as satisfactory performance of thoron exhalation model in case of monazite rich sands. Hence, the model can be used for thoron source term estimation in facilities processing these sands in the front end of thorium fuel cycle.

Table 3.4: Results for measurement of thoron emission parameters for sand samples of coastal regions of Chavara- Neendakara (CN), Kerala and Chhatrapur (CH), Odisha

Sample code	In-situ thoron flux (Bq $m^{-2}s^{-1}$)	Thoron mass emanation rate ($\times10^{-2}$Bq kg^{-1} s^{-1})	Bulk density ($\times10^{3}$ kg m^{-3})	Effective diff. length, ($\times10^{-2}$m)
CN1	11.57±1.45	17.3±0.1	2.43	2.76±0.34
CN2	10.53±1.38	18.8±0.1	2.48	2.26±0.30
CN3	12.58±1.51	23.4±0.1	2.38	2.26±0.28
CN9	7.72±1.17	13.3±0.1	2.38	2.44±0.37
CN12	4.52±0.88	10.8±0.1	2.29	1.83±0.36
CN16	4.19±0.90	10.7±0.1	2.40	1.63±0.35
CH11	3.03±0.71	6.05±0.01	2.03	2.46±0.57
CH18	2.41±0.84	4.63±0.01	2.02	2.58±0.89
CH21	4.19±0.85	8.84±0.02	2.04	2.32±0.47
CH26	0.45±0.24	1.45±0.01	1.46	2.11±1.12

3.2.4. Salient properties of thoron exhalation model

The diffusion based thoron exhalation model described in section 3.2.1 is very useful for determining the thoron exhalation rate from a wide range of porous matrices handled in the thorium fuel cycle. The only input parameters required are thoron mass emanation rate, bulk density of the material and thoron diffusion length in the material. Simple measurement setups were developed for determination of thoron mass emanation rate, which could be used for in-situ measurements in the facilities. A simple lab based setup was also developed to measure thoron diffusion length. This makes it feasible to use the model in actual facilities. It can be applied to calculate net thoron emission from open surface of any matrix such as monazite sand or powders stored in containers such as drums or trays. It also makes it possible for calculating thoron source term in some other unique situations encountered in thorium processing facilities such as powders adhering to drum filters or inner walls of centrifugal driers etc. This model is especially useful for predicting the thoron source term during the designing of thorium facilities itself so as to plan for radiological protection measures.

3.3. Factors affecting thoron exhalation from porous matrices

It can be observed from the thoron exhalation model that the thoron exhalation rate J_S is linearly dependent on mass emanation rate J_M and diffusion length l. Hence any factor that has an effect on them will also affect the exhalation rate. The ^{224}Ra activity content is a primary factor which will govern the thoron emission and it has been discussed in section 1.4. Some of the other important factors that can affect the thoron exhalation rate are discussed below.

3.3.1. Emanation coefficient

The thoron emanation from a solid *grain* of a porous medium is quantified by the parameter emanation coefficient (E) defined as the fraction of all the thoron atoms produced in the grain, that is emanated out of the grain. Mathematically it can be expressed as

$$E = \frac{J_M}{R_a \lambda} \qquad \textbf{3.13}$$

Thoron atoms produced in the solid grain can be emanated to the pores by two pathways: 1. by recoil of thoron atom near grain surface and, 2. by diffusion of thoron atom through solid grain structure. When ^{224}Ra is converted to ^{220}Rn by alpha decay, the newly produced ^{220}Rn atom is imparted a recoil energy. If the decayed ^{224}Ra is situated sufficiently close to the surface of the grain and the direction of recoil of the newly formed thoron atom is favourable, then it can come out of the grain into pore space. This mode of emanation is called as *recoil emanation*.

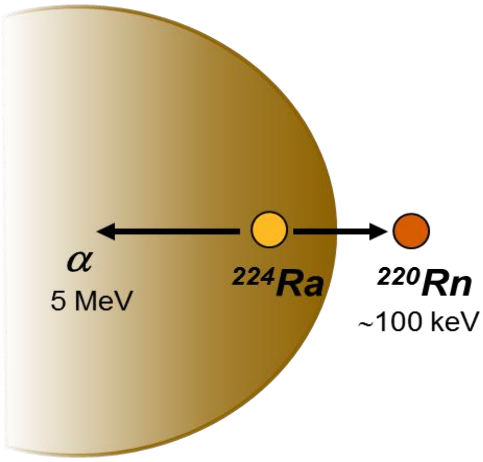

Figure 3.7 Emanation of thoron atom from a solid grain by recoil

The other case is that thoron atom formed in the grain diffuses through the solid grain to escape out, known as *diffusion emanation* and this generally occurs only at very high temperatures. Thus, the emanation co-efficient ***E*** can be considered to be consisting of two components as

$$E = E_{rec} + E_{diff} \qquad \textbf{3.14}$$

where E_{rec} is the part attributable to thoron emanation through direct recoil and E_{diff} is the part attributable to thoron emanation due to diffusion in solid grain.

At room temperature $E_{diff} \approx 0$ as thoron diffusion lengths in solid grains is of the order of just a few tens of nanometres [83] and becomes significant only at very high temperatures. In the next section the emanation due to recoil is discussed in detail to understand the factors that can influence it.

3.3.1.1. Modeling of Emanation coefficient based on Alpha recoil

The emanation co-efficient due to recoil E_{rec} can be modelled on the basis of grain geometry. If we consider the surface of a solid grain containing ^{224}Ra which decays to thoron, only those thoron atoms which move by recoil and end up in the volume above the surface will actually be emanated.

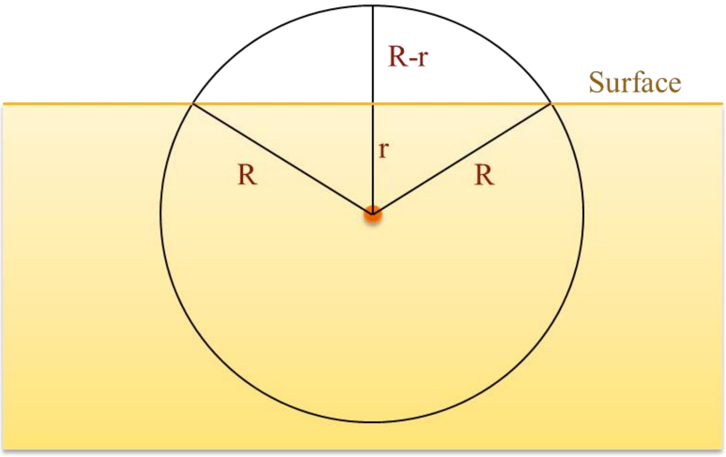

Figure 3.8 Schematic representation of emanation of thoron atom formed near the surface of a solid

Consider a ^{224}Ra atom inside the solid at a depth r from the surface of solid such that the distance r is less than the recoil range R of ^{220}Rn in the solid, as shown in Figure 3.8. The probability that the thoron atom formed by decay of the ^{224}Ra atom is emanated from the solid, ($p(r)$) is given by the ratio of surface area of the part of sphere with radius R that is above the surface of the solid to the total surface area of the sphere and can be calculated using equation [84]:

$$p(r) = \frac{2\pi R(R-r)}{4\pi R^2} = \frac{(R-r)}{2R} \qquad \textbf{3.15}$$

Since, only the thoron atoms which are formed within the depth R from surface have a chance of being emanated, we can estimate the fraction of thoron atoms formed within the depth R which will be emanated by integrating equation 3.15 over the range 0 to R as:

$$f = \frac{\int_0^R \frac{(R-r)}{2R} dr}{R} = \frac{1}{4} \quad \textbf{3.16}$$

Thus, if we have a grain with surface area *S* and volume *V*, with uniform distribution of ^{224}Ra, we can write expression for E_{rec} as:

$$E_{rec} = \frac{1}{4} \frac{RS}{V} \quad \textbf{3.17}$$

where *R* (m) is the recoil range of radon/thoron in the solid grain, *S* (m^2) is surface area of the grain and *V* (m^3) is the volume of the grain. This expression is applicable in cases where the size of the grain is considerably large as compared to recoil range *R*.

It can be seen from equation 3.15 that emanation coefficient for any material is dependent on R and *S/V* ratio. The *S/V* ratio in itself is dependent on the geometry, i.e. size and shape of the grain.

As the S/V ratio for normal geometries decreases with the increasing size, the emanation coefficient too decreases with the increasing size of the grains. This makes emanation a function of the geometry of the grain and to understand the exact nature of this dependence, geometry based models of emanation are required.

Flugge and Zimens [84] have obtained the theoretical expression for emanation coefficient based on recoil for small spherical grains as:

$$E_{Sph}^{r} = \frac{3R}{2d} - \frac{R^3}{2d^3} \qquad (d > R) \quad \textbf{3.18}$$

where *d* (m) is the diameter of spherical grains.

Sasaki et al., 2007[85] obtained a model for a cubic particle as:

$$E_{Cub}^{r} = \frac{3R}{2a} - \frac{3R^2}{a^2} + \frac{2R^3}{a^3} \qquad \textbf{3.19}$$

where *a* (m) is the length of the edge of cube.

For grains considerably larger than *R*, both the models predict same emanation coefficient for same grain size i.e. *d*=*a*. Since the natural materials are rarely found to have the shapes of perfect cube or sphere, emanation models corresponding to a few more shapes were derived in the present work. The basic procedure used was to estimate the volume of grain corresponding to a thickness equal of *R* just below the surface for different shapes and use the probability for recoil emanation obtained from equation 3.16. The emanation coefficients so obtained in this work are presented below.

1. For cylinder:

$$E_{Cyl}^{r} = \frac{R}{d} + \frac{R}{2h} - \frac{R^2}{d^2} - \frac{2R^2}{dh} + \frac{2R^3}{d^2h} \qquad \textbf{3.20}$$

where d (m) is the diameter of the cylinder and h (m) is the height of cylinder

2. For a Parallelepiped:

$$E_{Parld}^{r} = \frac{R}{2a} + \frac{R}{2b} + \frac{R}{2c} - \frac{R^2}{ab} - \frac{R^2}{ac} - \frac{R^2}{bc} + \frac{2R^3}{abc} \qquad \textbf{3.21}$$

where *a*, *b* and *c* are dimensions of three sides of parallelepiped. The expression obviously extends to a rectangular block. For the case of two sides to be equal (i.e. *a* = *b*), the expression simplifies as

$$E_{Parld}^{r} = \frac{R}{a} + \frac{R}{2c} - \frac{R^2}{a^2} - \frac{2R^2}{ac} + \frac{2R^3}{a^2c} \qquad \textbf{3.22}$$

3. For regular octahedron:

$$\frac{a^3-(a-2R)^3}{4a^3} \qquad \textbf{3.23}$$

The calculation of emanation coefficient by the models for different geometries was done for grain size range comparable to that of sand. The characteristic size selected for a particular geometry was the dimension which will allow the grain to pass through sieve hole with size greater than that dimension.

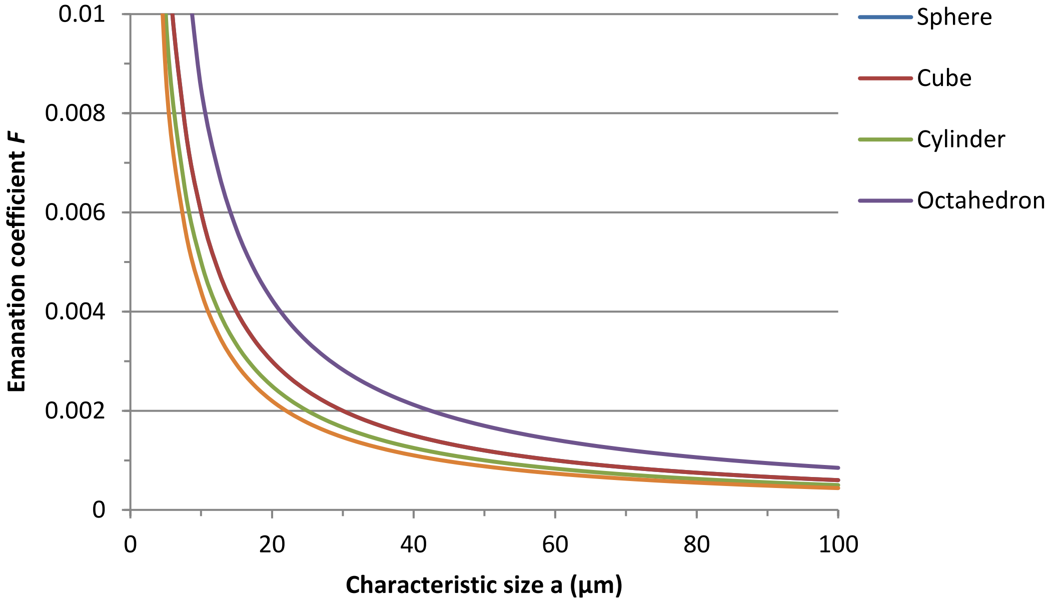

Figure 3.9: Plot of emanation coefficient predicted by models for various geometries as a function of characteristic size *a* and recoil length value of 0.04 µm

The results are presented in graphical form in Figure 3.9. The dimensions assumed in case of parallelepiped was $b=a$ *and* $c=8a$, in case of cylinder it was $h=a$ and $r=0.5a$, whereas for the shape of cylindrical rod, it was $h=5a$ and $r= 0.5a$.

It should be noted that the models derived above will be applicable for grain sizes greater than about ten times the recoil length of thoron in the grains. For grains of sizes smaller than these, the volumetric fraction of the *edges* of the grain, where the emanation probability is greater than that given by equation 3.16, will become significant and the actual emanation will be higher than that predicted by model.

3.3.1.2. Application of Emanation model to monazite bearing sand

As inferred from the theoretical modeling of thoron emanation coefficient, the variation of the emanation coefficient for a porous medium will depend on the grain size and shape. Hence in order to test this by actual measurements, the experimental determination of emanation coefficient for different sizes of a monazite rich sand sample was carried out.

3.3.1.2.1. Emanation coefficient for different sizes of the sand

To study the effect of size of sand grain on thoron emanation, the sand samples were sieved into different size ranges (75-105, 105-150, 150-212, 212-250 and 250-500 µm) using scientific sieves and standard protocol. The specific thoron mass emanation rate was determined for each of the fraction using procedure described in section 3.2.3.1. The specific ^{224}Ra content was determined using gamma spectrometry as described in detail in section 2.4.5. The two measured quantities were then used as input parameter in equation 3.13 to determine the thoron emanation coefficient. The results for these measurements are presented in Table 3.5. Both the thoron mass emanation rate and thoron emanation coefficient, were found to decrease considerably with increase in size of the grain. The plot of the measured emanation co-efficient against median grain size is shown in Figure 3.10. The emanation coefficient prediction of models for different shapes is also shown along with in the figure. The value of recoil range for the sand was obtained as 45 nm using the SRIM code [86].

Table 3.5: Results of measurement of thoron emanation parameters for the different sizes of the monazite rich sand

Sr. No.	Size Range (μm)	Mean grain size (μm)	Mass Exhalation Rate (Bq g^{-1} s^{-1})	^{224}Ra content (Bq g^{-1})	Emanation co-efficient
1	250-300	280	6.49×10^{-05}	22.6	2.30×10^{-04}
2	212-250	230	9.74×10^{-05}	34.1	2.29×10^{-04}
3	150-212	180	1.07×10^{-04}	25.4	3.36×10^{-04}
4	105-150	127.5	1.74×10^{-04}	27.9	4.99×10^{-04}
5	75-105	90	4.97×10^{-04}	47.9	8.29×10^{-04}

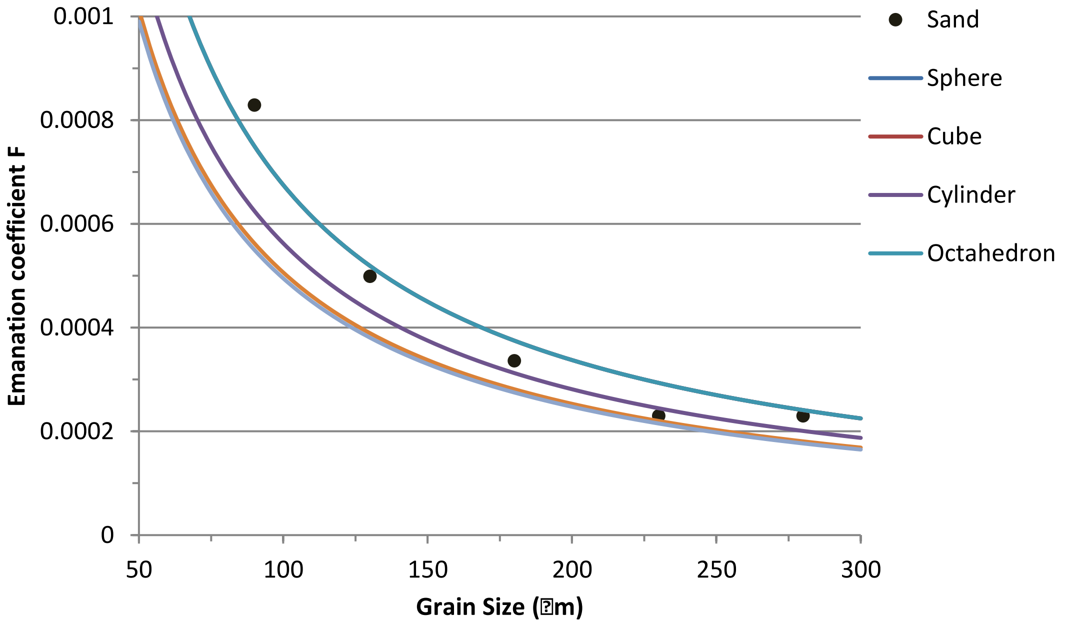

Figure 3.10: Plot of measured emanation coefficient against the mean size of sand and comparison with models for different shapes

It can be seen from the figure that the variation in the measured emanation coefficient with the size shows behaviour closer to that predicted by a model for an octahedron and by model for a cylinder. The image of sand grains obtained using a high resolution imager is shown in Figure 3.11. The grains of the sand seem to really have shapes which are closer to these two shapes. The measured data does not however match exactly with any of the two models.

This can be attributed to the fact that we consider the median diameter to be representative of whole size range. However, the sand sample in any size group will contain particles of varying sizes whose distribution is not known exactly. However, the comparison shows that the models developed in this work have high utility value.

Figure 3.11: Image of sand grains (25×) for monazite sand sample used in the emanation study

3.3.1.3. Study of thoron emanation from Powders

Most studies of radon and thoron emanation were performed on materials from natural earth. The literature of emanation from industrial powders, especially for thoron is very scarce. Emanation coefficient from powders has been mainly studied in context of specific applications such as determination of surface area and Emanation thermal analysis [87], [88].

Powders in almost all industrial processes related to thorium fuel cycle are primarily produced by precipitation. The characteristic of precipitation is formation of a *nucleus* in supersaturated solution, its growth to a certain sized *granulates* and then aggregation or coagulation of these *granulates* to form *particles* of powder [89]. This nature can be seen from the scanning electron microscopy images for two powders related to thorium fuel cycle shown in Figures Figure 3.12 and Figure 3.13.

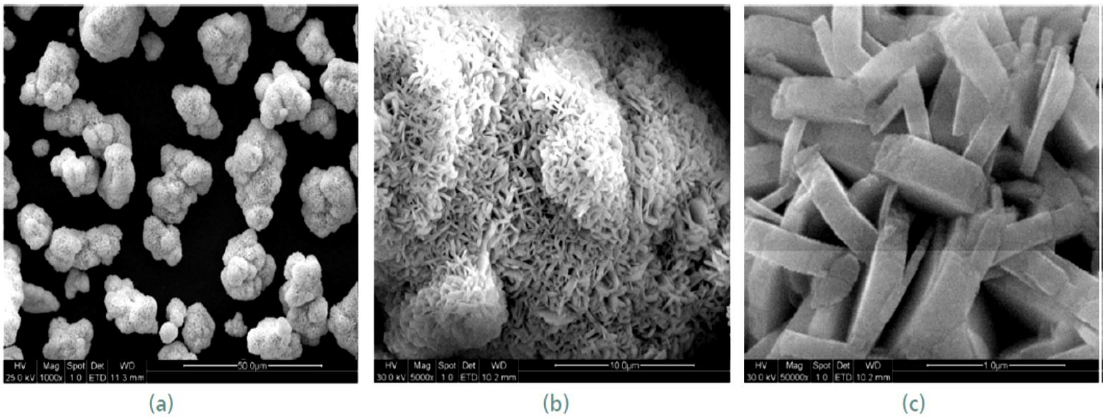

(a) (b) (c)

Figure 3.12: SEM images of ADU at different magnifications. (a) 500×, (b) 5000×, (c) 50,000× [90]

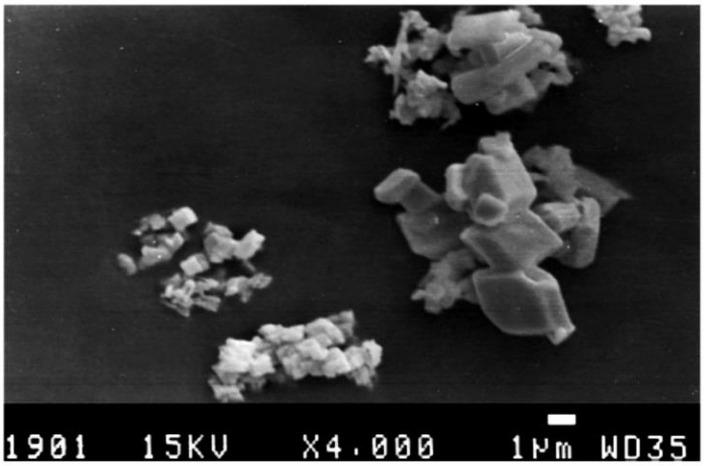

Figure 3.13: SEM micrograph of the thorium oxalate 4000× [91]

These images clearly indicate that the characteristic size of the particle changes according to the scale or level of measurements. This makes it difficult apply geometry based emanation models to powders. In an attempt to have some parameter which can be useful in predicting the thoron emanation coefficient, the basic emanation equation (3.13) is modified by introducing concept of specific surface area S_m, as:

$$E_{rec} = \frac{R}{4}\rho_b \frac{S}{M} = \frac{R}{4}\rho_b S_m \qquad \textbf{3.24}$$

where S (m^2) is the surface area of the powder, M (kg) is the mass of the powder and S_m (=S/M) (m^2 kg^{-1}) is the specific surface area i.e. surface area per unit mass of the powder. The specific surface area is an accurately measurable parameter for powders and hence a better option to correlate with emanation of powders.

Table 3.6: Thoron emanation coefficient and specific surface area values for powder samples

Sample code	**Estimated emanation coefficient, *E***	**Specific Surface Area S_M (m^2/g)**
ADU	0.079	14.73
Thorium Oxide 1	0.014	7.38
Thorium Oxide 2	0.074	11.09
Thorium Oxide 3	0.031	9.08
Thorium Oxalate	0.047	3.45

To check the feasibility of this approach emanation coefficient for five samples of powders handled in thorium fuel cycle was determined. The value of J_M was measured using the powder sandwich technique described in section 2.4.3 and the ^{224}Ra content R_a was determined by gamma spectrometry using procedure described in section 2.4.5.

The emanation coefficient was then determined using these values in equation 3.13. The specific surface area for the powder samples was determined using BET method. The results for the same are presented in Table 3.6.

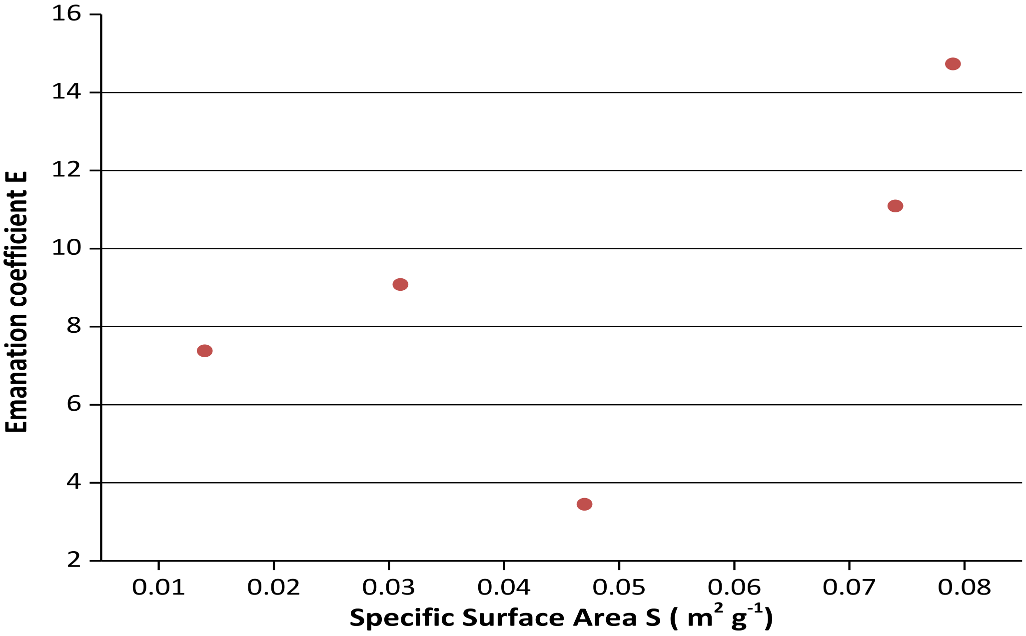

Figure 3.14: Plot of emanation coefficient against specific surface area for all studied powders

According to equation 3.24 the emanation coefficient for powders should be directly proportional to the BET specific surface area. But as can be seen from Figure 3.14 this is not observed when considering all samples together. When only thorium oxide powder is considered, this proportionality is present (Figure 3.15). But when a straight line fitting using least square method was done the value of slope was obtained as 0.0164. This compares well with the values of 0.0192 and 0.0088 reported by Balek, 1982 [24] and 0.006 reported by Zhabrova and Shibanova, 1967 [92]. However, substitution of the value of S_M and ρ_b in equation 3.24 suggest the value of emanation coefficient of about ten times higher than the measured value.

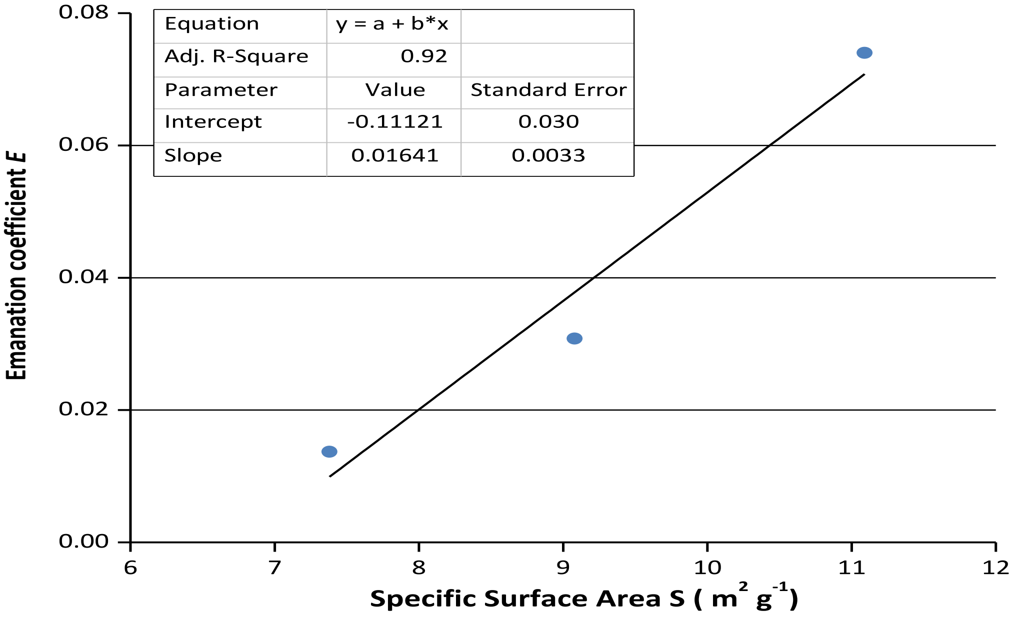

Equation	y = a + b*x	
Adj. R-Square	0.92	
Parameter	Value	Standard Error
Intercept	-0.11121	0.030
Slope	0.01641	0.0033

Figure 3.15: Plot of emanation coefficient against specific surface area for thorium oxide

This can be explained by the ‘agglomerate of granulates’ structure for powders as seen in figures Figure 3.12 and Figure 3.13. Since the thoron emanating granulates are closely spaced, a large fraction of the thoron atoms coming out by recoil from a granulate will easily cross the inter-granulate gap and get embedded into neighbouring grain. The theoretical estimation of emanation from such a system of aggregates of small particles is a very complex problem. Though some work has been done on this problem, the system of emitting particles considered are much simplified and well-ordered as compared to those for powders [93], [94]. Thus, it can be concluded that there is no theoretical model available which can predict thoron emanation coefficient for powders. However, empirical correlation can be established between the emanation coefficient and the specific surface area for the powders through actual measurements.

3.3.2. Moisture Content

The effect of moisture content on thoron exhalation from various earthen materials has been well documented [64], [95]–[97]. But a study of effect of moisture content on thoron exhalation from different chemical powders, especially those related to nuclear fuel cycle is still lacking. Hence an experiment was carried out to study the effect of moisture content on thoron exhalation from two powders. The presence of moisture in a porous matrix affects both emanation and diffusion of thoron. The effect of moisture on overall exhalation of thoron is a combination of its effect on these two individual parameters.

First the effect of moisture content on the overall thoron exhalation rate was measured for two powder samples: ammonium di-uranate (ADU) and thorium oxide. The powder to be studied was initially dried by heating in an oven at temperature of 150° C for three hours. The bulk density for the powder was measured according to standard procedure. The porosity η of the powder to be studied was determined using equation 3.25 [98].

$$\eta = 1 - \frac{\rho_b}{\rho_g} \tag{3.25}$$

where ρ_g is the grain density of the powder. The grain density for the powder was measured by using specific gravity values measured for completely dry powder and for pore volume completely filled with water.

In order to measure the thoron surface exhalation rate J_S, the powder sample to be studied was taken in an accumulation chamber with diameter of 6 cm and height of 20 cm. The powder was filled in the accumulator up to a height of 15 cm. The accumulator was connected with RnDuo thoron monitor in a closed loop arrangement. The exhalation rate J_S was determined by measuring the equilibrium thoron concentration and using equation 3.11. The measurement was started with completely dried powder. A measured amount of water was then added to the powder and the powder was mixed by shaking and left sealed overnight to achieve a uniform distribution of moisture throughout the powder. The weight of the powder was measured to check for any loss of water due evaporation. The pore moisture fraction m was then obtained from the water fraction by dry weight basis, θ_d as:

$$\mathrm{m} = \frac{\rho_b \theta_d}{\rho_w \eta} \qquad \mathbf{3.26}$$

where, ρ_{w} is the density of water.

The thoron exhalation rate was measured for both ADU and thorium oxide powder for m varying from 0 to 1. The results for the measurement are shown in Figure 3.16 for ADU powder and Figure 3.17 for thorium oxide powder. It can be seen that the general trend for variation of thoron exhalation rate with pore moisture fraction is similar for both powders. It rises initially, reaches a maximum and then decreases steadily reaching to very low levels for complete moisture saturation. In case of ADU, the maximum value of J_S was reached for a moisture saturation value of 0.3. The maximum J_S value was greater than the J_S value for completely dry powder by 35 per cent. On the other hand, the maximum J_S value for thorium oxide was observed corresponding to m value of 0.42 and it was greater than the J_S value for dry powder by 270 per cent. Thus, it can be seen that the extent to which J_S for powder is affected by m is different for different powders.

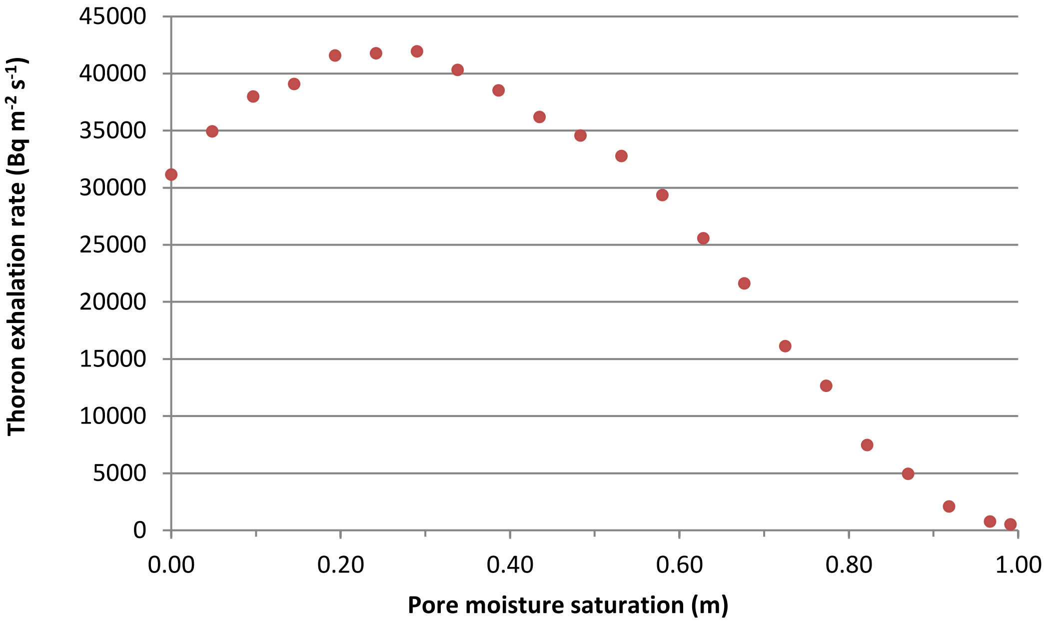

Figure 3.16: Plot for variation of thoron exhalation rate against pore moisture saturation for ADU

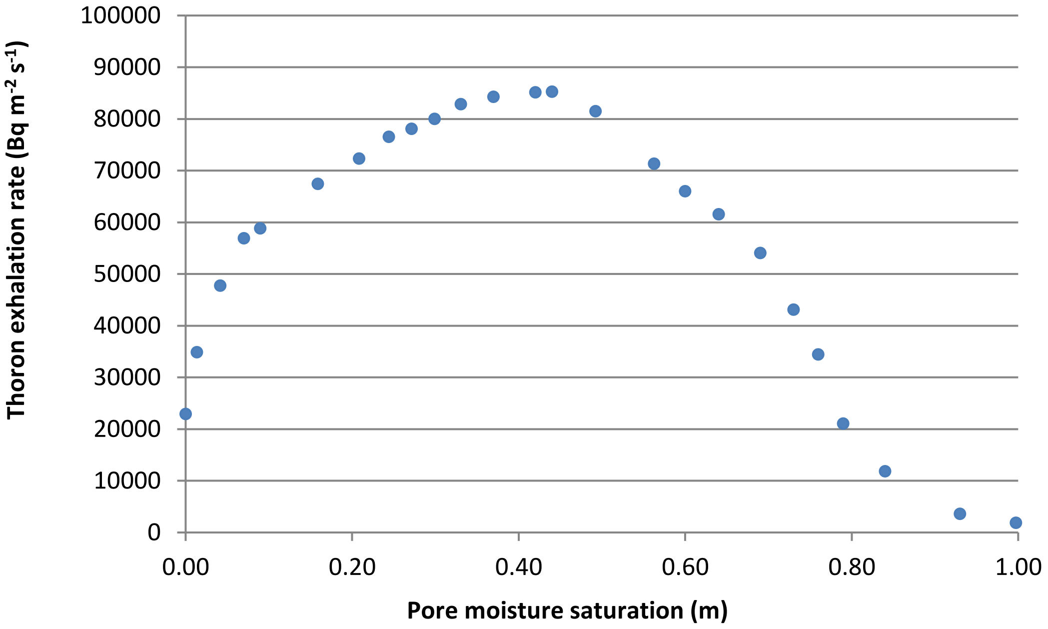

Figure 3.17: Plot for variation of thoron exhalation rate against pore moisture saturation for thorium oxide

To study how the moisture content affected J_M and thoron diffusion length l individually, the dependence of J_M on m was determined separately. For this a small quantity of powder was taken in a small plate and spread into a thin layer to avoid matrix absorption of thoron. The plate was then kept in a sealed accumulator of dimension diameter 6 cm and height 9 cm. The accumulator was connected with RnDuo thoron monitor in a closed loop setup to measure the C_{eq} value. The J_M value was then determined using equation 3.12. The results for the experiment are plotted in Figure 3.18 for ADU and Figure 3.19 for thorium oxide. It can be seen that the J_M for both powders increases initially with rise in m before getting saturated. The nature of rise is same as the rise in J_S for both the powders. Thus, it can be concluded that the initial rise in J_S with m is due to increase in J_M. This observation is similar to that for the cases of soils and other earthen materials.

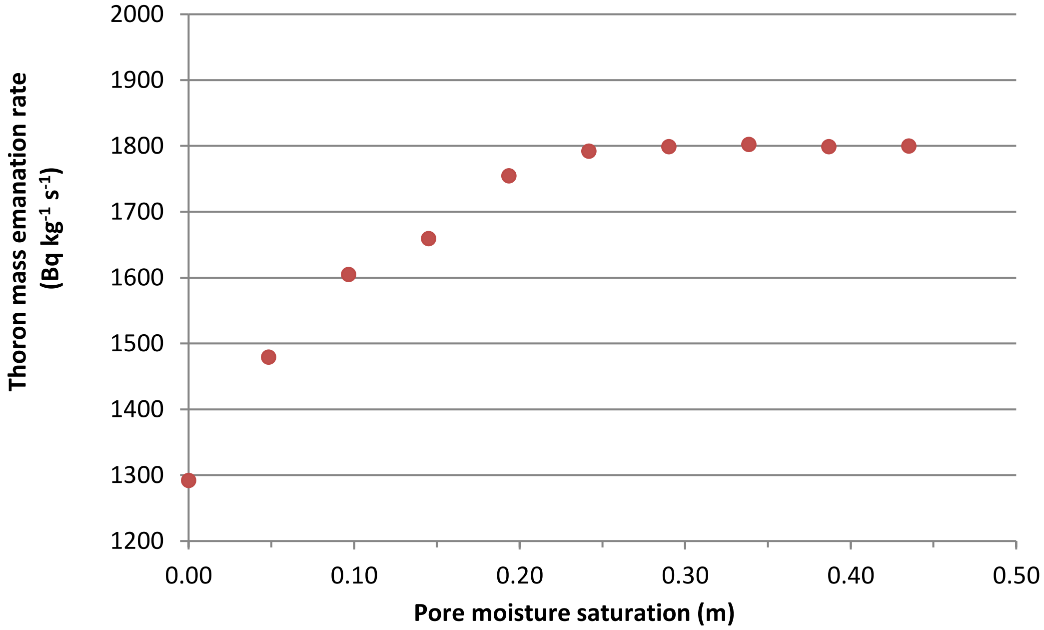

Figure 3.18: Plot for variation of thoron mass emanation rate against pore moisture saturation for ADU

This increase in emanation occurs because for initial increase in pore water content, it forms a film on surface of grains and reduces the distance travelled by recoiled thoron atoms emanating from the grain and stops them from getting embedded into neighbouring grain, keeping them in pore volume.

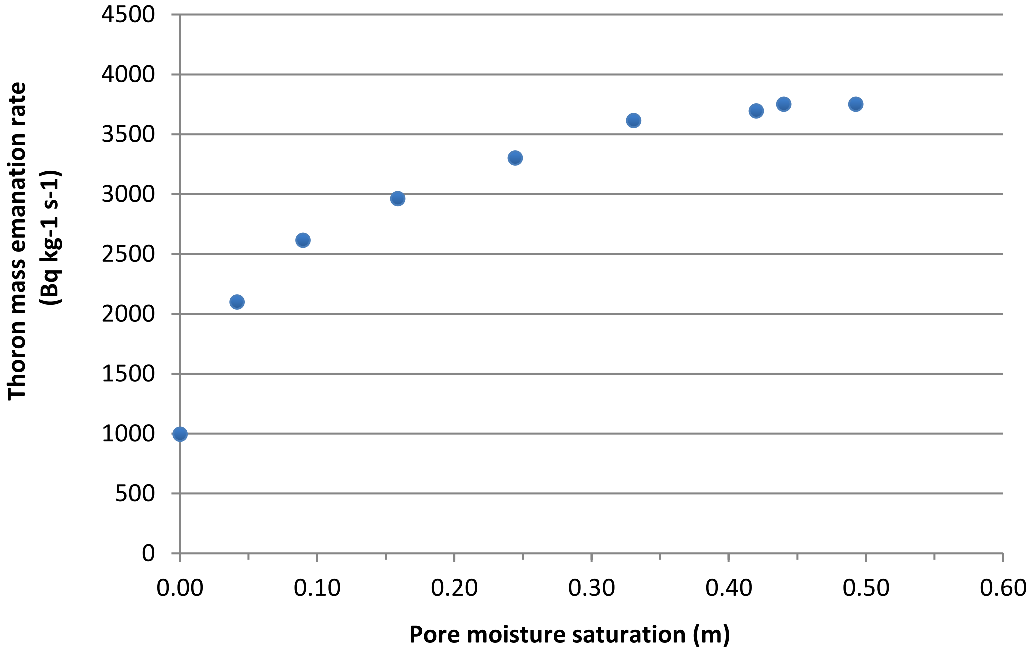

Figure 3.19: Plot for variation of thoron mass emanation rate against pore moisture saturation for thorium oxide

Once the variation of J_M over the complete range of moisture content was obtained it was used in the thoron diffusion model (equation 3.9) along with the J_S value to calculate l corresponding to the different values of m. The value of l was then used to calculate effective thoron diffusion coefficient D_{eff} (m^2 s^{-1}) using equation:

$$D_{eff} = l^2 \lambda \qquad \textbf{3.27}$$

The variation of effective diffusion coefficient with pore moisture content is shown in Figure 3.21 and Figure 3.20 for ADU powder. A few models are available in literature for dependence of D_{eff} on m.

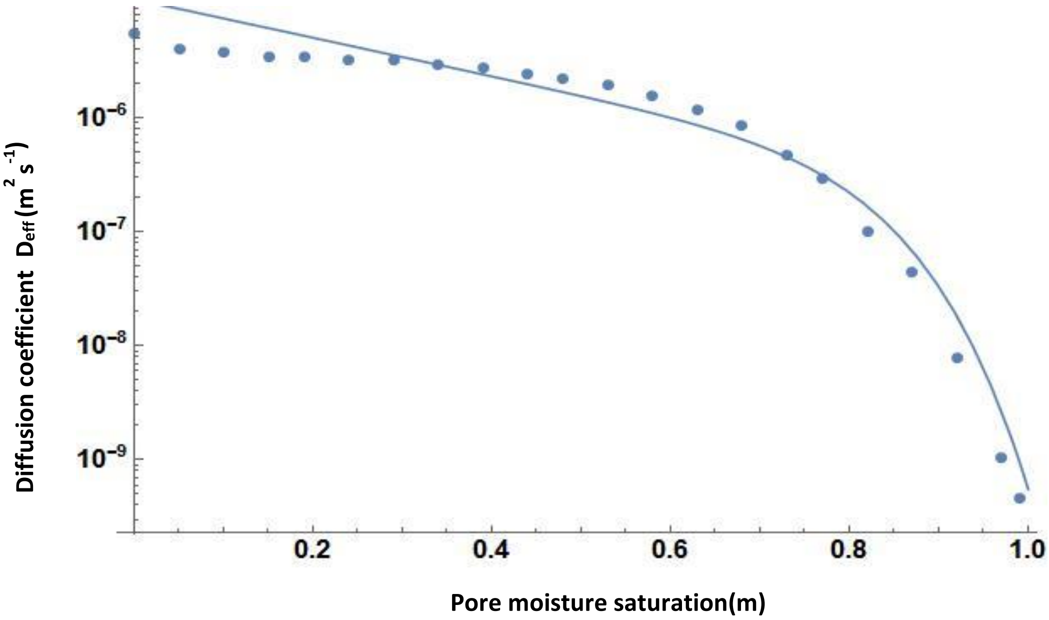

Figure 3.20: Plot of effective diffusion coefficient for thoron (on logarithmic scale) against pore moisture saturation for ADU powder with fitted value for Rogers Neilson Model

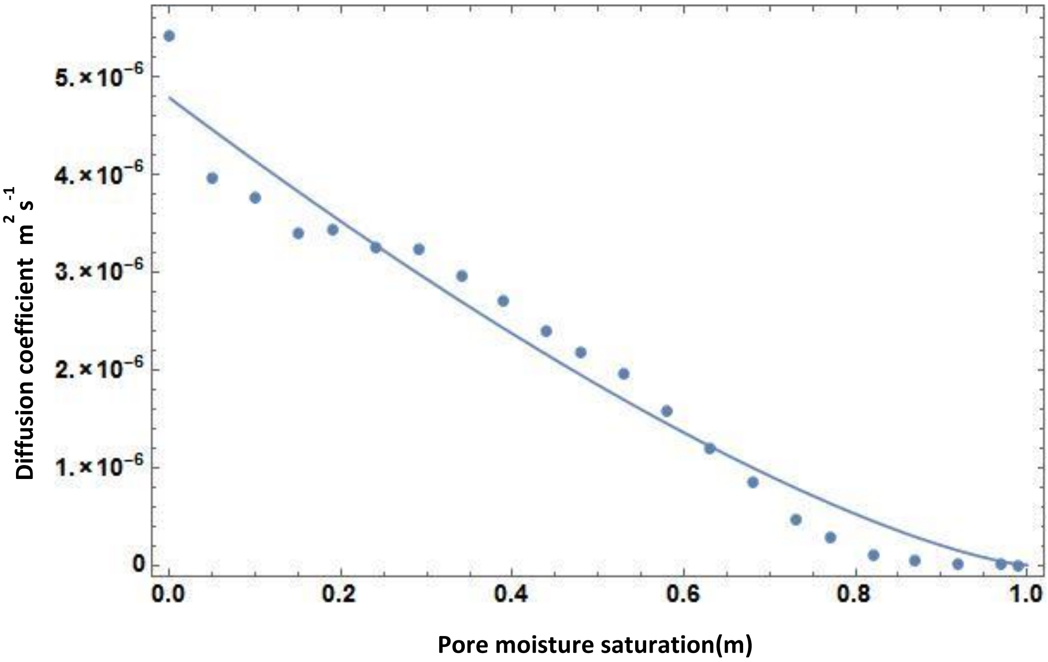

Figure 3.21: Plot of effective diffusion coefficient for thoron (on linear scale) against pore moisture saturation for ADU powder with fitted value for Adler Perrier model

The most commonly used model for soils is that proposed by Rogers and Neilson [99]. The fit of the model to the data for ADU is shown in Figure 3.20. It can be seen that the model matches well with the measurement for *m* values above 0.4 but shows a large deviation from measured values at m values lower than 0.3. A fit of model by Adler and Perrier [100] to the data is shown in Figure 3.21. It can be seen that the model matched well for m values up to 0.6 but could not predict the sharp decrease in D_{eff} after that.

Similar observations were made in case of thorium oxide powder, for which the data is shown along with the fit of Rogers and Neilson model Figure 3.22 in and with the fit of Adler and Perrier model in Figure 3.23.

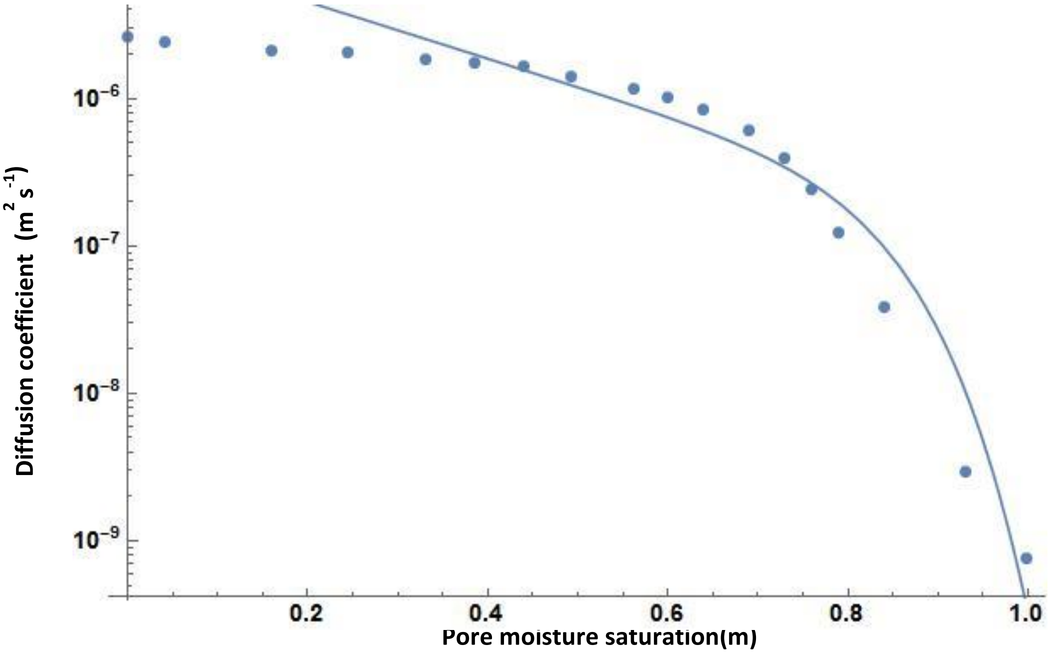

Figure 3.22: Plot of effective diffusion coefficient for thoron (on logarithmic scale) against pore moisture saturation for thorium oxide powder with fitted value for Rogers Neilson Model

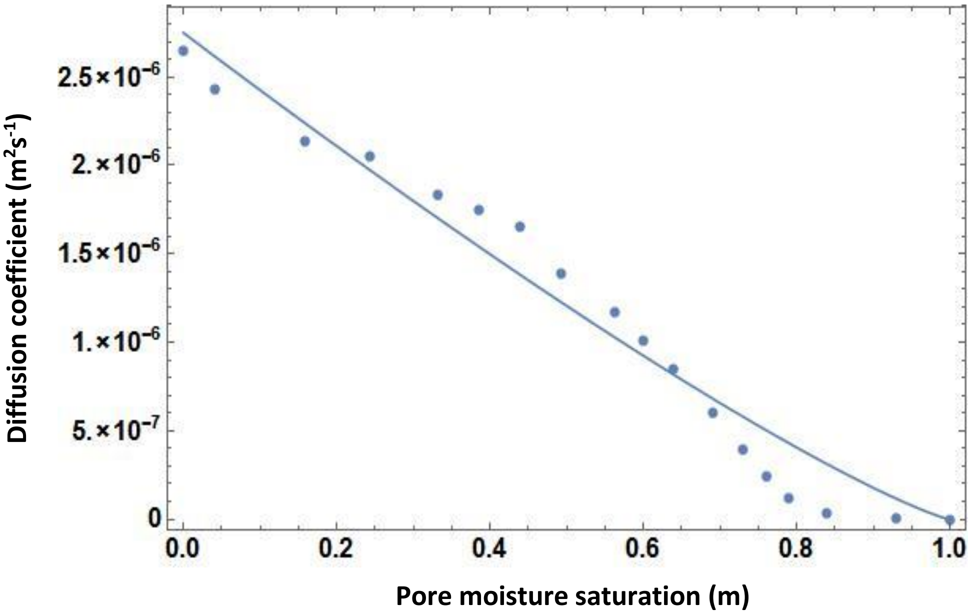

Figure 3.23: Plot of effective diffusion coefficient for thoron (on linear scale)against pore moisture saturation for thorium oxide powder with fitted value for Adler Perrier model

Hence, we can conclude that the variation in D_{eff} and hence in l is best explained by Adler and Perrier model for m values up to 0.6 whereas the decrease in D_{eff} for m values above 0.6 is better predicted by Rogers and Neilson model.

3.3.3. Heating

The thoron emission rate dependence on temperature is well known. Increase in temperature is known to affect both emanation coefficient as well as the diffusion length.

3.3.3.1. Effect of heating on emanation

As described in section 3.3.1, the emanation of thoron at room temperatures of 20-40 °C is almost completely due to recoil. The emanation due to diffusion of thoron atom through solids is very low due to small diffusion length attributable to short half-life of thoron. However, when the source matrix is subjected to heating to very high temperatures of above 700-800 °C the diffusion of thoron in solids also becomes significant. The dependence of emanation coefficient due to solid diffusion E_{diff} is given by equation [24]:

$$E_{diff}\left(T\right)=\frac{3}{y}(\coth y-\frac{1}{y}) \qquad \textbf{3.28}$$

where T (°K) is temperature and y is a function given as

$y=R\sqrt{\frac{\lambda}{D_s\left(T\right)}}$, where $D_S(T)$ is the diffusion coefficient of thoron in the solid at temperature T given as: $D_s\left(T\right)=D_{S0}\exp\left(\frac{-Q_{DS}}{RT}\right)$ in which D_{S0} is the thoron diffusion coefficient at reference temperature, Q_{DS} is the energy of activation for diffusion of thoron in solid, which are specific to the source matrix.

The plot for the variation of E_{diff} calculated using equation 3.28 for thorium dioxide powder is shown in Figure 3.24.

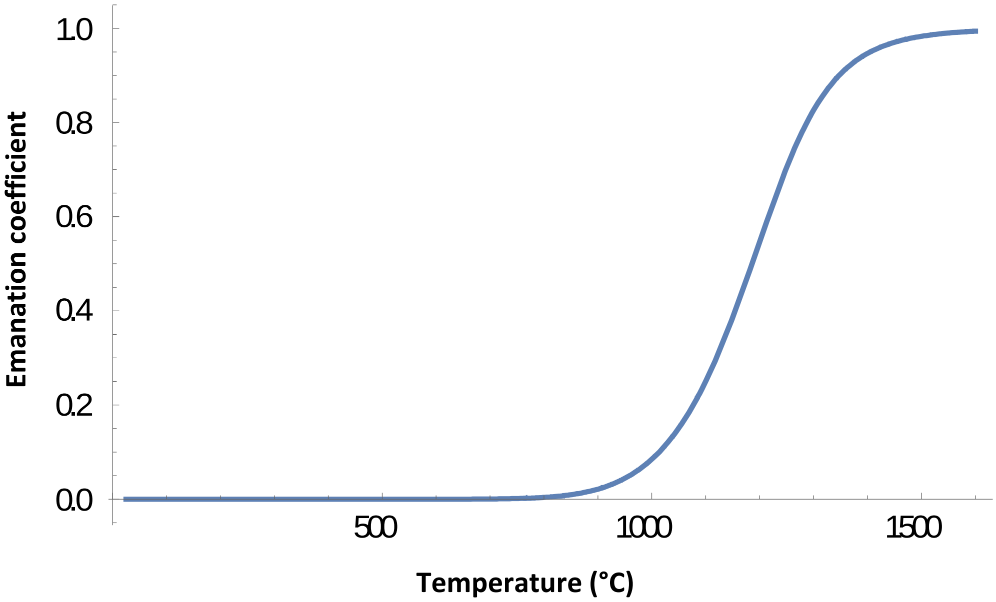

Figure 3.24: Plot of emanation coefficient due to solid diffusion as a function of temperature for thorium dioxide powder

It can be seen that the emanation coefficient due to diffusion increases significantly beyond temperature of 800 °C. Hence the emanation of thoron during processes such as calcination and sintering can be expected to be very high. The direct effect of temperature on recoil process of thoron is negligible considering the fact that the recoil energy of thoron is of order of 100 keV, whereas heating can only increase the energy of atoms in order of few eV. However, heating of powders can increase the overall thoron emanation due to recoil by the way of increase in the specific surface area. As discussed in section 3.3.1.3 the emanation coefficient is dependency on specific surface area S_M can be expressed as:

$$E_{rec}\left(T\right)=kS_M \qquad \textbf{3.29}$$

where k is a temperature independent constant specific to a particular powder.

The heating of different powders handled in nuclear fuel cycle to very high temperatures in processes such as calcination and sintering results in changes in specific surface area of the powder. Hence to be able to predict the effect of heating on thoron emanation from powders, the effect of heat on both emanation processes needs to be considered together. Due to the difference in physic-chemical processes occurring at high temperatures, the overall effect of heat on thoron emanation will be different for different powders.

3.3.3.2. Effect of heating on thoron diffusion

As discussed in earlier sections, after its emanation from grains, the thoron transport in and its exhalation from a porous matrix take place by diffusion. The dependence of diffusion coefficient for thoron on temperature can be determined using kinetic theory of gases and is expressed as:

$$D_a(T) = D_{a0}\left(\frac{T}{273}\right)^{\frac{3}{2}} \tag{3.30}$$

where D_{a0} is the thoron diffusion coefficient in air at reference temperature (273 K).

The diffusion length of thoron is given by equation:

$$l = \sqrt{\frac{D_a(T)}{\lambda}} \tag{3.31}$$

Combining equations 3.30 and 3.31 we can write

$$l(T) = l_0\left(\frac{T}{273}\right)^{\frac{3}{4}} \tag{3.32}$$

As the overall exhalation rate J_S is a linear function of l, the above relationship can be integrated in the diffusion model for including dependence of diffusion on temperature.

3.4. Thoron emission from liquids by bubbling

Thorium in form of liquid solution is required to be handled in different processes of thorium fuel cycle. Since the diffusion length of thoron in liquid is very short, only a fraction of thoron from a thin layer of liquid in surface is actually emitted. But sometimes the thorium solutions are subjected to air or gas sparging for purposes like precipitation, increasing reaction rates etc. Sparging is an operation in which air or a gas is bubbled continuously through the liquid solution. In case of sparging the thoron gas from liquid in contact with air bubble diffuses into the bubble and then comes out to the environment along with it. This leads to a significantly high amount of thoron emission.

Study of thoron or radon transfer from radium bearing liquid along with bubbled air has not been done previously. Experimental study of thoron gas transfer during bubbling is required to select and validate available models. The models describing transfer of dissolved gas during bubbling for normal gases cannot be applied directly to thoron because of its short lived nature. Hence a model was previously developed for transfer of dissolved thoron to a single bubble [101]. The same is described in brief below.

3.4.1. Model for liquid to bubble thoron gas transfer

Thoron is transferred from liquid to air inside the bubble by diffusion. Thoron gas steadily formed from the decay of ^{224}Ra in solution undergoes radioactive decay and diffuses into the bubble. An expression for the ratio of the concentration in the bubble to that in the liquid (transfer factor) at a given time can be written using the following assumptions:

i. Mass transfer into the bubble is governed by molecular diffusion and radioactive decay.
ii. The rise velocity of the bubble has negligible effect on mass transfer as compared to diffusion. The assumption is reasonable in view of the fact that thoron would diffuse only from a thin layer around the bubble that would be moving along with it.
iii. The concentration of thoron is uniform inside the bubble, since the diffusion rate inside the bubble will be much higher as compared to that in liquid.

The expression for transfer factor η is obtained by assuming a bubble released at time t=0 at the bottom of the vessel rising upwards. As the bubble rises, the concentration field of the thoron gas around it would be modified due to air-water gas exchange mechanism. With this, the transport equation describing the evolution of thoron concentration outside the bubble of diameter *a*, in liquid is given, in spherically symmetric co-ordinates, by

$$\frac{\partial C_1(r,t)}{\partial t} = D\frac{1}{r^2}\frac{\partial}{\partial r}\left[r^2\frac{\partial C_1(r,t)}{\partial r}\right] - \lambda\left[C_1(r,t) - C_L\right] \qquad a < r < \infty$$

where $C_1(r,t)$ (Bq m^{-3}) is the near field concentration in liquid, C_L (Bq m^{-3}) is constant far field concentration of thoron in liquid (sustained by constant production rate), D (m^2 s^{-1}) is the diffusion coefficient of thoron in water and λ (s^{-1}) is the radioactive decay constant.

Simultaneously the concentration inside the bubble will begin to rise due to an exchange flux from the liquid phase. Assuming a rapid mixing inside the bubble, we can treat it a spatially uniform and denote it by $C_2(t)$. This satisfies the equation

$$\frac{\partial C_2(t)}{\partial t} = \frac{3}{a}D\left.\frac{\partial C_1(r,t)}{\partial r}\right|_{r=a} - \lambda C_2(t) \qquad 0 < r < a$$

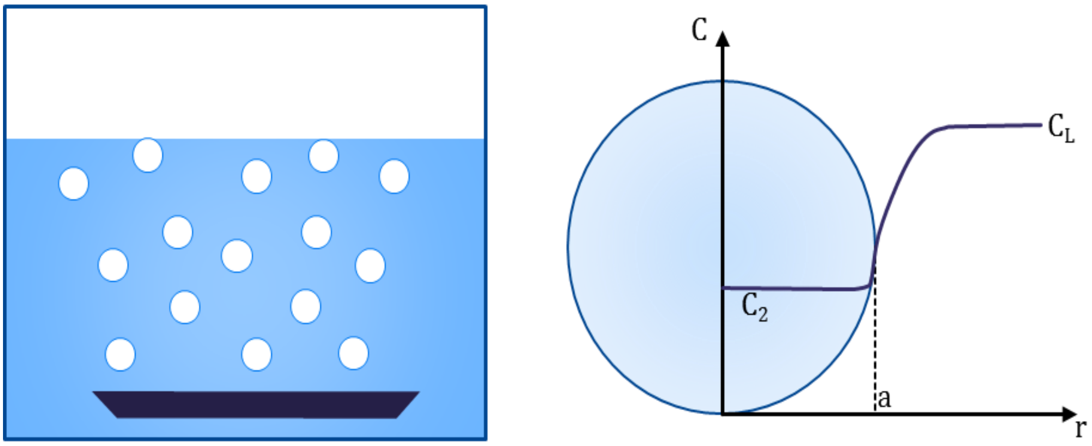

Figure 3.25: Schematic diagram for thoron concentration profile in liquid and bubble

On solving the two coupled equations with suitable boundary conditions, the expression for thoron transfer factor is obtained as:

$$\eta(t)=\frac{1}{k_T+a^2/\{3l_D(a+l_D)\}}-\frac{3}{\pi}e^{-\lambda t}\int_0^{\infty}\frac{(1+x)\,x^{3/2}e^{-x(Dt/a^2)}}{x^3+\{3K_T(1+x)-x\}^2\{x+\lambda a^2/D\}}\,dx \qquad \textbf{3.33}$$

Where $l_D = (D/\lambda)^{1/2}$ is the diffusion length of thoron in water and K_T is the partition coefficient of thoron between air and the liquid.

The model predicted thoron transfer is found to be dependent on the rise time of the bubble i.e. time spent by bubble between the instant of release and surfacing on the liquid, and the size of the bubble. The plot for prediction of thoron transfer factor in case of an aqueous solution of thoron is shown as a function of rise time in Figure 3.26 and as a function of bubble diameter in Figure 3.27.

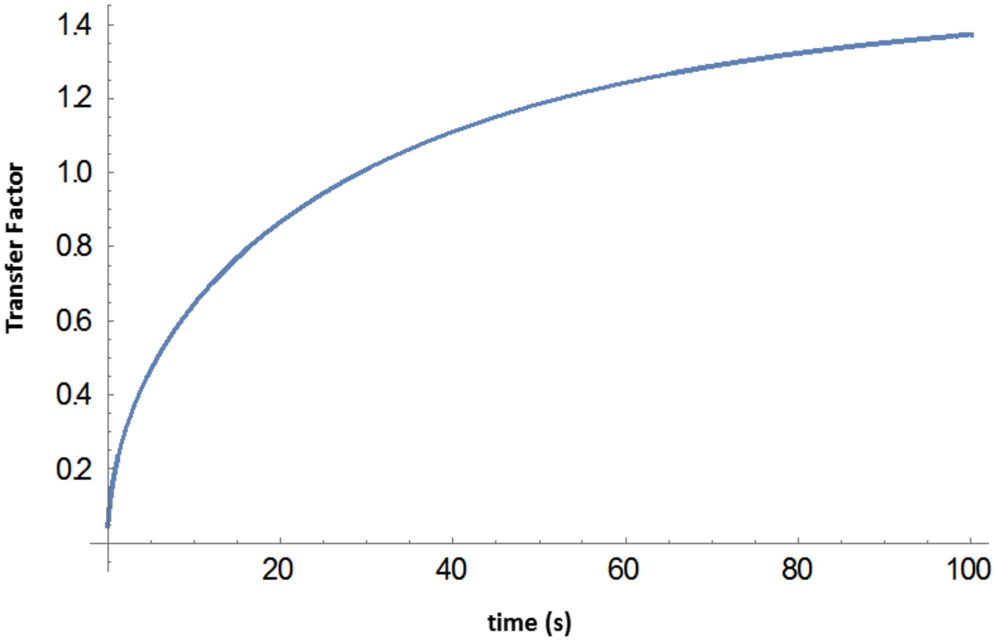

Figure 3.26: Plot of thoron transfer factor against rise time for bubbling of air in aqueous solution

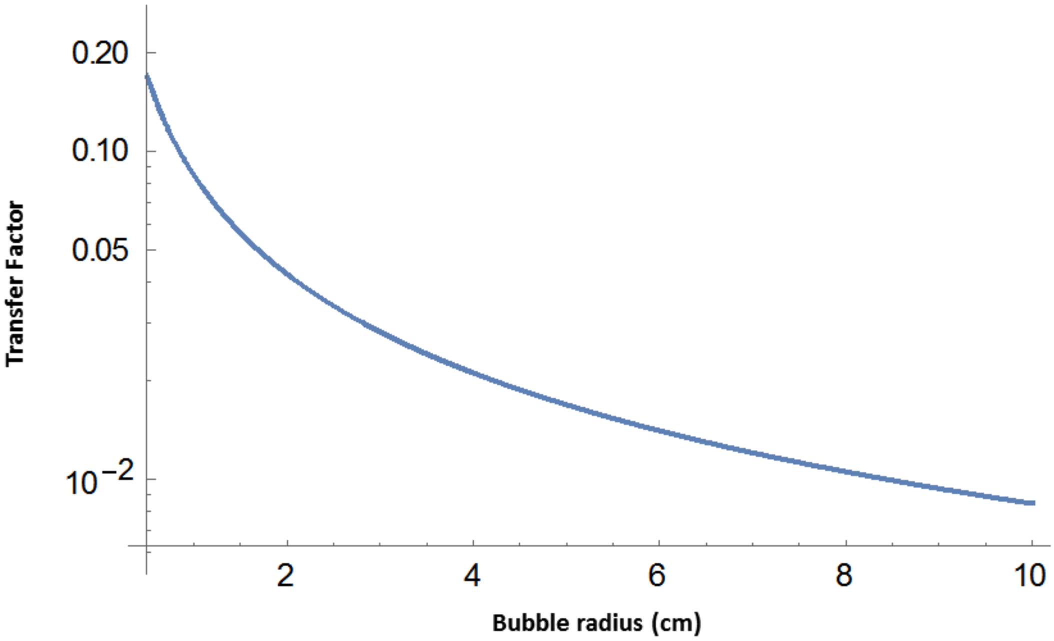

Figure 3.27: Plot of thoron transfer factor against bubble radius for bubbling of air in aqueous solution

3.4.2. Experimental validation of model for thoron transfer to bubble

In order to study the thoron transmission from liquids to bubbled air a new setup was developed. The schematic for the same is shown in Figure 3.28 along with a photograph of the experiment. A tall glass cylinder with a diameter of 10cm and height of 60 cm with sealed lid having two tubes connected to it was used. The cylinder was connected to a pump, flow regulator, flow meter and thoron monitor in closed loop setup. One of the tubes connected to the cylinder extended deep inside it and had a provision to attach nozzles of different size through which air could be released. The cylinder was then filled with thorium nitrate solution of known volumetric activity and thoron concentration. Air was released through submerged pipe with arrangement to vary the depth and orifice size. The bubbles formed at the tip of orifice travelled through the solution, rising to the surface. The air above the solution was collected and the thoron concentration was measured in it. The rising bubbles were photographed using digital camera and the size of the bubble was determined through image analysis using ImageJ software [102] and using an internal measurement reference. The rising bubbles were also video graphed at a high frame rate (120 fps) and the video was then analysed to manually obtain the bubble rise times and bubble rise velocities using software Shotcut [103]. The value of average thoron concentration in bubble air (C_2) was then estimated using the concentration measured by thoron monitor and a suitable correction factor.

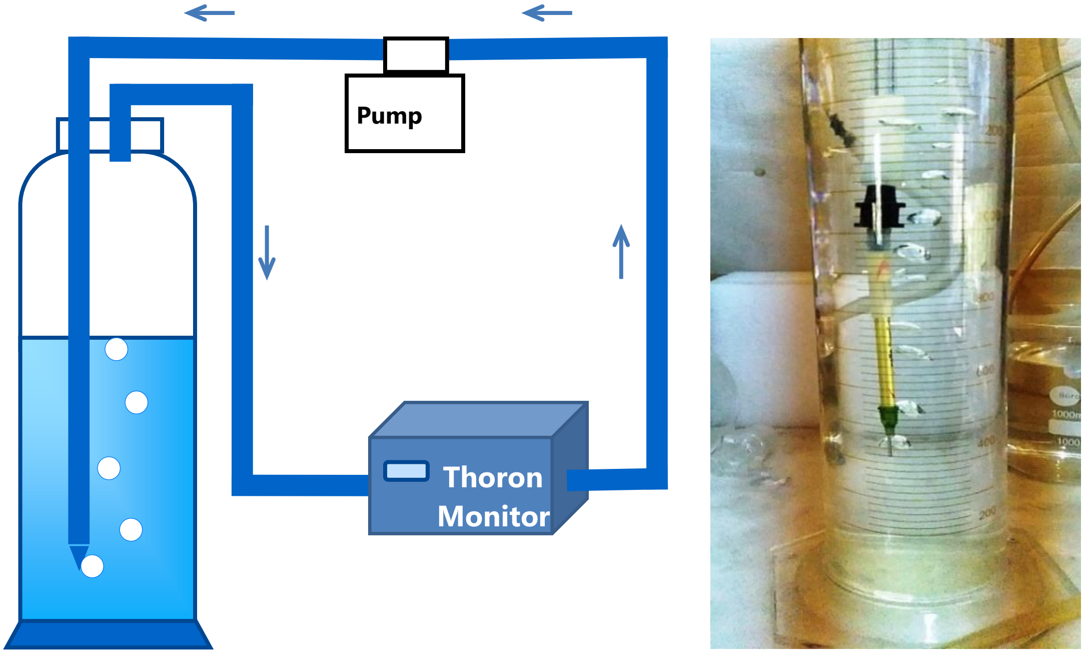

Figure 3.28: Schematic for experimental setup for study of thoron transfer factor with photograph of actual experiment

Measurements were carried out for bubbles of size ranging from 8.6 mm to 11.2 mm and residence time ranging from 0.28 s to 1.13 s. The values of the experimentally measured transfer factor and its comparison with corresponding values predicted by model are presented in Table 3.7 for the different sets of experiment.

Table 3.7: Results for the experimental measurement of thoron transfer factor and comparison with model predicted values

Rise time T (s)	Effective Experimental Diameter (mm)	Measured Transfer Factor	Model Transfer Factor	Per cent Deviation
0.28	11.17	0.067 ± 0.009	0.048	28
0.3	10.59	0.069 ± 0.011	0.049	30
0.57	9.77	0.060 ±0.008	0.051	16
0.87	10.30	0.065 ±0.009	0.051	21
0.88	9.48	0.060 ±0.008	0.052	12
1.025	9.35	0.068 ±0.010	0.053	23
1.13	8.68	0.065 ±0.008	0.054	16

It can be seen that the experimentally obtained values for transfer factor were always found to be higher than the model predicted values. The deviation between the two ranged from 16 % to 30 %. It can be seen that the model could predict the transfer factor with considerable accuracy. This is a definite progress as no model was available previously for this purpose and this model can be used to predict the thoron transfer from liquids during bubbling, albeit with a suitable safety factor to add a degree of conservatism in case of application for radiation protection.

3.5. Summary

The present chapter starts out by discussing the scenarios where thoron emission can be significant and pointing out the necessity of establishing tools and method to determine thoron source term. The work done towards development of diffusion based model for thoron emission from porous matrices and its validation for some thorium powders and monazite rich sands is presented. The model gives value of thoron surface exhalation rate using the thoron mass emanation rate, bulk density and diffusion length. Simple measurement setups developed to obtain the values of these parameters, which can even be used for in-situ measurements have been described. The typical values of the input parameters are discussed for application in model where actual measurements are not possible. The effect of different factors such as grain characteristics, moisture content and heating on thoron emission from porous matrices is discussed. Emanation model developed for grain shapes of cylinder, parallelepiped and octahedron are presented. Emanation from monazite sand and thorium bearing powders is discussed. The issue of thoron emission from thorium bearing liquids through bubbles during processes such as sparging has been addressed through experimental study of thoron transfer factor in laboratory. The comparison of measured transfer factor with prediction of model for thoron transfer to single bubble is presented.

The thoron emission model for porous matrices can be applied for calculation of thoron source term in most of the facilities by measuring the surface area available for thoron emission and multiplying it with corresponding exhalation rate. The thoron emission from thorium bearing liquid can also be predicted using the single bubble thoron transfer model. After developing the necessary methodology and tools for thoron source term estimation the next step naturally is to study the fate of thoron subsequent to its release in working environment and formation and properties of its decay products, which is presented in the next chapter.

Chapter 4

MODELING OF THORON AND ITS DECAY PRODUCTS IN CLOSED ENVIRONMENTS

4.1. Background

The thoron inhalation dose received by workers in thorium processing facilities will depend primarily on the thoron and its decay product concentration in the air. After establishing the thoron source term using methods described in previous chapter, the next step is to know its distribution in the working environment, formation of its decay products and their behaviour and properties. Thoron being a very short lived gas decays before it can disperse and mix completely in the environment. Hence its concentration exhibits a non-uniform profile with highest concentration near the source which decreases rapidly with distance from it. To determine the exact exposure to the gas, it is desirable to know the concentration profile. The radioactive decay of thoron gas results in formation of other radioactive decay products in its decay chain which are primarily particulates of solid suspended in air. The exposure of occupational personnel to this air results in inhalation and deposition of these radionuclides in the respiratory tract, leading to a significant internal dose. The size distribution of the decay products decides the pattern of their deposition in the respiratory tract and hence the resulting radiation dose (as different tissues of respiratory tract have different radio-sensitivity). In order to be able to predict the dose due to inhalation of thoron and its decay products accurately it is also important to know the size characteristics of the air-borne decay products along with their concentration in air.

Most of the studies for thoron and its decay products have been restricted to residential environments. A few studies that were carried out for industrial environments similar to thorium processing facilities, concentrated only on measurement of thoron and its decay product concentration and estimation of thoron dose using UNSCEAR dose conversion factor (DCF) [2]. Studies involving modeling of thoron decay product characteristics have been carried out for environments in homes [1], [104], [105]. However, the environments of thorium processing facilities are in general very different due to presence of greater quantity of ambient aerosols that are generated in different industrial processes, concentrated thoron source, forced ventilation etc. Though the basic physics and modeling principle remains same, suitable modifications to account for difference in environmental parameters such as aerosol particle size distribution, ventilation etc. need to be done. This chapter presents the work done towards various aspects of thoron and its decay product modeling in confined spaces in context of occupational environments of thorium fuel cycle facilities.

4.2. Thoron gas concentration profile

In radiation dosimetry for thoron, the dose conversion coefficient for thoron gas is considerably small in comparison to that of its decay products. In case of normal environments like homes and offices, thoron which is released from room surfaces usually decays out before travelling even a small distance. As a result, the concentration of thoron is very low and the resultant dose being negligible can be easily overlooked. However, the TENORMs handled in thorium fuel cycle result in thoron source terms which are higher by many orders of magnitude. Hence the concentration of thoron can be very high, especially at locations near the source and the resultant dose cannot be neglected. Because of the non-uniform concentration profile, the dose due to inhalation of thoron gas will also depend on the point of consideration. This makes it desirable to have a method to predict thoron gas concentration more accurately for estimation of dose. For this purpose, an analytical model was developed to obtain thoron concentration profile.

The model is based on the assumption that thoron emission is taking place from a point source and its transport thereafter takes place by diffusion. Assuming spherical symmetry, the one dimensional steady state diffusion equation in spherical co-ordinates, with source at the origin can be written as:

$$D\left[\frac{\partial^2 C}{\partial r^2}+\frac{2}{r}\frac{\partial C}{\partial r}\right]-C\lambda=0 \text{ for } 0<r \qquad \textbf{4.1}$$

where, C is the concentration of thoron, D is the diffusion coefficient of thoron in air and r is the radial distance from the source (origin). The equation is solved using the boundary conditions:

1) $0 < C(r) < \infty$ i.e. concentration C is finite at any point in medium, and

2) for source strength of S_0 (Bq s^{-1}), the activity crossing a sphere placed around a source in outward direction will tend to S_0 as $r \to 0$, i.e.

$$\lim_{r\to 0} 4\pi r^2 J(r) = S_0 \qquad \textbf{4.2}$$

The solution so obtained gives the value of thoron concentration $C(r)$ as a function of distance r from the source as:

$$C(r)=\frac{S_0}{4\pi l^2\lambda}\frac{e^{-\frac{r}{l}}}{r} \qquad \textbf{4.3}$$

where l (m) is the diffusion length of thoron in air and λ (s^{-1}) is the radioactive decay constant of thoron. The solution implies that the decrease in concentration of thoron with distance r is inversely proportional to the product $r.e^{r/l}$.

To see how the model performs in the real conditions, thoron measurement in closed space were done in two different cases. In the first case, a concentrated thoron source in form of thorium powder was placed at the centre of a room with a volume of about 40 m^3 and passive twin cup thoron detectors were placed around the source in different directions to measure thoron concentration at varying intervals. The setup for the same is shown in Figure 4.1.

Figure 4.1: Setup for measurement of thoron concentration around thoron source kept at the centre of room

In the other case, measurement of thoron concentration was done at varying distance from thorium powder kept in a drum as the thoron source, in a thorium processing facility with forced ventilation. In both the cases the measured thoron concentration was plotted against the corresponding distance from the source. The model (equation 4.3) was fitted to the data using least square regression. The fitted model for the data of second case is shown in Figure 4.2. The value of *l*, which is the variable parameter, was obtained for the best fit.

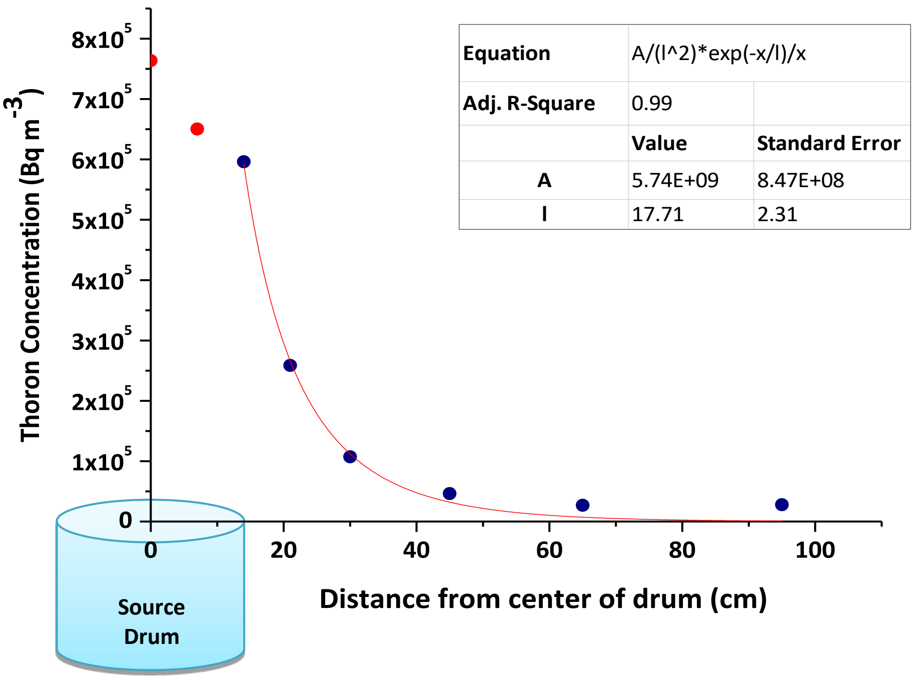

Figure 4.2: Fitting of the thoron concentration model to the plot of thoron concentration against distance from the source for measurement in an industrial environment

The fitting of the model gave a value of the diffusion length *l* as 8.2 cm for measurements in case 1 for a normal room, and 17.7 cm in case 2 which was a typical industrial environment. These values are greater than the molecular diffusion length of 3cm for thoron in stable air. The higher value of *l* indicates presence of some 'turbulence' and hence the value of *l* obtained from fitting the model can be called as turbulent diffusion length. The higher value obtained for turbulent diffusion length for thoron in case 2 can be attributed to the greater turbulence in air of the industrial environment due to higher ventilation rate (4 h^{-1}) as compared to that of normal room (estimated as 0.5 h^{-1}). To understand how the variation of diffusion length will affect the thoron concentration at different distances from the source, calculations were done using the model assuming same source strength for different values of diffusion length. The plot of the results is shown in Figure 4.3.

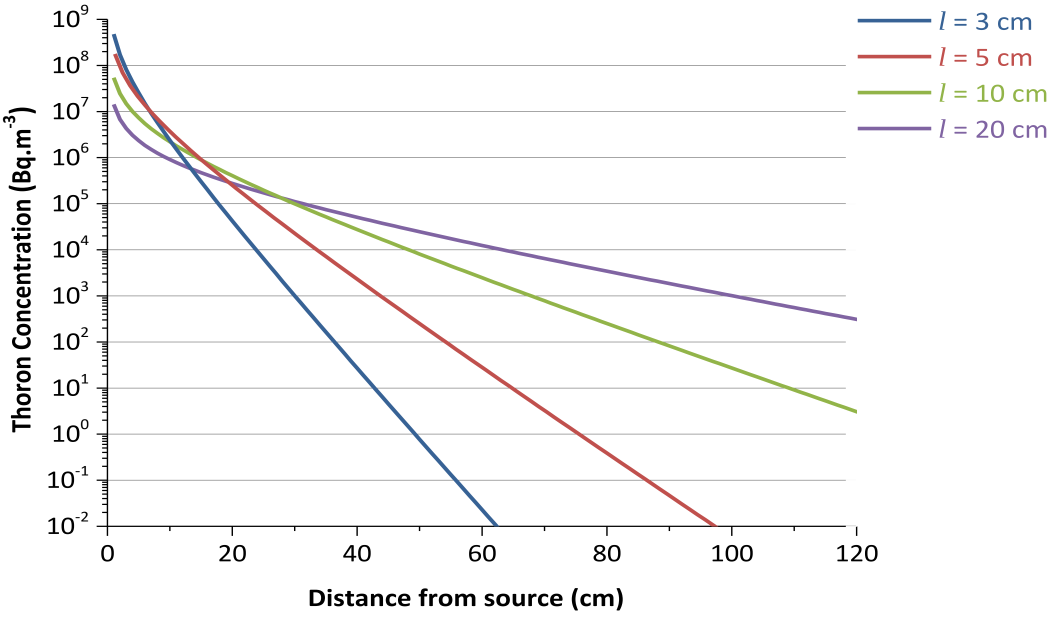

Figure 4.3: Thoron concentration profile for different values of *l*

It can be seen that as the turbulent diffusion length increases, the concentration of thoron very close to the source (< 30 cm) decreases. But for the distance beyond it the thoron concentration increases. For a distance of about 60 cm -100cm which is most probable inhalation zone for a worker working near the source, the increase can be by a few orders of magnitude. From the above plots, it is also clear that for any value of diffusion length, the concentration of thoron will increase by a couple of orders of magnitude as the distance from the source is decreased by a few tens of centimetres. In cases where the thoron gas concentration is the only quantity to be used for estimation of overall dose due to thoron and decay products, a measurement of thoron gas at a distance of about 20 cm is recommended. As seen from Figure 4.3, the influence of change in diffusion length on the concentration is least at this distance. An equilibrium factor derived on the basis of the measurement at the same distance can be reliably used for calculating the decay product concentration.

It is to be noted that the model has been mainly derived to obtain approximate thoron concentration at typical working distances from source of dimension of few centimetres. For cases where the thoron emitting areas are larger (of about 1 m^2 or greater) the expression for thoron concentration near a wall, as given in equation 4.4 can be used.

$$C(r) = \frac{J_s e^{-\frac{r}{l}}}{l\lambda} \qquad \textbf{4.4}$$

where, J_s (Bq m^{-2} s^{-1}) is the thoron surface exhalation rate for the source.

4.3. Modeling of thoron decay products in closed occupational environments

Once thoron is emitted from the source, it decays to its decay products in air. The decay products undergo various processes like formation of clusters, attachment to aerosols, removal by ventilation, deposition and radioactive decay, etc. It is necessary to understand how these processes affect the concentration of air-borne decay products and their size characteristics, in order to estimate the inhalation dose accurately. A model was developed to predict the thoron decay product concentration, unattached fraction and size distribution of thoron decay product in the industrial environment of thorium processing facilities. The model is based on the principles used in Jacobi's model for decay products of radon in mines which was modified for indoor environment by Porstendörfer [106]. The same model was modified for thoron in indoor environment of homes by Meisenberg and Tschiersch [104]. The basic physical processes considered here are same as those used by Meisenberg and Tschiersch, but the model was modified to include multiple aerosol size modes of thoron decay products and derive attachment rates and deposition rates corresponding to these modes. Nikezić and Stevanovic [105] have proposed a 'three modal model' on similar lines but have considered all possible processes for all the decay products in thoron decay chain.

The model presented here considers only those decay products of thoron which are dosimetrically important, and only the physical processes which are of consequence in affecting decay product properties, as described in detail by Meisenberg and Tschiersch [35].

4.3.1. Derivation of thoron decay product model

To begin, the average thoron concentration in the room volume of the facility was estimated. The source term for thoron can be calculated by multiplying thoron exhalation rates J_{Si} (Bq m^{-2} s^{-1}) determined using the methods described in previous chapter, with corresponding emitting area A_i (m^2) and summing up for all sources (i) in the room. The emitted thoron mostly undergoes a fast radioactive decay, while a very small fraction of it is lost by ventilation. Hence, the change in average concentration of thoron in a room, C_{Tn} (Bq m^{-3}) can be expressed using mass balance equation as:

$$\frac{dC_{Tn}}{dt} = \frac{\sum_i J_{Si} A_i}{V} - \lambda C_{Tn} - \lambda_v C_{Tn} \tag{4.5}$$

where, the summation in the first term on right side of the equation gives the net thoron source term (Bq s^{-1}); V (m^3) is the volume of the room, λ_v (s^{-1}) is the radioactive decay constant of thoron and λ_v (s^{-1}) is the ventilation rate. At equilibrium, solution of the equation will give value of C_{Tn} as:

$$C_{Tn} = \frac{\sum_i J_{Si} A_i}{V\left(\lambda + \lambda_v\right)} \tag{4.6}$$

Thoron gas decays to ^{216}Po, which has extremely short half-life (0.145 s) and is always in secular equilibrium with ^{220}Rn. Hence, for all practical purposes we can assume that the concentration of ^{216}Po, C_{Po216} is equal to C_{Tn}.

It is well known that the decay products of ^{220}Rn which are of dosimetric importance are ^{212}Pb and ^{212}Bi [36], [106], [107]. Hence the properties of only these two decay products need to be considered. ^{216}Po decays to ^{212}Pb, which is formed as an independent atom but immediately reacts with vapour and trace gases to form small cluster of size of about 1-3 nm [1] within a few seconds. Such clusters are traditionally called *unattached particles*. The unattached clusters of ^{212}Pb gradually attach to the ambient aerosols present in the environment to form '*attached particles*' or are lost by the processes of deposition to surfaces, removal by ventilation or radioactive decay. The equation for activity concentration of ^{212}Pb in form of unattached particles C_{Pb}^{unatt} (Bq m^{-3}), can be written using mass balance as:

$$\frac{dC_{Pb}^{unatt}}{dt} = C_{Tn}\lambda_{Pb} - \left(\lambda_{Pb} + \lambda_v + \lambda_d^{unatt} + \lambda_a\right)C_{Pb}^{unatt} \qquad \textbf{4.7}$$

where, λ_{Pb} (s^{-1}) is the radioactive decay constant of ^{212}Pb, λ_v (s^{-1}) is the ventilation rate, λ_d^{unatt} (s^{-1}) is the deposition rate of unattached particles and λ_a (s^{-1}) is the attachment rate of the unattached particles.

The attachment of unattached particles of ^{212}Pb to ambient aerosols in the environment results in formation of attached particles of ^{212}Pb. The aerosols generally present in the environment are best approximated by lognormal distributions. Depending on the sources of aerosols the aerosols will be mixture of different sizes of particles and can be described as a combination of multiple lognormal distributions, termed as '*modes*', each characterised with distinct parameters: Activity Median Aerodynamic Diameter (AMAD) and Geometric Standard Deviation (GSD). The attachment rate of unattached particles to the aerosols of a particular mode '*m*' and the deposition rate for particles of that mode are size dependent. Hence the equation for concentration of attached ^{212}Pb in each mode C_{Pb}^{att-m} (Bq m^{-3}) can be written as:

$$\frac{dC_{Pb}^{att-m}}{dt} = \lambda_a^m C_{Pb}^{unatt} - \left(\lambda_{Pb} + \lambda_v + \lambda_d^m\right) C_{Pb}^{att-m} \qquad \textbf{4.8}$$

where, λ_a^m (s^{-1}) is the attachment rate of unattached particle for the particular mode *m*, λ_v (s^{-1}) is the ventilation rate and λ_d^m (s^{-1}) is the deposition rate of attached particles of ^{212}Pb in mode *m*. The total concentration of attached particles of ^{212}Pb, C_{Pb}^{att} (Bq m^{-3}) will be the sum of concentration of attached ^{212}Pb in all the modes present:

$$C_{Pb}^{att} = \sum_m C_{Pb}^{att-m} \qquad \textbf{4.9}$$

and the attachment rate λ_a (s^{-1}) used in equation 4.7 is the sum of attachment rate for all modes:

$$\lambda_a = \sum_m \lambda_a^m \qquad \textbf{4.10}$$

The solution of equations 4.7 and 4.8 at the equilibrium gives the values of concentration of unattached ^{212}Pb and attached ^{212}Pb in different modes as:

$$C_{Pb}^{unatt} = \frac{\lambda_{Pb} C_{Tn}}{\lambda_{Pb} + \lambda_v + \lambda_d^{Unatt} + \lambda_a} \qquad \textbf{4.11}$$

and

$$C_{Pb}^{att-m} = \frac{\lambda_a^m C_{Pb}^{unatt}}{\lambda_{Pb} + \lambda_v + \lambda_d^m} \qquad \textbf{4.12}$$

^{212}Pb decays to ^{212}Bi, which is the next product in thoron decay chain. The unattached particles for ^{212}Bi will be formed only from the decay of unattached ^{212}Pb as the probability of detachment of ^{212}Bi formed by decay of attached ^{212}Pb is small due to low recoil energy in beta decay. Once formed, unattached ^{212}Bi will be lost by processes of attachment, ventilation or radioactive decay. Hence the equation for concentration of unattached ^{212}Bi, C_{Bi}^{unatt} (Bq m^{-3}) can be written as:

$$\frac{dC_{Bi}^{unatt}}{dt} = \lambda_{Bi} C_{Pb}^{unatt} - \left(\lambda_{Bi} + \lambda_v + \lambda_d^{unatt} + \lambda_a \right) C_{Bi}^{unatt} \qquad \mathbf{4.13}$$

where, λ_{Bi} (s^{-1}) is the radioactive decay constant of ^{212}Bi, λ_v (s^{-1}) is the ventilation rate, λ_d^{unatt} (s^{-1}) is the deposition rate of unattached particles and λ_a (s^{-1}) is the attachment rate of the unattached particles. The values of λ_a and λ_d are dependent only on the particle sizes and will remain unchanged for same particle sizes for both ^{212}Pb and ^{212}Bi.

The attached ^{212}Bi particles will be formed either by decay of attached ^{212}Pb or by attachment of unattached ^{212}Bi to the aerosols of different modes present in environment. They will also undergo loss by the processes of attachment, ventilation or radioactive decay. The equation for concentration of attached ^{212}Bi in a particular aerosol size mode *m*, C_{Bi}^{att-m} (Bq m^{-3}) can be written as:

$$\frac{dC_{Bi}^{att-m}}{dt} = \lambda_{Bi} C_{Pb}^{att-m} + \lambda_a^m C_{Bi}^{unatt} - \left(\lambda_{Bi} + \lambda_v + \lambda_d^{att-m} \right) C_{Bi}^{att-m} \qquad \mathbf{4.14}$$

where, λ_a^m (s^{-1}) is the attachment rate of unattached particle for the particular mode *m*, λ_v (s^{-1}) is the ventilation rate and λ_d^m (s^{-1}) is the deposition rate of attached particles of ^{212}Bi in mode *m*. The total concentration of attached particles of ^{212}Bi, C_{Bi}^{att} (Bq m^{-3}) will be:

$$C_{Bi}^{att} = \sum_{m} C_{Bi}^{att-m} \quad \textbf{4.15}$$

The solution of equations 4.13 and 4.14 at the equilibrium gives the values of C_{Bi}^{unatt} and C_{Bi}^{att-m} for different modes as:

$$C_{Bi}^{unatt} = \frac{\lambda_{Bi} C_{Pb}^{unatt}}{\lambda_{Bi} + \lambda_{v} + \lambda_{d}^{unatt} + \lambda_{a}} \quad \textbf{4.16}$$

and

$$C_{Bi}^{att-m} = \frac{\lambda_{Bi} C_{Pb}^{att-m} + \lambda_{a}^{m} C_{Bi}^{unatt}}{\lambda_{Bi} + \lambda_{v} + \lambda_{d}^{att-m}} \quad \textbf{4.17}$$

The equilibrium equivalent thoron concentration EETC (Bq m^{-3}) can then be obtained by using the equation [108]:

$$EETC = 0.917 C_{Pb} + 0.083 C_{Bi} \quad \textbf{4.18}$$

where C_{Pb} (Bq m^{-3}) is the total air-borne concentration of ^{212}Pb activity and C_{Bi} (Bq m^{-3}) is the total concentrations of ^{212}Bi activity.

From equations 4.11, 4.12, 4.16 and 4.17, it is clear that for evaluation of the concentrations of ^{212}Pb and ^{212}Bi in unattached form and as attached particles in different modes, the values for attachment rates of unattached particles to the aerosols in different size modes, and the deposition rates for unattached particles and the attached particles in different modes are required.

4.3.2. Estimation of attachment rate

The unattached particles formed in the air collide with the ambient aerosol due to the Brownian motion and get stuck to them. The probability of attachment depends on the sizes of aerosols and hence attachment rate depends on the sizes of the aerosol and is characterized by the parameter *attachment coefficient*, $\beta(d)$ (m^3 s^{-1}). The attachment coefficient, gives the probability that the unattached particle of thoron decay product will attach to an aerosol particle, as a function of particle size as [1]:

$$\beta(d) = \frac{2\pi D_0 d}{\frac{8D_0}{dv_0} + \frac{d}{d + {l_0}/{2}}} \qquad \textbf{4.19}$$

The value of attachment coefficient β was calculated using the typical values of parameters for unattached particles as: diffusion coefficient $D_0 = 6.8\times10^{-6}$ (m^2 s^{-1}), mean thermal velocity $v_0 = 1.72\times10^2$ (m s^{-1}) and mean free path length $l_0 = 4.9\times10^{-8}$ (m). The plot for variation of attachment coefficient with particle size is shown in Figure 4.4 for aerosol size range from 1nm to 10000 nm.

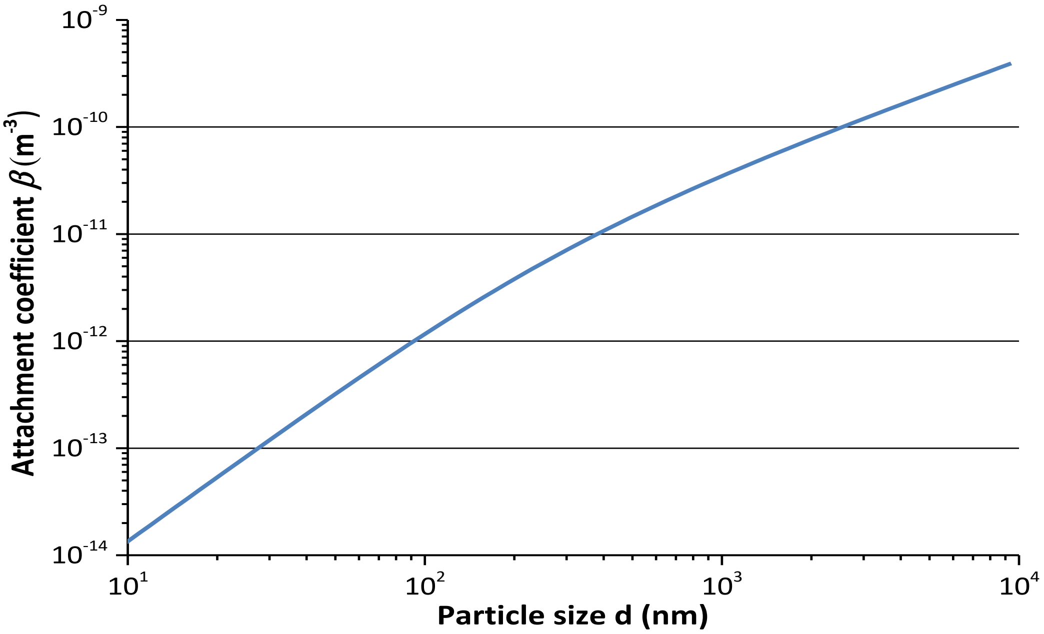

Figure 4.4: Variation of attachment coefficient β with particle size

The wide range of variation of β with change in particle size is clearly evident from the plot. Due to this, the attachment rate for different modes of aerosols will also be different and will be required to be evaluated separately.

The overall attachment rate of unattached particle for a particular mode of aerosols λ_a^m (s^{-1}) is given as:

$$\lambda_a^m = \int \beta(d) Z(d) \mathrm{d}d \qquad \mathbf{4.20}$$

where $Z(d)$ (m^{-3}) is the number concentration of aerosol particles with diameter d.

As the aerosol particle sizes in any mode are described by a lognormal distribution, $Z(d)$ was calculated using the lognormal distribution function with characteristic parameters mean diameter (d) and geometric standard deviation (σ_g). The value of σ_g corresponding to each value of d was obtained by using the continuous function recommended by ICRP 66 [109] shown in equation 4.21.

Calculation of attachment rate λ_a^m (s^{-1}) for varying mean diameter (d) of aerosol mode was done by solving equation 4.20 numerically for a total aerosol concentration N of 1 m^{-3}. A module was also written to obtain the attachment rate using specified values of d and σ_g, to be included in the program for thoron decay product model in software *Wolfram Mathematica*.

$$\sigma_g = 1.5\left(1 - \frac{1}{100d^{1.5} + 1}\right) + 1 \qquad \mathbf{4.21}$$

The results for calculation of specific attachment rate λ_{a-sp}^m (s^{-1} (particle $m^{-3})^{-1}$) corresponding to aerosol mode mean diameter d (nm) (count median diameter) are shown graphically in Figure 4.5 for aerosols of nucleation mode and Figure 4.6 for aerosols of accumulation and coarse modes.

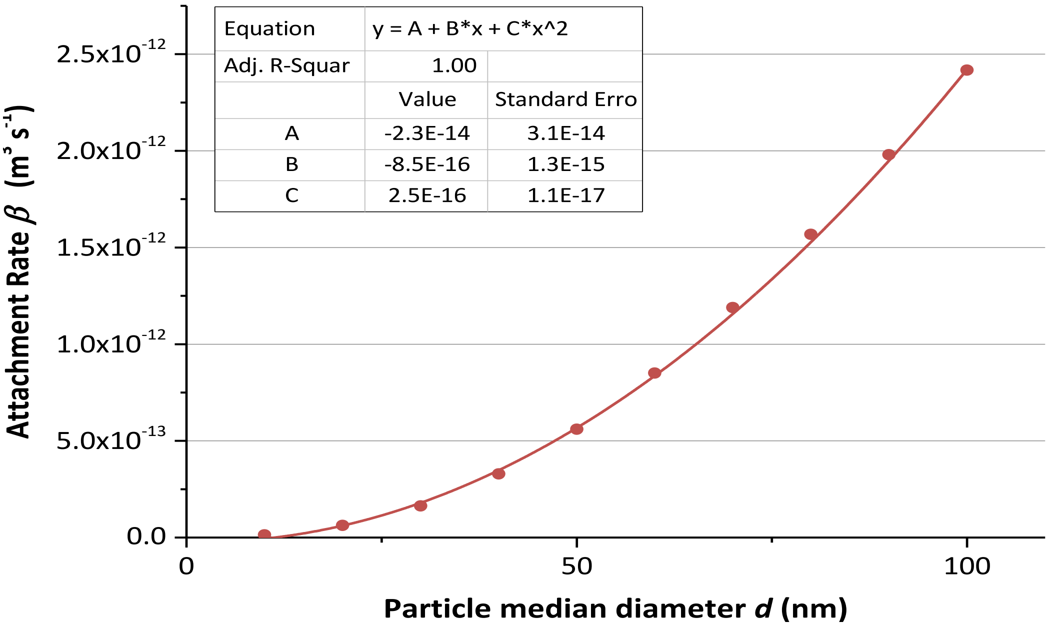

Equation	y = A + B*x + C*x^2	
Adj. R-Squar	1.00	
	Value	Standard Erro
A	-2.3E-14	3.1E-14
B	-8.5E-16	1.3E-15
C	2.5E-16	1.1E-17

Figure 4.5: Variation of attachment coefficient with aerosol median diameter for nucleation mode

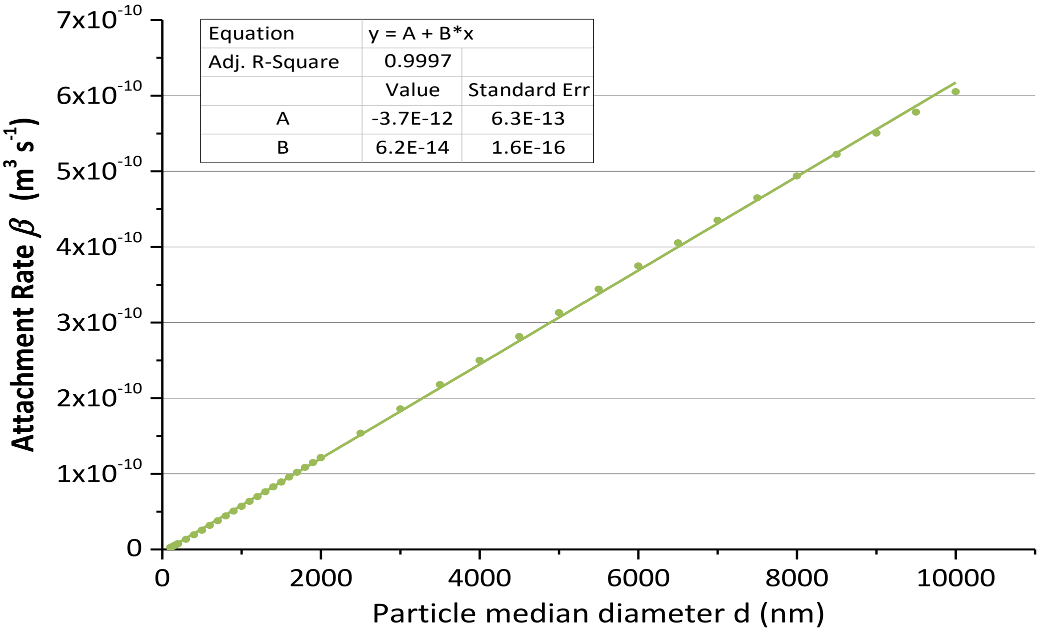

Equation	y = A + B*x	
Adj. R-Square	0.9997	
	Value	Standard Err
A	-3.7E-12	6.3E-13
B	6.2E-14	1.6E-16

Figure 4.6: Variation of attachment coefficient β with aerosol median diameter for accumulation and coarse modes

The plots were fitted with suitable equations to obtain simple working relationship for calculating the attachment rate using the value of median diameter for a particular aerosol mode. These are given by equation 4.22 for nucleation mode:

$$\lambda_{a-sp}^{f} = 3\times10^{-16} d^2 - 9\times10^{-16} d - 2\times10^{-14} \tag{4.22}$$

and equation 4.23 for accumulation and coarse modes.

$$\lambda_{a-sp}^{c} = 6\times10^{-14} d - 4\times10^{-12} \tag{4.23}$$

The values obtained above need to be multiplied with the number concentration of aerosol N (particle m^{-3}) to obtain attachment rate λ_a^m (s^{-1}). The information about typical aerosol size distribution and concentration in facilities associated with processing of thorium in different stages of thorium fuel cycles is normally available. Hence the above method can be used to obtain the rates of attachment corresponding to these particles to be used in the decay product model (section 4.3.1) for predicting the properties of thoron decay products. In some cases, the information about the activity size distribution of thoron decay products is directly available. In such a case the attachment rate for unattached thoron decay products can be obtained using the relationship given by Stevanovic et al. [110] as:

$$\lambda_a = \frac{N}{\int \frac{f(d)}{\beta(d)} \mathrm{d}d} \tag{4.24}$$

where $f(d)$ is the fraction of activity of thoron decay products associated with particles of size d and N (particles m^{-3}) is the number concentration of aerosol particles.

4.3.3. Estimation of deposition rate

Deposition of thoron decay products onto walls and other surfaces is an important removal process in indoor environments which influences their concentration.

Deposition can be quantified by the parameter deposition velocity v_d (m s^{-1}) [1], [111] defined as:

$$v_d = \frac{J(d)}{Z(d)} \tag{4.25}$$

where, $J(d)$ (particles m^{-2} s^{-1}) is the number of particles with diameter d deposited per unit surface area per unit time (particle flux) and $Z(d)$ (m^{-3}) is the number concentration of aerosol particles with diameter d. The rate of deposition of particles onto surfaces λ_d (s^{-1}) can be calculated from deposition velocity using the relation:

$$\lambda_d = v_d \frac{S}{V} \tag{4.26}$$

where, S (m^2) is the area of total surface available for deposition and V(m^3) is the volume of the indoor room.

In general the deposition of aerosol particles is governed by the physical processes of sedimentation by gravity, impaction by inertial forces and deposition by Brownian motion [1]. Considering that the flux of particles onto a surface can be expressed in form of equation as [1], [112]:

$$J(d) = -\left(D_0(d) + D_T(z)\right)\frac{dZ(z,d)}{dz} + V_s(d)Z(z,d) \tag{4.27}$$

where D_0 (m^2 s^{-1}) is the molecular diffusion coefficient for particles of diameter d, $D_T(z)$ (m^2 s^{-1}) is the turbulent diffusion coefficient at a distance z from the surface, Z(z, d) is the concentration of particles of diameter d at distance of z (m) and V_s (m s^{-1}) is the settling velocity of the particle. Due to the nature of gravitational setting, V_s will carry a negative sign for surfaces facing upward and will have a value of zero for vertical surfaces.

In case of environments with turbulent flow, the fraction of deposition flux due to turbulent diffusion ($D_T dZ/dz$) is much larger than that due to molecular diffusion ($D_0 dZ/dz$) and gravitational settling ($V_s Z$). The deposition of particles on to surfaces due to turbulent air flow takes place in two steps: 1) the particle is transported from the bulk volume towards the surface and 2) the particle is precipitated on the surface. The most commonly used model for deposition of particles in indoor environments is the Lai-Nazaroff model [113]. It is a three layer model in which the width of the layers and the turbulent functions are based on the results of direct numerical solution. It is applicable over a wide range of aerosol particle size. According to the model, the deposition velocity on a vertical surface $v_{d\mathrm{v}}$ (m s^{-1}) due to turbulence is given as:

$$v_{d\mathrm{v}} = \frac{u^*}{I} \qquad \textbf{4.28}$$

where u^* (m^2 s^{-1})is the friction velocity defined in equation 4.29, and I is the integral defined in equation 4.30.

$$u^* = \sqrt{\frac{\tau_w}{\rho_a}} \qquad \textbf{4.29}$$

where τ_w is the shear stress at the wall and ρ_a is the air density

$$I = \int_{r^+}^{30} \left(\frac{v}{D_T\left(z\right) + D_0} \right) \mathrm{d}z^+ \qquad \textbf{4.30}$$

where υ (m^2 s^{-1}) is the kinematic viscosity, z+ is the normalised distance (= z u*/ υ) and r^+=(d/2)($u^*/\ \upsilon$).

The deposition velocity for the upward facing horizontal surface $v_{d\mathrm{u}}$ (m s^{-1}) is given by:

$$v_{d\mathrm{u}} = \frac{v_s}{1 - \exp\left(-\frac{v_s}{v_{d\mathrm{v}}} \right)} \qquad \textbf{4.31}$$

The deposition velocity for downward facing horizontal surface v_{dd} (m s^{-1}) is given by

$$v_{d\mathrm{d}} = \frac{v_s}{\exp\left(\frac{v_s}{v_{d\mathrm{v}}}\right) - 1} \qquad \textbf{4.32}$$

The gravitational setting velocity v_s (m s^{-1}) is given as:

$$v_s = \int \frac{\rho d^2 g C_C}{18\mu} \qquad \textbf{4.33}$$

where ρ (kg m^{-3}) is the particle density, g (m^2 s^{-1}) is the acceleration due to gravity, C_C is the Cunningham slip correction factor, and μ (kg $m^{-1}s^{-1}$) is dynamic viscosity of the air.

It is evident from the model that the deposition velocity is also dependent on particle size for airborne aerosols. Hence the value of average deposition rate for unattached fraction and aerosol modes with different sizes will also be different and need to be evaluated. Here the interest is in the deposition of the activity of thoron decay products and not the ambient aerosol itself. So, the averaging is done on the activity size distribution of thoron decay products which again follows a lognormal distribution with parameters activity median aerodynamic diameter AMAD (d) and geometric standard deviation σ_g (obtained using equation **4.21** for calculations). The average deposition velocity $\bar{v}_{di}$ (m s^{-1}) for a particular activity size distribution and a particular surface orientation 'i' is then given as:

$$\bar{v}_{d\mathrm{i}} = \int v_{d\mathrm{i}}(d, u^*) f(d) \mathrm{d}d \qquad \textbf{4.34}$$

where $f(d)$ is the fraction of activity of thoron decay products associated with particles of size d, and index i will have values corresponding to a particular orientation of surface i.e. v for vertical, u for upward facing or d for downward facing. The average deposition velocity was calculated for varying values of *d* (AMAD) ,using equation 4.34 in conjunction with equation 4.28, 4.31 or 4.32 for a particular surface orientation. A module written in Wolfram Mathematica was used for solving the equations numerically. The results for the calculations are shown graphically in Figure 4.7. It can be seen that the deposition velocity on all surfaces is high for small particles with aerosol distributions having AMAD of about 5nm (unattached clusters), due to higher deposition by diffusion. It then decreases steadily with increasing AMAD up to 100 nm. It further decreases for vertical and downward facing surfaces. But for upward facing horizontal surface, it starts increasing with increase in diameter beyond 100nm due to increase in contribution of gravitational settling in the deposition process.

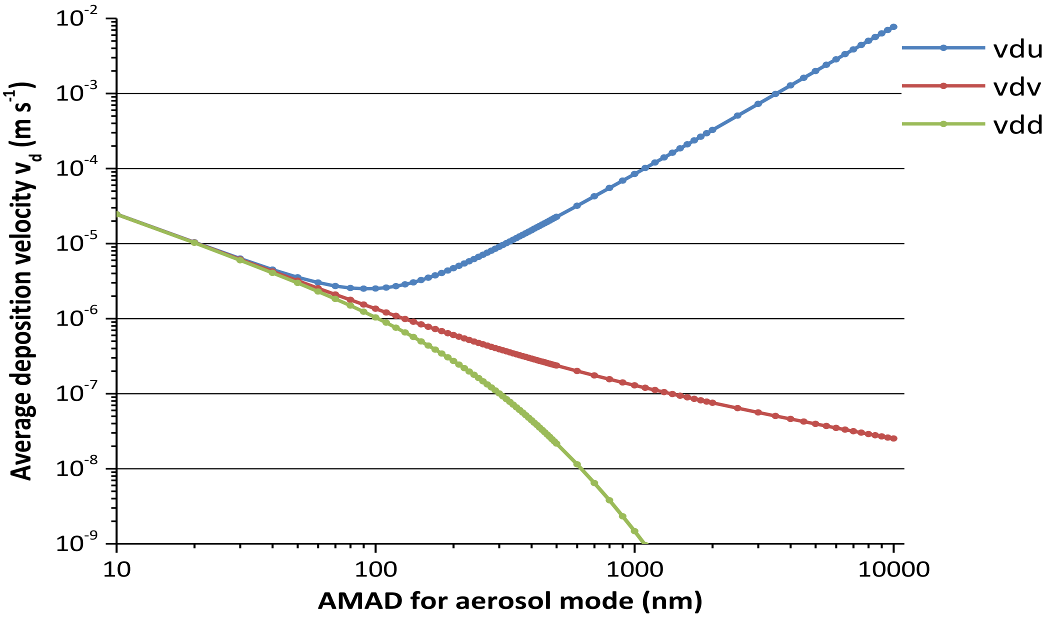

Figure 4.7: Variation of average deposition velocity $\overline{v}_d$ (m s^{-1}) with aerosol AMAD

A plot for variation of the calculated average deposition velocities for aerosols with AMAD (nm) and a GSD value recommended by ICRP 66 [109], is shown in Figure 4.8 along with the plot of deposition velocities for mono-dispersed particles with diameter d (nm) equal to the AMAD. The considerable difference between the two values for same diameter highlights the need to use particle size averaged deposition velocities for practical calculations. This is especially true for aerosol distributions with larger particle sizes, which are more probable in case of environments of thorium processing facilities. However, this approach has been seldom followed in previously published literature.

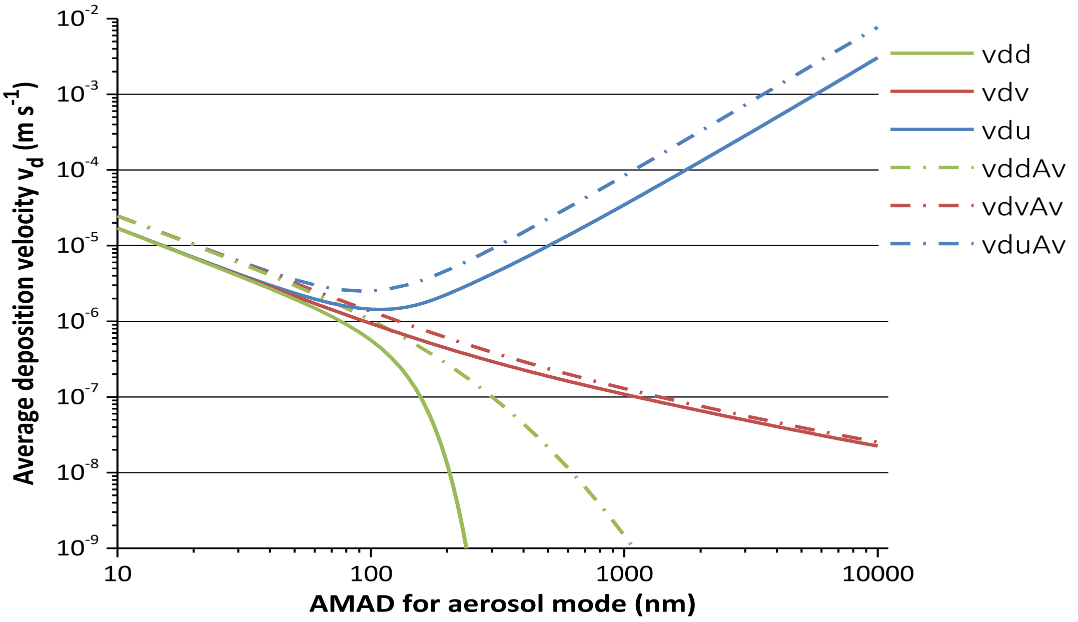

Figure 4.8: Difference between average deposition velocity for lognormal aerosol distribution and aerosol deposition velocity of mono-dispersed particle with size same as AMAD

Like in the case of attachment rate (section 4.3.2) equations giving simple working relationship for calculating the average deposition velocity $\bar{v}_{di}$ (m s^{-1}) using the value of AMAD (nm) for aerosol modes with AMAD greater than 100 nm. These relationships, obtained empirically by fitting power function of form a×AMAD^b using least square regression (R^2>0.99), are represented by equations 4.35, 4.36 and 4.37 for upward facing, vertical and downward facing surfaces.

$$\bar{v}_{d\mathrm{u}} = 10^{-10} AMAD^{1.93} \qquad \mathbf{4.35}$$

$$\bar{v}_{d\mathrm{v}} = 4\times10^{-5} AMAD^{-0.8} \qquad \mathbf{4.36}$$

$$\bar{v}_{d\mathrm{d}} = 4.435\times10^{5} AMAD^{-5} \qquad \mathbf{4.37}$$

Once the average deposition velocities corresponding to the prevalent decay product size distribution are estimated, the overall deposition rate λ_d (s^{-1}) corresponding to the aerosol mode can be calculated using the equation:

$$\lambda_d = \frac{\bar{v}_{d\mathrm{v}} A_\mathrm{v} + \bar{v}_{d\mathrm{u}} A_\mathrm{u} + \bar{v}_{d\mathrm{d}} A_\mathrm{d}}{V} \qquad \mathbf{4.38}$$

where $\bar{v}_{d\mathrm{i}}$ (m s^{-1}) is the average deposition velocity and A_i (m^2) is the area of the surface with corresponding orientation (i), and V(m^3) is the volume of the room. The overall deposition rate will thus depend on the size distribution of the decay product aerosols, turbulence characterised by friction velocity $u*$ and room dimensions. The friction velocity is usually directly proportional to the ventilation rate of the room [114] and hence greater ventilation will increase the deposition rate for aerosol particles.

A program was written in Mathematica to implement the methodology described in sections 4.3.1, 4.3.2 and 4.3.3, to predict the characteristics of thoron decay products like concentration of unattached fraction, and concentration and size distribution of attached fraction using input parameters: thoron source term, ambient aerosol concentration and size distribution, ventilation rate and room dimensions.

4.4. Measurements in thorium facility: Case study or validation of model

The model for prediction of thoron decay products based on the input parameters was tested in a thorium processing facility associated with powder processing. The facility was a large room of volume 240 m^3. Measurements for determining various parameters related to thoron and its decay products were carried out in the facility and the same were compared with the values obtained by the Thoron decay product model. The details of the same are described below.

4.4.1. Determination of thoron source term

The thoron surface exhalation rates $J_{S,i}$ (Bq m^{-2} s^{-1}) was measured for all available surfaces either by actual on-site measurement using accumulator technique (section 2.4) or predicted using the exhalation model (section 3.2.1) with input parameters based on in-situ measurements, in cases where direct flux measurement was not possible. The surface area A_i (m^2) corresponding to each of the source was determined. The total thoron source term S_{Tn} (Bq s^{-1}) was then estimated using equation:

$$S_{Tn} = \sum_i J_{Si} A_i \qquad \textbf{4.39}$$

The net source term obtained in this way was 25.4 kBq s^{-1}. The average thoron concentration obtained by using this in equation 4.6 was 7.68 kBq m^{-3}.

4.4.2. Determination of decay product aerosol characteristics

Grab filter paper sampling technique (described in section 2.4.2.1) was used for determining the concentration of thoron decay products. The air-borne decay products were sampled on a glass fibre filter paper for overnight sampling. The filter paper was then counted for alpha activity using a ZnS (Ag) based alpha counter. The counting was carried out at three distinct intervals of order: of a few minutes, a couple of hours and overnight. ^{212}Pb activity concentration (Bq m^{-3}) was obtained using the calculation method described in section 2.4.2.1 [61]. The value of ^{212}Pb activity concentration obtained from three sets of measurement was126 ± 32 Bq m^{-3}.

The ^{212}Bi concentration was assumed to be twenty per cent of ^{212}Pb[40], [60]. The determination of activity size distribution of thoron decay products was done using eight-stage Cascade impactor (section 2.4.2.5) which is an inertial impaction based particle separator. The sampling was carried out at a flow rate of 0.47 $m^3 s^{-1}$ for a period of 18 hours. The sampled aerosols were collected on glass fibre filter papers and the corresponding activity concentration was determined using the alpha measurements according to the method described earlier. Two sets of measurements were carried out: one during normal operations and other during powder transfer operations when the thoron concentration and airborne aerosols increase due to greater dispersion of powder during the operation.

The activity median diameter, total aerosol activity concentration and fractional contribution of the size modes of the aerosol were obtained from the measurements. In both cases the air-borne thoron decay product activity was found to follow a bimodal size distribution. The first mode had AMAD of 680 nm with σ_g of 2.1 and accounted for 90 % of the decay product activity whereas the second mode had an AMAD of 2.05 µm with a σ_g of 3.2 and accounted for 10% of the decay product activity. The results for the measurement are shown in Figure 4.9. The unattached fraction for decay products was obtained using DTPS based integrated sampler, described in detail in section 2.4.2.4. The sampler collected air-borne activity on two substrates: a wire mesh and a glass fibre filter paper. The wire mesh collected the unattached decay products while the filter paper collected the remaining activity associated with attached decay products. The deposited activities were counted using DTPS kept facing the two substrates. The SSNTD films from the DTPS were removed and processed to determine the unattached fraction. The value of the unattached fraction obtained from four sets of measurement and using a coverage factor of 1, was 0.07 ± 0.03.

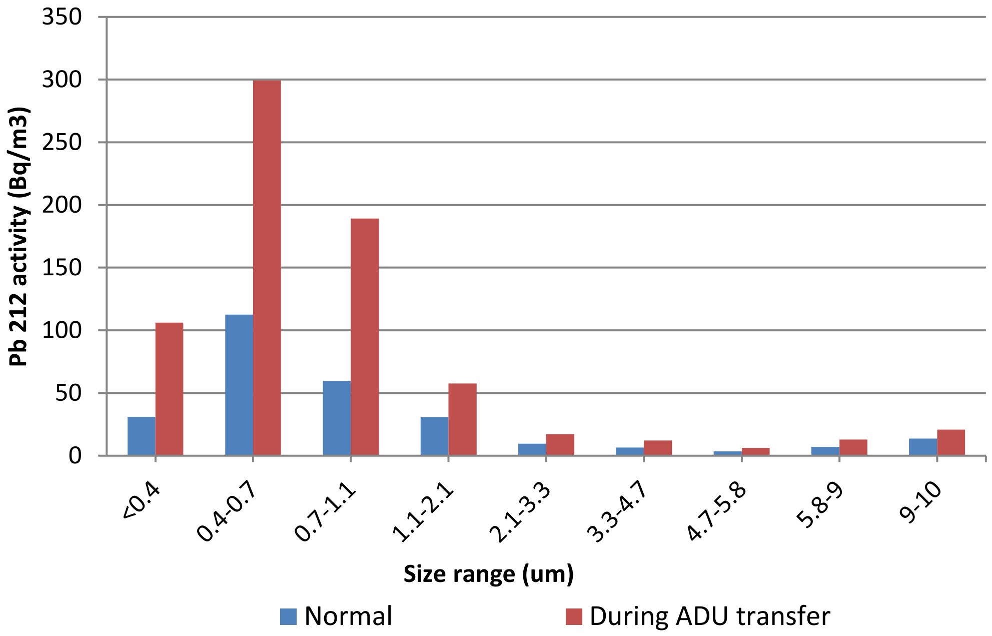

Figure 4.9: Activity size distribution of ^{212}Pb measured using eight stage Cascade Impactor

4.4.3. *Measurement of deposition velocity*

The surface deposition rate for thoron decay product was determined by using DTPS detectors. Seven DTPS badges were exposed for a period of 15-20 days in vertical orientation. After the exposure the SSNTD films from DTPS were processed according to standard protocol to obtain the track density. The average deposition rate of decay products J_d (Bq m^{-2} s^{-1}) was obtained using the measured track density T (tracks/cm^2), the track registration efficiency η_{tr} (tracks/atom) and the exposure period t(s) using equation

$$J = \frac{T}{\eta_{tr} t \lambda_{Pb}} \qquad 4.40$$

Using this value of deposition rate along with the measured air-borne decay product concentration (Bq m^{-3}), the average deposition velocity was obtained as $1.2 \pm 0.4\times10^{-5}$ m s^{-1}.

4.4.4. Comparison with model calculation

The thoron decay product model described in section 4.3.1 was used to predict the properties of thoron decay products in the facility. The input parameters for the model are thoron source term, ventilation rate, attachment rate and deposition rate. The estimation of thoron source term has been discussed in previous section. The attachment rate for two different modes was determined using equation 4.24, with the value for total number concentration *N* as 10^9 particles m^{-3}obtained on the basis of the data in literature where information on the particle size distribution (AMAD or MMAD, and GSD) was provided along with total airborne activity content or actual mass load (mass/m^3) and particle density [115]. The standard methods of conversion of aerosol parameters provided by Hinds(1982) were used [63].

This value of *N* also matched well in case of comparison of attachment rate calculated using this value and the aerosol size modes, with experimentally measured values. Though a higher aerosol generation is expected in the facility, the value of *N* is found to be in the range of aerosol number concentration for normal indoor environments. This may be attributed to the fact that a higher ventilation rate maintained for the facility with particle filtration results in greater aerosol removal and a lower number concentration of aerosol. The ventilation rate of 4 h^{-1} maintained at the facility was also used in the model. The measured AMAD values for the two distributions were used for calculation of deposition velocity. Combining it with the measured room volume and surfaces available for deposition, the total deposition rate was obtained. The value of average deposition velocity was obtained as 0.84×10^{-6} m s^{-1}. The concentrations of ^{212}Pb and ^{212}Bi in attached and unattached form were also obtained using the model.

The value for ^{212}Pb concentration obtained from the model was 126 ± 32 Bq m^{-3}. The unattached fraction for the decay products was obtained as 6.5%.

The comparison of the model predicted parameter values with that obtained by actual measurements is presented in Table 4.1.

Table 4.1: Comparison of model predicted and experimentally measured values for thoron decay products in thorium processing facility

Parameter	Theoretical Estimate	Measured value
Deposition Velocity (m/s)	0.84×10^{-6}	$1.2 \pm 0.42 \times10^{-5}$
Unattached Fraction	0.065	0.07 ± 0.03
^{212}Pb Concentration (Bq m^{3})	114	126 ± 32

It can be seen that the model predicted values agree well with the measurement values. This can be considered as the validation of the decay product model and the included methodology, for occupational environment.

4.5. Case study for validation of model: residential environment

As the basic physics of the thoron decay product behaviour in indoor spaces remains same for occupational and residential environment, a case study was also done to see the performance of the model in residential environment. For houses, the source of thoron is exhalation from wall. However, a lack of a method for direct measurement of thoron flux from wall made the estimation of thoron source term a challenging task. The use of direct measurement of thoron gas concentration was unreliable due to the associated uncertainties resulting from the inherent large variability in its concentration profile.

Hence a new wall mounting accumulator was developed to reliably measure the thoron flux from wall. The accumulator can be mounted on to the wall by using vacuum and the thoron exhalation rate can be measured accurately.

Figure 4.10: Photograph of the Wall mounting accumulator being used for measuring thoron flux from wall of a house

A photograph of the accumulator being used to measure thoron exhalation from wall of a house is shown in Figure 4.10.

Measurements were carried out in 24 dwellings across two states of India: Kerala and Uttarakhand, which are quite distinct in terms of geographical and geological aspects. The thoron exhalation rate was measured for all the thoron exhaling surfaces including walls, ceilings and roofs. The houses studied were mostly constructed with concrete and bricks with a couple having mud plaster on wall. Total thoron emission rate to indoor air (i.e. source term) was estimated by multiplying with respective exhaling surface area. Measurements were also carried out to determine the deposition velocities for the dwellings using DTPS detectors as described in section 4.4.3. The measurement of thoron decay product concentration was done by using grab filter paper sampling technique described in section 2.4.2.1. Measurements were done for total decay product concentration, i.e. attached and unattached fraction together. Hence the model was modified in this respect and calculation was done to predict typical equilibrium factor for residential environment.

The average value of deposition rate λ_d and ventilation rate λ_v obtained from the measurements were $3.6 \pm 1.1 \times 10^{-05}$ s^{-1} and $4.5 \pm 1.9 \times 10^{-04}$ s^{-1}. These were used in the model to predict the equilibrium factor F for the residential environment. The model predicted value of F obtained by using the average values of λ_d and λ_v was 0.036 ± 0.014. This was in good agreement with the value of 0.037 ± 0.013 obtained from direct measurements of thoron and its decay products in the dwellings of Uttarakhand and Kerala.

4.6. Application of model to study parameters affecting the decay product properties

After the validation of the decay product model, it was used to study the parameters that can affect thoron decay product properties. The model was used to obtain an insight into which input parameters have a greater effect on the decay products. For the calculations, the basic room dimensions used were same as the facility for which the model was validated. However, only one mode of aerosol was assumed to be present, resulting in only one mode for the attached thoron decay products. Study was done by keeping the values of parameters used for validation constant and varying one (or in some cases two) parameter over suitable range and predicting the decay product properties using the model. The results for the same are discussed in following sections.

It is evident from the measurements as well as the model predictions that the main dose to thoron decay products is contributed by ^{212}Pb. Moreover, the aerosol size distribution of ^{212}Bi is also same as that of ^{212}Pb. Hence study of ^{212}Pb activity alone is enough to make prediction for thoron dose.

4.6.1. Effect of friction velocity

The friction velocity (u*) characterises the turbulence for an environment. Any change in this will have a direct effect on the deposition rate of the aerosols by turbulent diffusion, in turn affecting their concentration in environment. In occupational environments a greater turbulence and hence a higher u* value is expected and it is useful to have a better knowledge of the effect of u* on deposition rate (λ_d). This can be understood by the results of model prediction shown in Figure 4.11. The graph shows variation of λ_d with u* for different AMAD values of attached decay products. It can be seen that there is a distinct increase in λ_d for decay product with u* for AMAD up to 0.1 µm. However, the rate of increase in λ_d with u*, decreases with the increase in AMAD. For an increase in u* value from 0.02 m s^{-1} to 0.1 m s^{-1}, the value of λ_d increases by 112 per cent for 0.025 µm AMAD, but for an AMAD of 0.1 µm this increase is by only 13 per cent. For the decay product AMADs above 0.25 µm the effect of u* on λ_d is negligible. This behaviour can be explained by the fact that for fine sizes of aerosols the main pathway for deposition is by diffusion and hence any change in u* will greatly affect the overall deposition rate. But in case of larger aerosols the main contribution to deposition is from the processes of settling and impaction. Hence even if change in u* causes change in deposition due to diffusion, it is masked due to the smaller contribution in overall deposition.

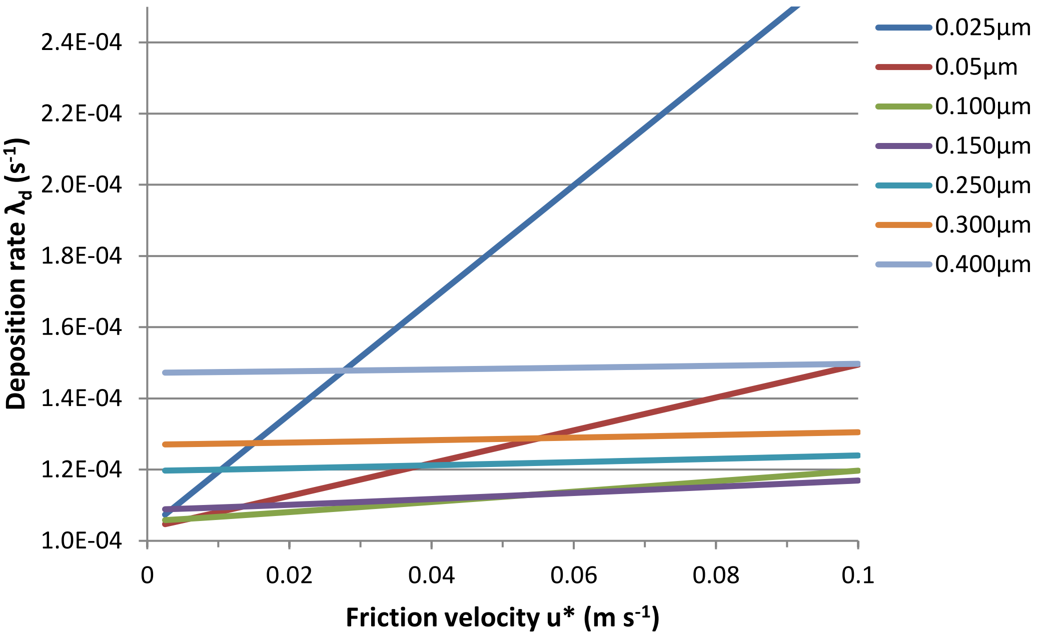

Figure 4.11: Plot for variation of deposition rate with friction velocity for different AMAD of aerosol

4.6.2. Effect of size distribution of environmental aerosol

The presence of aerosols generated from the industrial processes is one aspect which differentiates occupational environment from residential or office environments. The aerosol concentration and properties like size distribution are then dependent on the processes being carried out. This in turn affects the properties of thoron decay product in the environment. As discussed in section 4.3.2 the attachment coefficient β is function of particle size (diameter). The probability of attachment of unattached decay product cluster with aerosol is higher for larger aerosols. This results in the activity size distribution of decay products being different from that of the actual aerosols i.e. the activity median aerodynamic diameter AMAD, for thoron decay product is different from count median diameter CMD of aerosols.

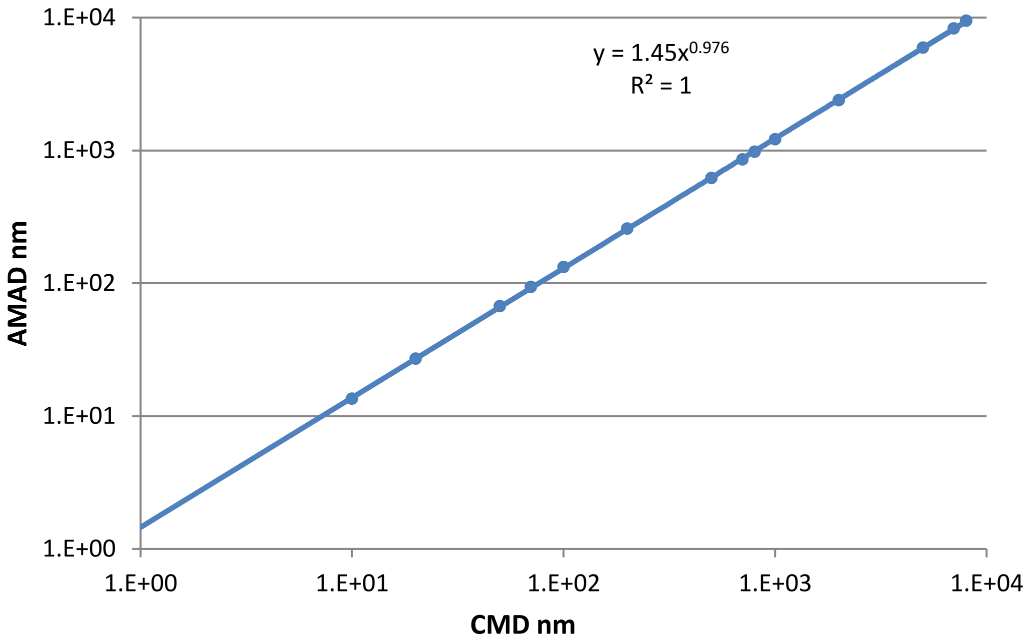

Figure 4.12: Plot of AMAD of thoron decay products against CMD of environmental aerosol

This will also lead to fraction of activity associated with the mode of aerosol with larger size being greater than the fraction of aerosol number concentration associated with the same mode. The correct knowledge of thoron decay product activity size distribution is desirable for more accurate dose prediction. Hence to obtain the relationship between the two parameters, the AMAD corresponding to varying CMD values was generated using the attachment module described in section 4.3.2. The results for the same are shown graphically in Figure 4.12. A least square regression fitting for a straight line was carried out to obtain the relationship between the CMD of environmental aerosols and AMAD of thoron decay products. The simple working relationship shown in equation can be particularly useful for prediction of the AMAD (nm) of thoron decay products in facilities where the CMD (nm) for aerosols is known.

$$\mathrm{AMAD} = 1.45\mathrm{CMD}^{0.976} \qquad \textbf{4.41}$$

The dependence of attachment rate on the aerosol particle sizes will also result in the CMD of aerosols affecting the unattached fraction for thoron decay products. The value of unattached fraction *f* was obtained for varying CMD of environmental aerosol. The results for the same are shown graphically in Figure 4.13. It can be observed that the unattached fraction is very high for aerosol CMD less than 0.05 µm, as the attachment rate corresponding to this range is very low and most unattached decay products will be removed by deposition, ventilation or decay before getting attached to the aerosols. In contrast to this, the unattached fraction is low for particle sizes above 0.5 µm as the attachment rate for them is high.

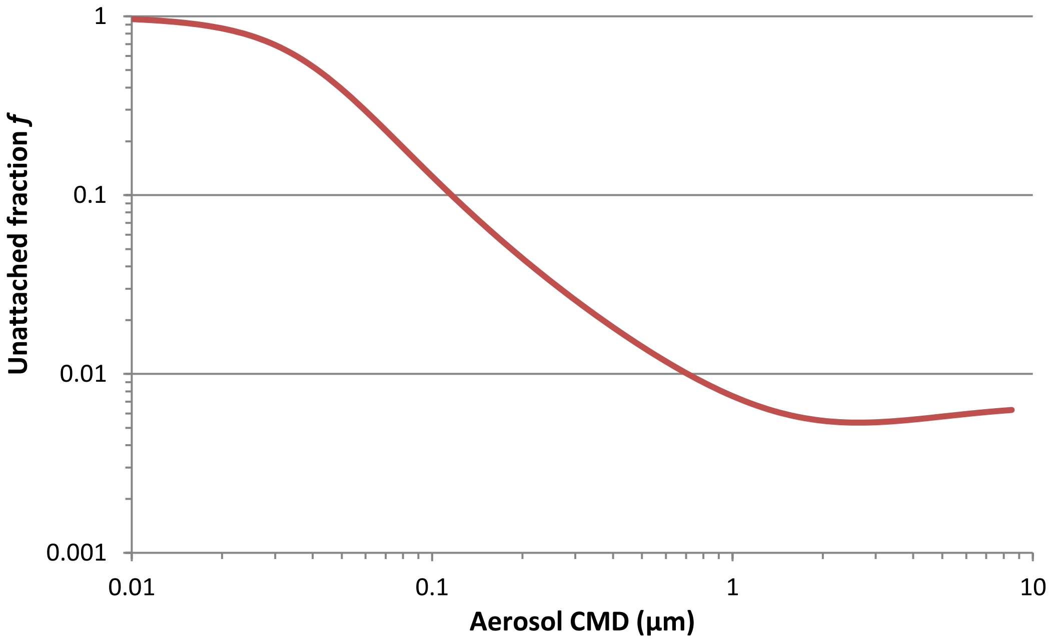

Figure 4.13: Plot for dependence of unattached fraction on CMD of environmental aerosol

4.6.3. Effect of number concentration of Aerosol in the environment

The study using model showed that the aerosol number concentration mainly affected the attachment rate λ_a and the unattached fraction *f*. The variation of λ_a with the number concentration of aerosols N, for different count median diameter CMD, of environmental aerosol is shown in Figure 4.14. It can be seen that the λ_a increases with *N* and the rate of this increment increases with the value of CMD for aerosols. This is as expected from equation 4.20, as the attachment coefficient for aerosols increases with the particle size. For the case of unattached fraction *f*, its variation with N for different values of CMD is shown in Figure 4.15. The unattached fraction decreases considerably with increase in N. The rate of this decrease is again more for larger value of CMD due to a greater attachment rate. The straight line in the log-log scale plot over a large range of particle number concentration suggests a power law relationship.

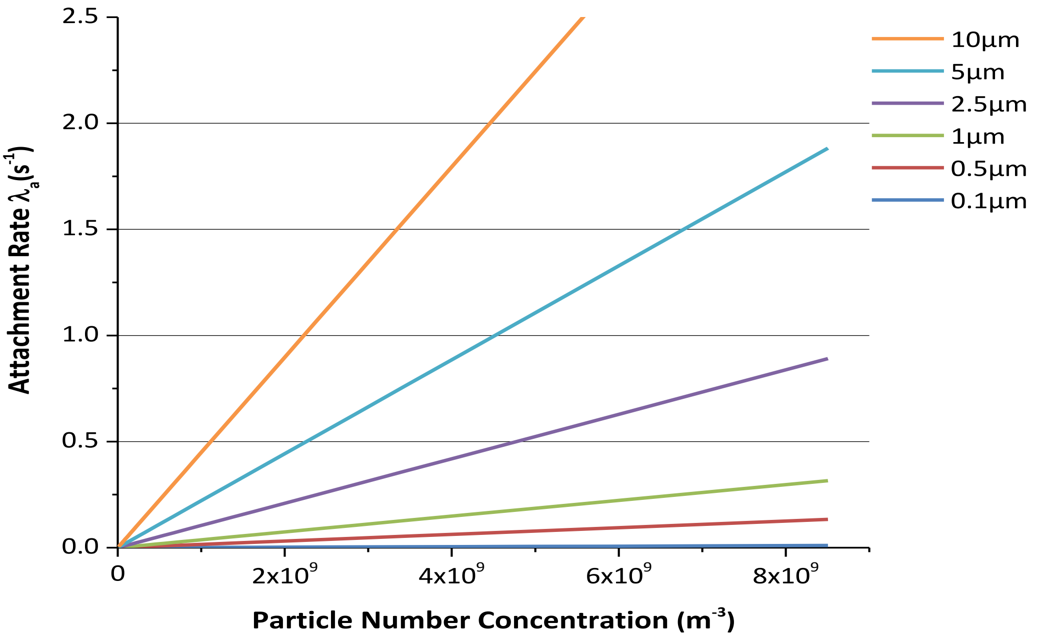

Figure 4.14: Plot for variation of Attachment rate with aerosol number concentration for different CMDs

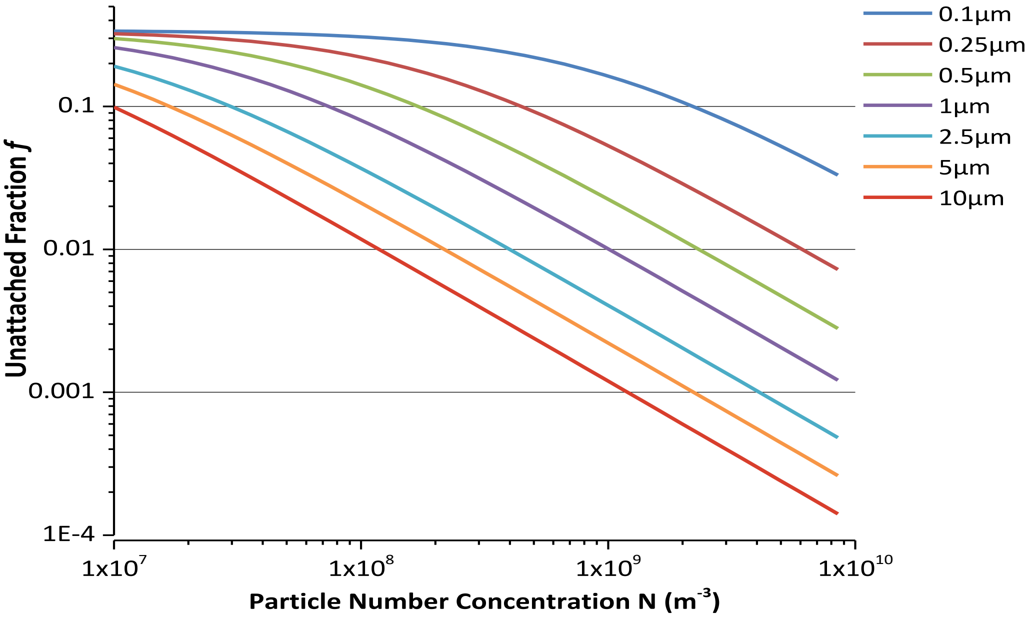

Figure 4.15: Plot for variation of unattached fraction with particle concentration for different CMD (nm)

4.6.4. Effect of ventilation rate

Ventilation rate is an important parameter which controls the characteristics of thoron decay products. The normal ventilation rate for homes and offices is usually around 0.5-1 h^{-1}. But in case of thorium fuel cycle facilities this rate can be much higher due to requirement of forced ventilation. As the thoron decay products (in particular ^{212}Pb) have long half-life, ventilation remains a key process affecting their removal. Thus, the thoron decay product concentration and hence the equilibrium factor will decrease with ventilation rate. The plot of model predicted equilibrium factor for different ventilation rates is shown in Figure 4.16 for different AMAD values of attached thoron decay products.

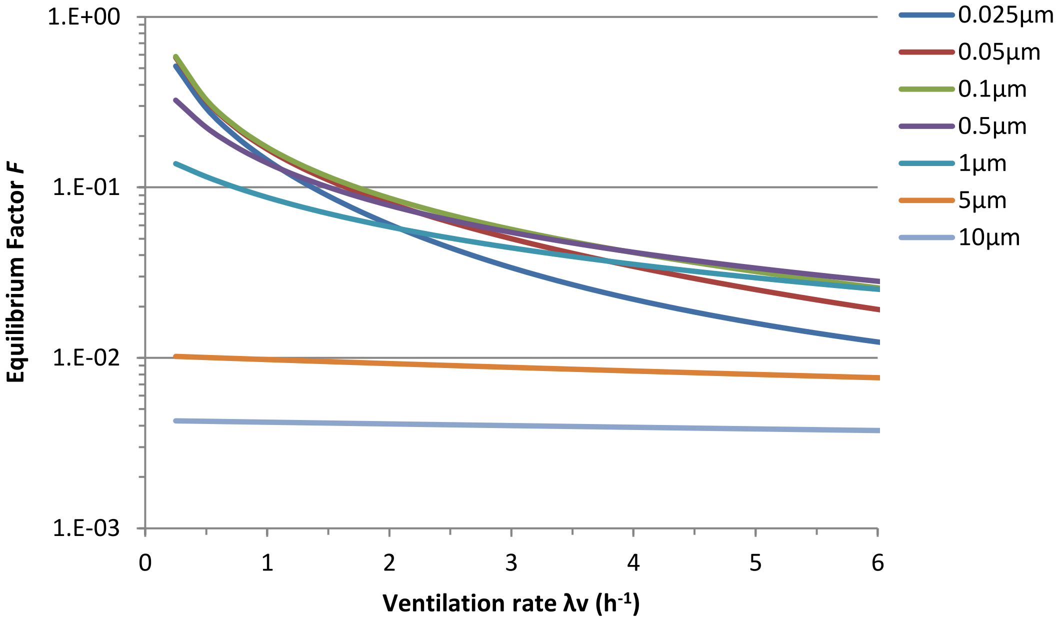

Figure 4.16: Plot of Equilibrium factor against ventilation rate for different AMADs

It can be seen from the graph that in general *F* decreases with increase in ventilation. The effect of λ_v on *F* is found to increase with decrease in the AMAD values. The fastest decrease in equilibrium factor with ventilation is observed for AMAD in nucleation modes. The extent to which λ_v affects *F* decreases when the AMAD increases and is found to be negligible for AMADs above 2.5 µm. However, the equilibrium factor itself is highest for AMAD of 0.1 µm where the deposition rate is lowest.Though removal of particles by ventilation is not dependent on the size of the particles, λ_v affects the unattached fraction *f* by controlling the time available to particles for attachment before being removed from the environment. Hence the unattached fraction depends upon the relative rate of removal of aerosols compared to rate of attachment. As a result, it will also be dependent on the size of aerosol particles. The variation of *f* with λ_v is shown in Figure 4.17 for different AMAD of the attached thoron decay products. Here the number concentration of aerosols is also calculated for the different ventilation assuming a constant aerosol generation rate.

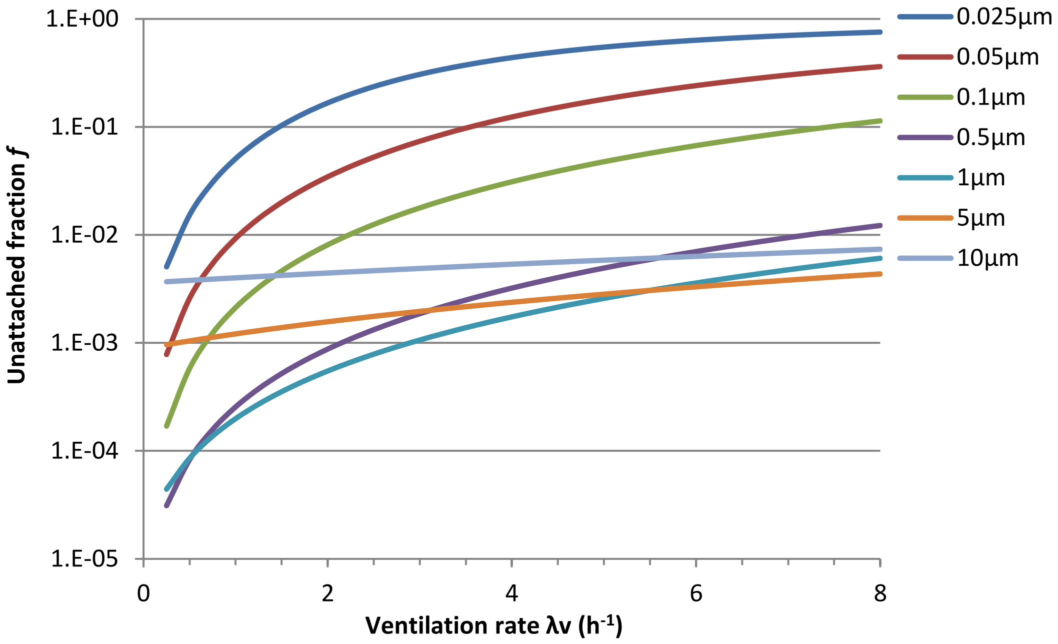

Figure 4.17: Plot of unattached fraction against ventilation rate for different AMADs

It can be seen that in general the value of f increases with increase in λ_v. The rate of increase is found to be more for AMADs less than 1µm. The rate of increase in f with λ_v is also found to be higher for initial rise in λ_v where it grows in relative magnitude in comparison with λ_a. The effect of λ_v on f is found to be very low in case of coarse particles (AMAD > 1) as λ_d value for these particles is considerably higher than λ_v (due to high amount of deposition by gravitational settling) and controls the removal rate. The amount of time spent by aerosol in the environment also decides the ratio of the concentration of decay products ^{212}Bi:^{212}Pb, as a longer residence time will lead to greater proportion of ^{212}Pb decaying to ^{212}Bi. Moreover, since the decay rate of ^{212}Pb is lower than the attachment rate, almost all of the ^{212}Bi formed is from the decay of attached ^{212}Pb. The results for variation of ^{212}Bi:^{212}Pb ratio with λ_v obtained using the model are plotted for various AMAD of decay product aerosols in Figure 4.18.

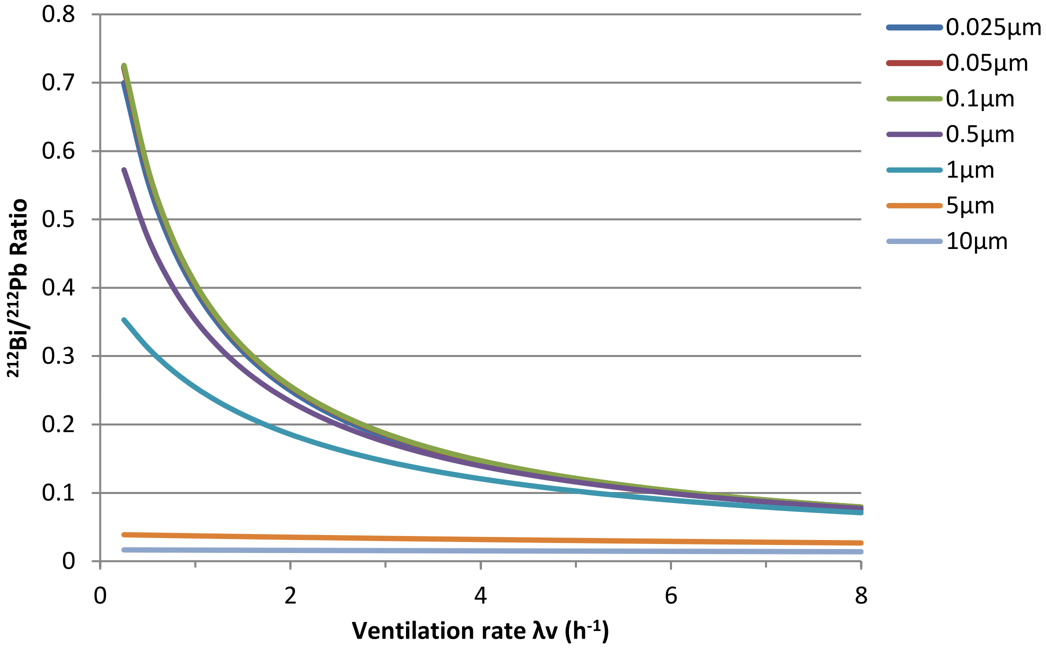

Figure 4.18: Plot of ^{212}Bi:^{212}Pb ratio against ventilation rate for different AMADs

It can be seen that the ^{212}Bi:^{212}Pb ratio is very high for ventilation rate lower than 1 h^{-1}, especially for AMADs less than 1 µm. The ratio increases as the λ_v increases, as the residence time for decay product also decreases. It can also be seen that ^{212}Bi:^{212}Pb ratio is maximum for decay product AMAD values of 0.1-0.25 µm, where the deposition rate is also minimum. The effect of λ_v is negligible for AMADs above 1 µm as the removal of ^{212}Pb is controlled by deposition rate dominated by gravitational settling, which is also the reason for a low ^{212}Bi:^{212}Pb ratio observed for them even at low values of λ_v.

4.7. Summary

The work towards study of thoron behaviour subsequent to its release into the working environment and that of its decay products has been presented in this chapter. The diffusion-based model for prediction of thoron concentration assuming point source geometry was derived and validated for two different environments. A model was developed to predict the concentration and size distribution of thoron decay products in the environment. It used size averaged attachment and deposition rates as input. The model was validated for environment of a thorium processing facility by comparison with comprehensive in-situ measurements of thoron and its decay products. Its performance was also tested by comparison with measurements done in residential environments of 24 houses. A software program written to implement this model was used to study the effects of various parameters on the thoron decay products in a typical environment of occupational facility. The analysis gave an insight into how the different parameters affected thoron decay products while considering other parameters acting in the environment. The methodology presented in the chapter is useful for predicting the thoron decay product properties in environment of thorium fuel facilities which can be used for more accurate radiation dose estimation for exposure of occupational personnel in such environments.

Chapter 5

INHALATION DOSE ESTIMATION

5.1. Background

The previous chapter presented the study of air-borne decay products and their characteristics in indoor environments of thorium processing facilities. If the occupational workers working in such facilities are exposed to the thoron bearing air it will lead to inhalation of the air-borne radionuclides and result in an internal radiation dose. The primary pathway for exposure to thoron and its decay product in the working environments is by inhalation. The exposure to radon and thoron decay products has been known to increase the risk of lung cancer in human populations exposed to them [14]–[16]. Since the exposure to thoron and its decay product is through inhalation, the thoron dose will depend on the characteristics of airborne radioactivity as well as individual factors like breathing rate and physiology of the exposed person. As the different tissues in the respiratory tract have different radio-sensitivities, the effective radiation dose also depends on the deposition pattern of radionuclides in the lungs, which in turn depends on the inhaled radioactive aerosol particle sizes.

Conventionally thoron dosimetry has been done by measuring the concentrations of thoron and its decay product in air and using the dose conversion factors (DCFs) given by UNSCEAR [2], [116] and ICRP[14], [38] to calculate dose to individual. However, the UNSCEAR dose conversion factor is a single value for dose per unit exposure which does not take into account the dependence of dose on the type of environment (residential, office or industrial) and the different properties of the decay product aerosol particles amongst them. ICRP 137 [40] has recently provided separate thoron

DCF values for indoor workplaces and mines. However, the value of DCF for indoor workplaces was obtained by using the data from measurements for houses and office workspaces. The working environment in thorium processing facilities is industrial in nature with larger rooms, forced ventilation and considerably higher concentration and a much different size characteristic of aerosol particles due to their generation in the different industrial processes. Hence the ICRP thoron dose conversion factor for the indoor workplaces is not representative of this environment. A more specific assessment of thoron inhalation dose is desirable for the case of different facilities of thorium fuel cycle. But thoron dosimetry in industrial environments is a neglected area and not much information is available for modeling the exposure and inhalation dose due to thoron and its decay products for them.

Considering this, a systematic study of the thoron inhalation dose for the environment of thorium processing facilities was carried out to obtain more reliable estimates, and the same is presented in this chapter. A dosimetric method based on the latest ICRP biokinetic and dosimetric models [40], [117], [118] was developed to calculate the thoron dose due to inhalation. The method was applied to study the effects of different thoron decay product and individual dependent parameters on the thoron dose. Calculations were done using the representative values of aerosol parameters in the different type of facilities to estimate thoron dose conversion factor for Indian worker. The importance of dose due to thoron gas itself in case of these facilities is pointed out.

5.2. Methodology for thoron dose calculation

Use of ICRP recommended models is the most accepted method for calculation of radiation doses for application in radiation protection. The evaluation of dose due to inhalation of thoron and its decay products requires: 1) determination of deposited fraction of inhaled decay products in the different regions of human respiratory tract, 2) calculation of transport, removal and decay of the radioactive decay products in various tissues/organs and 3) evaluation of total number of nuclear transformations (radioactive decays) in the different parts of the body and calculation of the tissue/organ equivalent doses and the effective dose. It is known that almost the entire radiation dose resulting from exposure to thoron and its decay product by inhalation is imparted to the airways of human respiratory tract by the non-penetrating alpha and beta radiations and any study for dose committed from thoron and its progeny can be focused only on the respiratory tract [119]. Hence a method was developed to estimate the thoron inhalation dose to human respiratory tract, based on the latest versions of ICRP Human Respiratory Tract Model (HRTM) and Internal dose calculation methodology [117], [118], [120]. A program was written in '*Wolfram Mathematica*' software to implement this method and carry out the calculations. The same is described in detail below.

5.2.1. Calculation of thoron decay product deposition in respiratory tract

The deposition model provided by ICRP 66 [109], along with the modifications done by ICRP 130 [117] was used to estimate the deposition pattern of the thoron decay product aerosols in the respiratory tract. In order to model the deposition pattern and the fate of the inhaled radioactive decay products, the model divides the respiratory tract into five broad anatomical regions: 1) Extrathoracic region (ET1) consisting of the anterior nasal passage, 2) extrathoracic region (ET2) consisting of the posterior nasal passages, larynx, pharynx, and mouth 3) the bronchial region (BB), consisting of the trachea and bronchi (generation 0 to 8) 4) the bronchiolar region (bb), consisting of the bronchioles and terminal bronchioles (generation 9 to 15), and 5) the alveolar interstitial region (AI), consisting of the respiratory bronchioles, the alveolar ducts and sacs (generation 15 to 23). The mathematical model for deposition treats each of the above regions as a particle filter. Each breath of individual is represented by a tidal flow of air that carries particles through each of the filter in sequence as shown in Figure 5.1. In case of breathing through nose nine filters in series are involved whereas for breathing through mouth there are seven filters involved. Mathematically, each of the filter j is characterized by two parameters: the volume v_j and the filtration efficiency for inhaled particles η_j, defined as the fraction of particles entering the filter that deposits in it. The deposition fraction DE_j is the fraction of the number of particles inhaled from environment I_0, which is deposited in the jth filter. It can be calculated by using equation:

$$DE_j = \eta_j \ \varphi_j \prod_{jj=0}^{j\text{-}1} \left(1 - \eta_{jj}\right) \qquad \mathbf{5.1}$$

where φ_j is the volumetric fraction and η_j is the deposition efficiency for a filter j.

The deposition efficiency depends on parameters like particle size, airway wind speed, transit times etc. and is different for different regions of respiratory tract. Particles are deposited in all compartments during both inhalation and exhalation. ICRP 66 has provided equations to calculate the deposition efficiencies for all filters. These are empirical equations based on the relevant particle size, wind velocity in airway and transition time through it.

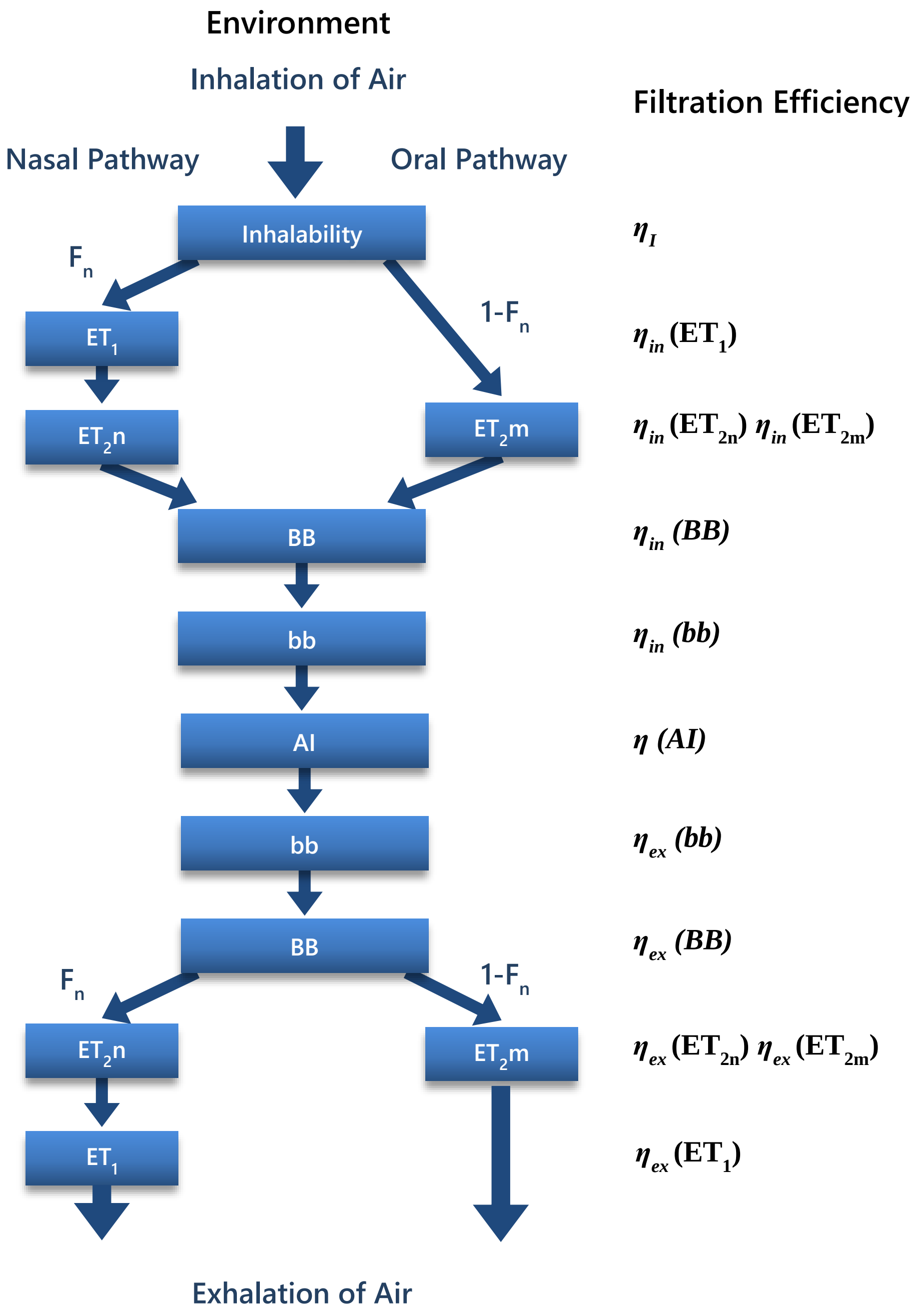

Figure 5.1:Model for deposition in different regions of HRTM (ICRP 66)[109]

The equations have been primarily obtained for ‘reference worker’ and include *scaling factor* to modify the deposition efficiencies for other subjects, depending on the body size. In current work, the scaling factors were obtained for an Indian occupational worker, considering the physical and physiological parameters for Indian adult male

[121], [122]. The volumetric fraction φ_j of the tidal volume V_t which reaches the filter j on inhalation is given by equation:

$$\varphi_j = \begin{cases} 1 & For\ \ j = 0 \\ 1 - \frac{1}{V_t}\sum_{i=0}^{j-1} v_i & For\, 1 \le j \le \frac{N+1}{2} \\ \varphi_{N-j+1} & For\, \frac{N+3}{2} \le j \le N \end{cases} \tag{5.2}$$

where, v_i is the volume of the preceding filters and N is the number of filters, i.e. deposition regions in the respiratory tract, for the complete breathing cycle (Figure 5.1). On exhalation, the volume of air returning through each filter is equal to the volume that passed through the filter on inhalation.

For Indian male, due to the smaller body size in comparison to the Caucasian counterpart, the factors like different lung volumes, airway sizes and organ sizes were also small. However the overall breathing rates reported for Indian male was comparable to that of Caucasian male and hence the ICRP reference worker [121], [123].

A program was written in Wolfram Mathematica to do calculations as per the described framework. The program was validated by carrying out deposition calculations for the ICRP standard worker for different particle diameters and compared with the values published by ICRP 130. The values of deposition fraction obtained in the calculations were found to deviate from the ICRP published values normally by 3-5% with maximum difference observed being 10%.

Using the method described above, the total and regional depositions of inhaled particles were calculated for Indian worker for different sizes. The particles were assumed to have a unimodal size distribution with specified AMAD and a GSD value recommended by ICRP 66 [109]. A breathing rate of 1.2 m^3h^{-1} and complete breathing through nose were assumed for the calculation. The results for the same are presented graphically in Figure 5.2. The general variation of deposition pattern was on the expected lines and similar to deposition in other human subjects [109]. It was seen that very small particles with a size of few nanometres, almost complete deposition in the respiratory tract took place with more than 90 per cent of it being deposited in ET region. The deposition for particles in this size range takes place mainly by Brownian diffusion.

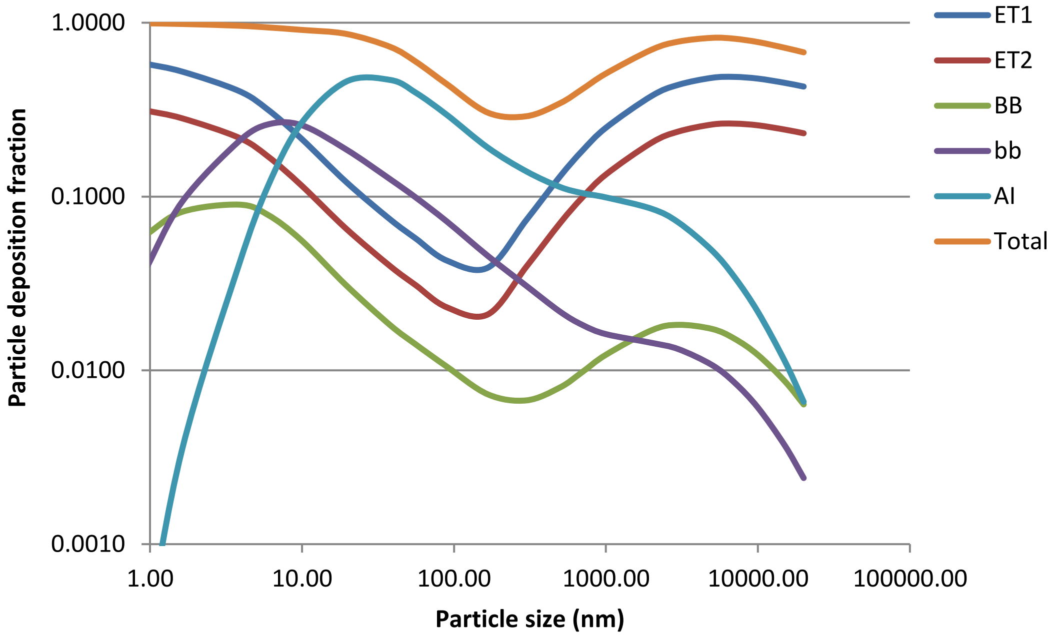

Figure 5.2: Variation of deposition fraction in respiratory tract of Indian worker with sizes of inhaled particles

With a further increase in the particle size, the deposition fraction in the ET region decreased due to lower diffusion; and more particles pass through and reach deeper parts of lung. Hence the deposition fractions in AI and bb region start increasing. As the inhaled particle size is increased further, the deposition fraction in all regions, and hence the total deposition, decreases due to lower diffusivity. The minimum deposition of particles is observed at a size of 200-300 nm. With further increase in particle size, more particles start depositing in ET region due to increased inertial impaction and the overall deposition increases. The deposition fraction again decreases beyond a size range of about 10 micrometres as the ‘inhalability’ of the particles decreases.

5.2.2. Calculation of number of nuclear transformations of radio-isotopes in HRT

Since ^{212}Pb and ^{212}Bi are the only decay products of thoron which control the inhalation dose [34], [119], the calculation for thoron dose was done considering inhalation of these two radionuclides only. The particles deposited in the respiratory tract are cleared mainly by means of two ways: 1) by mucociliary transport up the airways and transfer to gastro-intestinal (GI) tract and 2) by absorption into blood or the lymph system. The rates at which the deposited particles are cleared by each route depend on the location of deposition in the respiratory tract, the physic-chemical form of the material and the time spent by the particle in particular region. The mucociliary transport results in translocation of deposited particles from one region of respiratory tract to other. The radioactive particles deposited in the respiratory tract will also undergo nuclear transformation according to its decay constant.

The distribution and retention of the radionuclide particles in the different regions, following their deposition in respiratory tract, is given by the generic compartmental bio-kinetic model of ICRP Human Respiratory Tract Model (HRTM). The latest version of HRTM published in ICRP 130 divides the respiratory tract into 11compartments as shown in Figure 5.3. Of the five regions considered in calculation of deposition, the ET2 region is further divided into ET’ and ET_{seq} compartments, bb region is subdivided into bb’ and bb_{seq} compartments, BB region is subdivided into BB’ and BB_{seq} compartments, and AI region is subdivided into ALV and INT compartments considering the different translocation rates for activity that is sequestered into the tissues and that which remains on the surface of the tissue. Two more compartments, LN_{th} and LN_{et} representing the lymph nodes in thoracic and extra thoracic regions are also included. The rates of particle transport between the compartments are also provided (Figure 5.3) and it is assumed that these rates are same for all materials but different in different regions.

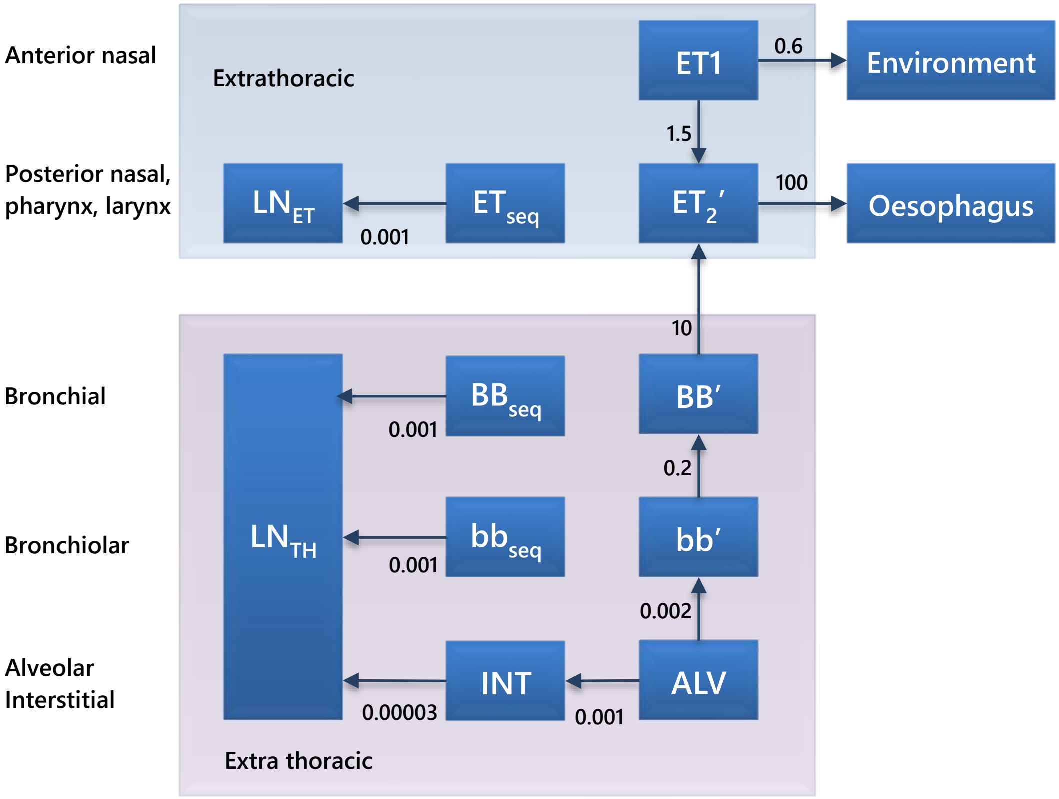

Figure 5.3: Compartmental biokinetic model of ICRP 130 HRTM along with rates (d^{-1}) of particle transport [117]

For particle clearance by absorption into blood, the rate of absorption is assumed to be same for all regions (but different for different materials), except ET1 for which no absorption takes place. The absorption occurs by two steps: 1) dissociation of particle into soluble form, called as dissolution and 2) absorption of the soluble material into blood called as uptake.

The rates for both steps can be time-dependent and are represented by compartment model to represent time-dependent dissolution, as shown in Figure 5.4. It is assumed that a fraction f_r dissolves relatively rapidly at a rate s_r, and the remaining fraction $(1 – f_r)$ dissolves more slowly at a rate s_s. The uptake normally occurs instantaneously, except for some elements, for which a fraction is 'bound' to respiratory tract components and is absorbed slowly. The fraction of the dissolved material in the bound state f_b, enters blood at a rate s_b; and the remaining fraction $(1 – f_b)$ is absorbed in to the blood instantaneously (Figure 5.4).

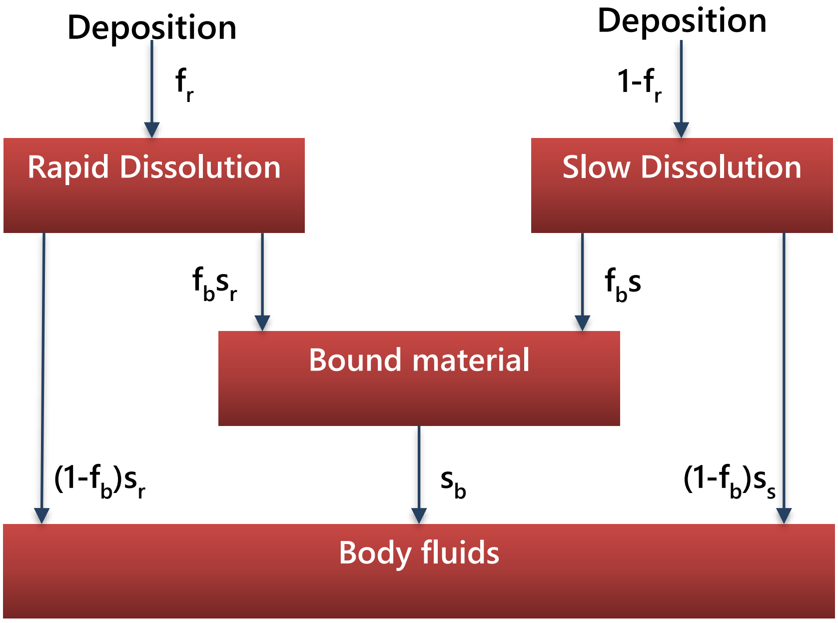

Figure 5.4: Compartment models representing time-dependent dissolution and uptake into blood [109]

On the basis of the biokinetic model the time variation of the activity of any radionuclide n in any compartment i can be represented by a general differential equation of the form shown in equation 5.3:

$$\frac{dq_{n,i}}{dt} = \sum_j m_{ji} q_{n,j} + q_{n-1,i}\lambda_n - (s_n + \sum_j m_{i,j} + \lambda_n) q_{n,i} \qquad \textbf{5.3}$$

where, where $q_{n,i}$ is the activity of radionuclide n in compartment *i*, $m_{i,j}$ is the transfer rate from compartment *i* to compartment *j* , λ_n is the decay constant of radionuclide *n* and radionuclide ‘*n-1*’ is the radioactive parent of nuclide n.

For calculation associated with estimation of thoron dose, the initial deposition of radionuclides ^{212}Pb and ^{212}Bi in respiratory tract was considered. The initial deposited activity of these radionuclides in each region of respiratory tract was determined using the deposition fractions obtained from the deposition model and the total value of inhaled radioactivity for these decay products. The total activity deposited in each region of respiratory tract was divided amongst the corresponding compartments according to the ratios given by ICRP 130, shown in Table 5.1 .

Table 5.1: Partition of deposit in each region of HRT amongst compartments [117]

Region of HRT	Compartment	Fraction of deposit
ET1	ET1	1
ET2	ET2’	0.998
	$ET2_{seq}$	0.002
BB	BB’	0.998
	BB_{eq}	0.002
bb	bb’	0.998
	bb_{seq}	0.002
AI	ALV	1
	INT	0

Though ^{212}Pb and ^{212}Bi were the only thoron decay products considered for initial deposition, the other decay products, viz. ^{212}Po and ^{208}Tl formed in the body by their decay, were also considered for actual dose calculation. The rate of change of activity content in a compartment *j* was calculated using equation5.3 for the radionuclides ^{212}Pb, ^{212}Bi, ^{212}Po and ^{208}Tl respectively.

The values of parameters for blood absorption used in the calculations were the element specific values applicable for them as the decay product of radon and are presented in Table 5.2.

Table 5.2: Values of parameters for blood absorption for thoron decay products [117]

Thoron Decay Product	Dissolution parameters			Uptake parameters	
	f_r	s_r (d^{-1})	s_s (d^{-1})	f_b	s_b (d^{-1})
^{216}Po	1	3	–	0	–
^{212}Pb	0.1	100	1.7	0.5	1.7
^{212}Bi	1	1	–	0	–
^{208}Tl	1	1	–	0	–

The above set of equations was solved using the initial condition as the initial concentration of the respective decay product in each region. The solution of these set of equations gave the expression for time variation of activity content of the radioisotope in these compartments as a function of time. Integration of the activity over a period of 50 years gave the total number of radioactive transformations occurring in the particular compartment during this period. This was required in accordance with the commitment period of 50 years recommended by ICRP for calculation of committed effective dose for an adult [109]. A module written in Wolfram Mathematica was used to perform the calculations.

5.2.3. Calculation of equivalent and committed effective dose

Each nuclear transformation taking place inside the respiratory tract will impart some radiation to the body and contribute to the overall radiation dose. In order to calculate the committed equivalent doses to the tissues and the committed effective dose, the dosimetric model provided by ICRP 130 was used [117]. According to it, the committed equivalent dose to a target region r_T of the body is given by equation 5.4:

$$H\left(r_T\right) = \sum_{i,rs} A_i \, S_W\left(r_T \leftarrow r_s\right)_i \qquad \textbf{5.4}$$

where, A_i (Bq s) is the number of nuclear transformations of a radionuclide *i* occurring in source region r_S, S_W (Sv (Bq s)$^{-1}$), called as S coefficients, is the radiation-weighted equivalent doses in target region r_T per nuclear transformation of radionuclide *i* in source region r_S. To calculate the committed equivalent dose due to any radionuclide, the nuclear transformations and the resulting dose from all the decay products of its decay chain need to be considered. The compartments of biokinetic models are associated with anatomical regions in the body termed as source regions. In cases of dose to the respiratory tract, the two main anatomical sections of extra thoracic region and Lungs consist of multiple target tissues and in order to calculate the dose to them, fractional weighting of the equivalent dose to the constituent tissues is done. The fractional weights of target regions used for this purpose are provided in Table 5.3.

The radiation-weighted S coefficient for a radionuclide is calculated as:

$$S_W\left(r_T \leftarrow r_s\right) = \sum_R w_R \sum_i E_{R,i} Y_{R,i} \Phi\left(r_T \leftarrow r_s, E_{R,i}\right) \qquad \textbf{5.5}$$

where, $E_{R,i}$ is the energy of the i^{th} radiation of type R emitted in nuclear transformations of the radionuclide; $Y_{R,i}$ is the yield of the i^{th} radiation of type R per nuclear transformation ($(Bq\ s)^{-1}$); w_R is the radiation weighting factor for radiation type R and $\Phi\left(r_T \leftarrow r_s, E_{R,i}\right)$ is the SAF, defined as the fraction of energy $E_{R,i}$ of radiation type R emitted within the source tissue r_S that is absorbed per mass in the target tissue r_T (kg^{-1}).

Table 5.3: Target region fractional weights f (r_T, T) [117]

Tissue, T	r_T	f (r_T, T)
Extrathoracic region	ET1 basal cells	0.001
	ET2 basal cells	0.999
Lungs	Bronchi basal cells	1/6
	Bronchi secretory cells	1/6
	Bronchiolar secretory cells	1/3
	Alveolar Interstitial	1/3

The values of all the required S coefficients (SW) were calculated using Φ values provided by ICRP for different energies of different types of nuclear radiations. In case of calculation for Indian worker the *Φ* values were corrected for the smaller organ masses of Indian worker using the ratio 'ICRP lung mass: Indian lung mass' as correction factor. This assumption is based on the fact that actual fractions of radiations emitted within the source tissue that is absorbed in different target tissue do not change much due to body size. This is valid in case of thoron decay products as almost the entire dose is due to alpha and beta ratios which are absorbed in the same organs where they are emitted. This approach has also been adopted by ICRP for calculating SAF values for body types other than reference subjects [109].

For the calculations, S_W values provided for alpha energy of 6.0 MeV were used for ^{212}Bi and for 8.5 MeV were used for ^{212}Po. For the beta decay of ^{212}Bi and ^{208}Tl the S_W values were calculated by weighing with the spectral data instead of using mean values. The electron energy spectrum for the beta decays were obtained from DecData published in ICRP 107 [124].

The committed effective dose was calculated by weighting the equivalent dose to tissue with tissue weighing factor and summing the same, as given in equation 5.6.

$$E = \sum_T w_T \, H_T \qquad \textbf{5.6}$$

where, w_T is the tissue weighting factor for target tissue T. The nuclear transformation of thoron decay products occurring in various regions of the respiratory tract results mostly in emission of alpha and beta radiations. Hence the dose imparted by them is to the organs in which they are deposited. Moreover, the activity of the decay products is concentrated mainly in the respiratory tract region. Hence the contribution by committed equivalent dose to lungs and extra thoracic region accounts for more than 98 per cent of the committed effective dose due to thoron and its decay products[119]. Hence the effective dose to the whole body was estimated by determining the effective dose to lungs and extra thoracic region and assuming that it was 98 per cent of the whole-body dose. The tissue weighting factor of 0.12 for lungs and 0.00923 for extra thoracic region, obtained by dividing the factor 0.12 provided for the group of “Remainder tissues” by the 13 individual tissues included in the group, as recommended by ICRP 130 [117].

5.3. Dose conversion factor for Indian worker

To obtain the dose conversion factor, an exposure to unit concentration of activity (1 Bq m^{-3}) for unit time (1 h) was considered and then the dose was calculated as per the procedure described above. The dose coefficient was calculated for Indian worker for exposure to varying particle sizes of ^{212}Pb and ^{212}Bi separately. Exposure to a unimodal lognormal activity size distribution with activity median particle diameter (thermodynamic diameter for up to size 1000 nm and aerodynamic diameter for size from 1000 nm and above) was assumed. The results for the same are shown in Figure 5.5 and Figure 5.6 respectively.

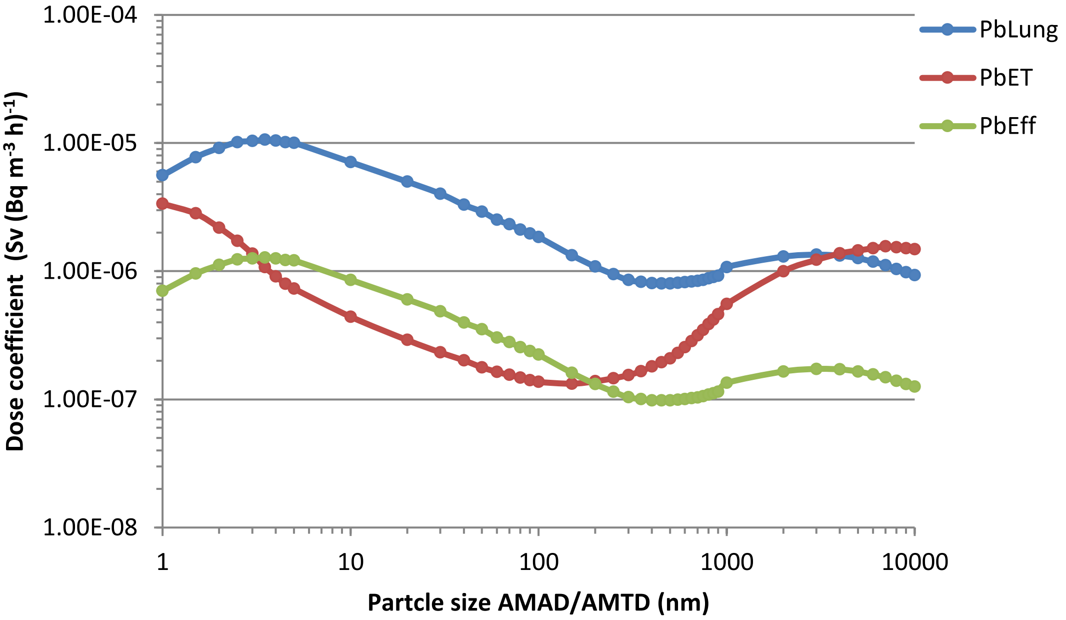

Figure 5.5: Variation of Effective dose coefficient and equivalent dose coefficient for lung and extra thoracic region for ^{212}Pb as a function of particle size

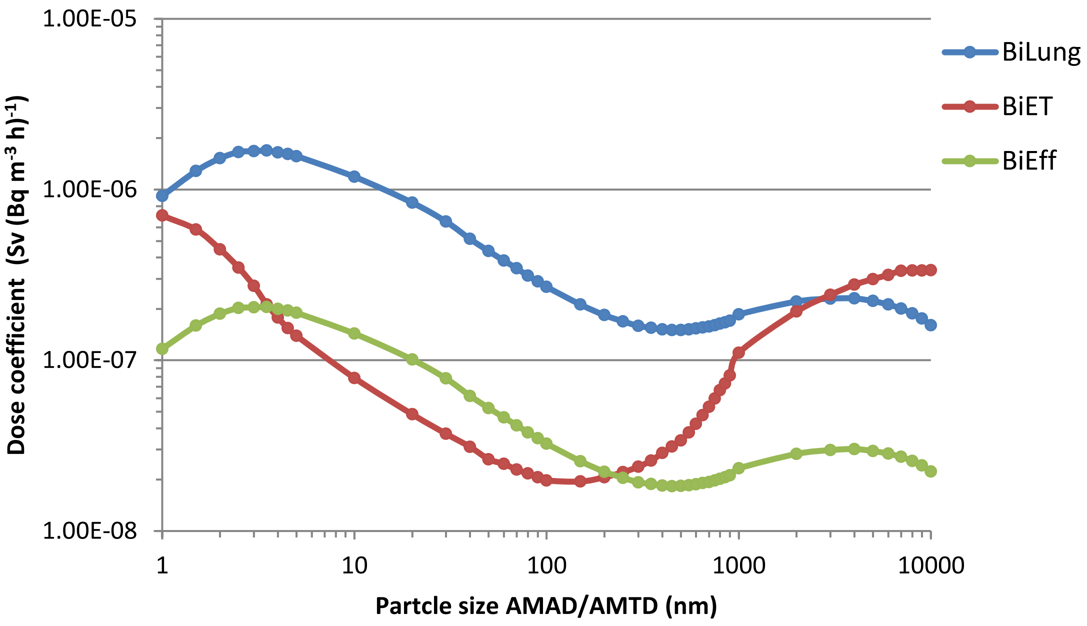

Figure 5.6: Variation of Effective dose coefficient and equivalent dose coefficient for lung and extra thoracic region for^{212}Bi as a function of particle size

The figures also show variation of the equivalent dose coefficient for lung and extra thoracic region with particle size for the two decay products. It can be seen that the general trend of variation of the overall effective dose coefficient and equivalent dose coefficients to the lung and extra thoracic regions is similar for both ^{212}Pb and ^{212}Bi. However, the value of dose coefficients for ^{212}Bi is always lower than ^{212}Pb, due to the small contribution of ^{212}Bi to equilibrium equivalent concentration of thoron (EETC). The maximum dose due to both the decay products is for particles with AMTD of 3 nm, which corresponds to the size of unattached particles of thoron decay products. In most practical cases, the unattached fraction of thoron decay products is constituted of ^{212}Pb only and the effective dose coefficient for ^{212}Pb corresponding to this size is 1050 nSv (Bq m^{-3} h)$^{-1}$. As the size of particle increases, the effective dose co-efficient decreases and reaches a minimum value at particle size of about 500 nm. From there on it increases with the particle size up to a size of 4000 nm and again decreases gradually.

It can also be observed that the effective dose coefficient mostly follows the trend of equivalent dose coefficient of lung and is less influenced by variation in the equivalent dose to extra thoracic region. This can be explained by the fact that the tissue weighting factor for lungs is 13 times higher than that for extra thoracic region.

For the estimation of an overall effective dose conversion factor for thoron, the individual dose coefficient of ^{212}Pb and ^{212}Bi are multiplied with the fraction of individual activity in unit concentration, i.e. 1 Bq of overall equilibrium equivalent concentration of thoron decay products (EETC), and summed. For multi-modal aerosol distribution, the above step is carried out for each of the individual aerosol modes and the overall dose coefficient is obtained by summing the dose coefficients for all modes, as shown in equation 5.7:

$$E = \sum_{m} f_m \sum_{i} C_{m,i} e_{m,i} \qquad \textbf{5.7}$$

where E (Sv (Bq EETC m^{-3} h)$^{-1}$) is the dose conversion factor for thoron, index m represents a particular mode of aerosol, f_m is the fraction of activity in a particular aerosol size mode, index i refers to the decay product ^{212}Pb or ^{212}Bi, $C_{m,i}$ is the concentration of decay product i in size distribution m that contribute to 1 Bq of EETC and $e_{m,i}$ is the effective dose coefficient for the decay product i with size distribution of mode m.

5.4. Comparison of dose to ICRP standard worker and Indian worker

The ICRP thoron dose conversion factors are obtained by dosimetric calculations done for ICRP standard worker based on the parameters for Caucasian body structure. The body structure of Indians is smaller as compared to Caucasians. This difference in the body structure is expected to lead to a different dose conversion factor owing to the changes in the lung deposition pattern and the different sizes of the organs. To study the exact difference that can arise because of the difference in body structure, which is human respiratory tract in present calculations, the dose coefficients to Indian worker were calculated with exposure conditions same as used for calculation of ICRP 130 dose factors. The dose coefficient for exposure to a single mode of log normally distributed decay products of a particular AMTD or AMAD with the corresponding geometric standard deviation (σ_g) specified by ICRP were calculated. For the particle sizes below 5nm, the AMTD and σ_g value of 1.3 were used, for particles in the size range from 5 nm and up to less than 1000 nm, the AMTD and σ_g value of 2.0 were used; whereas for particle sizes from 1000 nm and above, the AMAD and σ_g value of 2.5 were used for calculations. Since particles sizes of less than 5 nm corresponds to unattached decay products, and in case of thoron only ^{212}Pb can constitute this fraction, the exposure only to ^{212}Pb with a concentration corresponding to 1 Bq m^{-3} EEC of thoron (=1.1 Bq m^{-3}) was assumed. For all the particle size modes above this a ^{212}Pb:^{212}Bi ratio of 1:0.25 was assumed and the concentrations resulting in 1 Bq m^{-3} EEC of thoron (= 1.072 Bq m^{-3} of ^{212}Pb and 0.0225 Bq m^{-3} of ^{212}Bi) were used to calculate the dose conversion factor for thoron.

The variation of dose coefficient for Indian worker calculated in this study, with the inhaled particle sizes is shown in Figure 5.7, along with the corresponding ICRP dose coefficient for inhalation of the thoron decay products. The values of dose coefficient provided by ICRP 137 were in the units of mSv WLM^{-1}, and were converted to the units of nSv (Bq EETC m^{-3} h)$^{-1}$ for direct comparison [40].

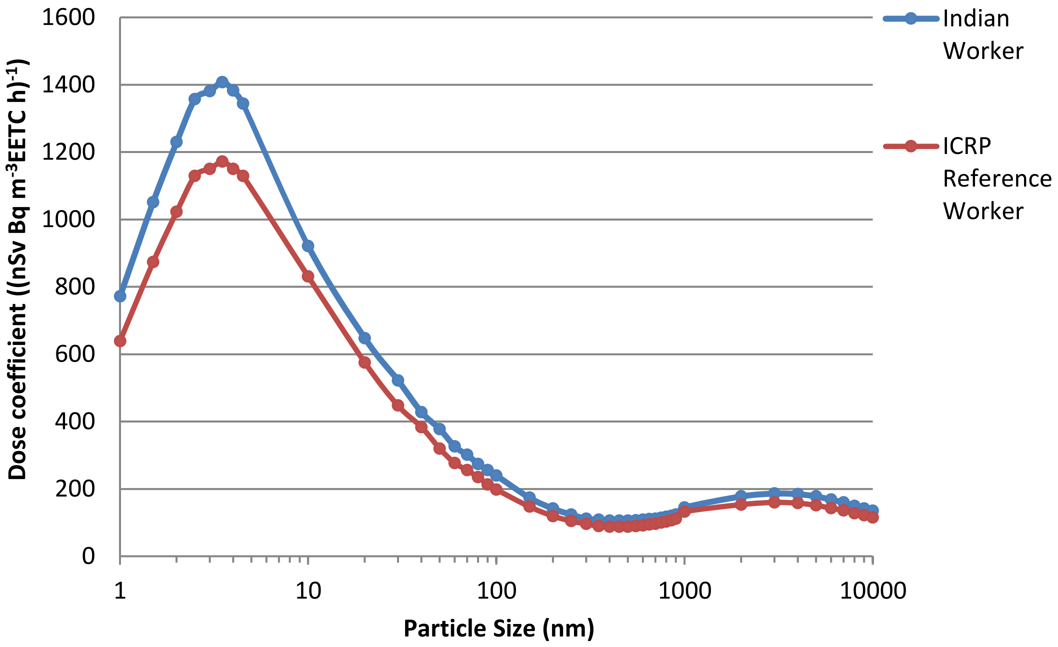

Figure 5.7: Comparison of thoron dose conversion factor calculated for Indian worker and ICRP dose conversion factor

It can be seen that though the general nature of the graph for variation of dose with respect to inhaled particle size was similar for the two cases, the dose conversion factor for Indian worker was higher than that of ICRP by 10 to 20 per cent. This may be attributed to the fact that the intake of radioactivity per unit time of exposure was same for both, but due to the smaller organ sizes, the dose to Indian worker was larger for same amount of radiation energy absorbed. Thus, it can be concluded that the effect of body structure of exposed individual can affect the dose conversion factor for thoron by 20 per cent. The dose conversion factor to Indian workers calculated for these conditions is presented in

Table 5.4.

Table 5.4: Size dependent dose conversion factor for Indian worker considering exposure to thoron decay product activity with unimodal size distribution

Unattached mode		Nucleation and Accumulation modes				Coarse mode	
σ_g=1.3		σ_g=2.0				σ_g=2.5	
AMTD (nm)	nSv h^{-1} (Bq m^{-3} EETC$)^{-1}$	AMTD (nm)	nSv h^{-1} (Bq m^{-3} EETC$)^{-1}$	AMTD (nm)	nSv h^{-1} (Bq m^{-3}EETC$)^{-1}$	AMAD (nm)	nSv h^{-1} (Bq m^{-3} EETC$)^{-1}$
1	781	10	921	300	112	1000	145
1.5	1051	20	648	350	108	2000	178
2	1229	30	522	400	106	3000	186
2.5	1357	40	428	450	106	4000	184
3	1380	50	378	500	106	5000	178
3.5	1407	60	326	550	107	6000	168
4	1382	70	301	600	108	7000	160
4.5	1344	80	274	650	110	8000	150
10	921	90	256	700	111	9000	142
20	648	100	240	750	114	10000	135
30	522	150	173	800	117		
40	428	200	141	850	120		
50	378	250	123	900	123		

5.5. Study variability of thoron dose in different facilities of thoron fuel cycle

As discussed previously, the dose conversion factors provided by ICRP for thoron in workplaces have been primarily arrived at by considering the work environment for indoor offices. But since the decay product aerosol properties in thorium fuel cycles are very different, specific consideration of the same is required for determining the dose conversion coefficient. It is also desirable to see how the variation of the decay product aerosol properties in the environment of thorium processing facilities can affect the resultant thoron dose conversion factor.

5.5.1. *Effect of attached decay products*

Different facilities of thorium fuel cycle are involved in different kind of activities, resulting in different aerosols in ambient environment. This in turn results in properties of attached thoron decay product aerosols also being different for different facilities. The typical thoron decay product AMAD for facilities associated with 1) Solvent Extraction and Precipitation, 2) Powder Handling, 3) Compaction and Sintering and 4) Pelletizing workshop were obtained by using the values reported for aerosols from the literature [115], [125]–[129] and thoron decay product model described in section 4.3. The results for the same are shown in Table 5.5. The dose coefficients for the attached decay products considering these size ranges were calculated using the procedure described in section 5.2 and the result for the same is also presented in Table 5.5.

Table 5.5: Typical size of attached thoron decay products and corresponding dose range in different types of thorium handling facilities

Type of Facility	Typical Attached mode AMAD (μm)	Typical Dose range nSv (Bq m^{-3} EETC)$^{-1}$ h^{-1}
Solvent Extraction and Precipitation	0.5 - 5	105-180
Powder Handling	3 - 7	160-185
Compaction and Sintering	5-12	130-180
Pelletizing workshop	10-18	80-135

The calculations show that a variation of about 15-70 per cent in the value of dose coefficient for the attached decay products can be expected for same type of facility. An overall variation of up to 100 per cent can be seen when comparing different types of facilities. This shows the importance of considering the sizes of attached thoron decay products for determination of dose in thorium facilities.

5.5.2. Effect of unattached fraction on thoron dose

The unattached fraction of thoron decay products are very small clusters with size ranging between 0.5 nm to about 3 nm. The fraction of unattached decay products with respect to the overall thoron decay product concentration can vary depending upon factors like net environmental aerosol concentration and ventilation rate, as described in section 4.6. The normally expected range for unattached fraction in thorium processing facility is from 3-5 per cent to 15-25 per cent.

The dose conversion factor for unattached decay products was calculated using a lognormal size distribution having AMTD equal to 1 nm and σ_g equal to 1.3. As stated earlier, due to the low concentration of unattached ^{212}Bi in the environment its small fraction in contribution to EETC, the dose due to unattached fraction for thoron decay products can be considered to be only due to ^{212}Pb. The dose conversion coefficient for unattached ^{212}Pb was obtained as 781 nSv (Bq m^{-3} EETC)$^{-1}$ h^{-1}. As this value of dose conversion coefficient is quite high in comparison with the dose conversion coefficients of attached decay products, the overall thoron dose conversion factor will increase considerably with an increase in the unattached fraction. However, the exact nature of this increase will also depend on the nature of attached thoron decay products. The thoron dose conversion factor corresponding to varying value of unattached fraction was calculated for different AMAD of attached decay products considering a unimodal distribution. The results for the same are shown graphically in Figure 5.8.

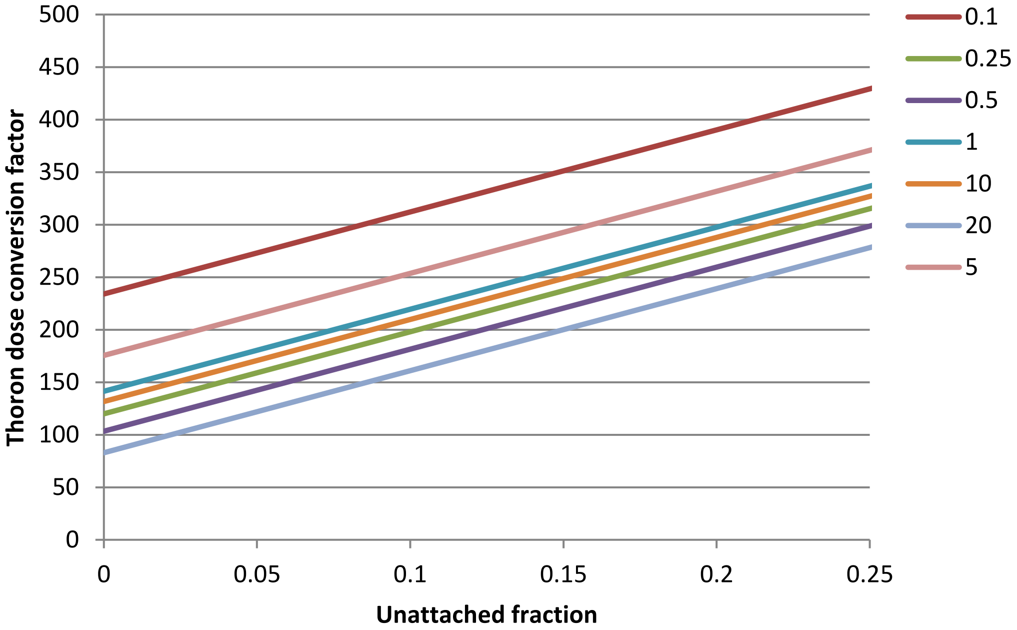

Figure 5.8: Plot for variation of thoron dose conversion factor (nSv (Bq m^{-3} EETC)$^{-1}$ h^{-1}) with the unattached fraction (*f*) for different AMADs of attached decay product size distribution

5.5.3. Dose due to inhalation of thoron gas

ICRP 103 has also given a revised dose co-efficient for inhalation of thoron gas only, obtained from using latest biokinetic and dosimetric model and parametric data. The value of thoron dose co-efficient is 0.15 nSv (Bq m^{-3})$^{-1}$ h^{-1}. The dose due to inhalation of thoron gas itself is normally less than that due to its decay product by an order of 100. Hence the contribution of dose due to thoron gas is normally overlooked when considering the overall thoron dose. However, in case of thorium fuel handling facilities, the contribution due to thoron gas itself can go up to very high levels and cannot be neglected. As discussed in section 4.2 Thoron gas concentration of order of hundreds of kBq m^{-3} can be found at a distance of few tens of centimetres from thorium powders. The radiation dose for exposure to this amount of thoron gas results in a dose rate of the order of 10 µSv h^{-1}, which is quite high significant.

This suggests that there is a potential for dose due to inhalation of thoron gas to reach high levels in case of thorium handling facilities and hence should not be neglected, especially for a small working distance from the source. Proper precautions must be taken by personnel working with thorium bearing materials directly because the thoron gas dose will rise very fast, as one moves nearer to the thoron source. It should also be noted that the particulate filter based respiratory masks which may be very effective for protection against the thoron decay products and help reduce the overall thoron dose substantially, will not be useful against thoron gas.

5.6. Determination of thoron risk from Inhalation Dose

Epidemiological studies carried out in different parts of the world for populations of miners and people exposed to radon in homes have established an increased risk of lung cancer due to exposure to radon [4], [14]. This is also supported by the dosimetric study for radon and knowledge of the biological effects of alpha radiation. Since thoron and its decay products behaviour with respect to the human exposure and dosimetry is very similar to radon, the risk analysis for radon is also applicable in case of thoron. The risk of developing lung cancer is nothing but the probability that a person will be diagnosed with lung cancer. The risk is usually calculated for large population and predicts an average probable number of cases. Because of the probabilistic nature, it cannot be used for deriving any certain conclusions in individual cases.

The risk in case of radon is normally described by the terms of excess relative risk (ERR) using Relative risk models, which assume that the increase in lung cancer risk due to exposure to radon is proportional to background risk. This can be mathematically expressed as:

$$R_{RnExp} = Risk_{Bckgnd}(1 + ERR) \qquad \textbf{5.8}$$

where R_{RnExp} is the net risk of lung cancer after exposure to radon, $Risk_{Bckgnd}$ is the background risk of lung cancer and ERR is the excess relative risk due to exposure to radon.

The ERR is quantitatively expressed using mathematical model obtained from statistical analysis of epidemiological data for exposed populations. The most prominent among them, especially for the case of risk due to occupational exposure to radon is the Exposure-age-duration (EAD) model proposed by Sixth committee on the biological effects of ionizing radiation (BEIR-VI). The model gives excess relative risk (ERR) per unit exposure as:

$$ERR = \beta\left(w_{5-14} + \theta_{15-24}w_{15-24} + \theta_{25+}w_{25+}\right)\varphi_{age}\gamma_z \qquad \textbf{5.9}$$

where, the parameter β represents the rate of increase in risk per unit exposure. Exposure at any particular age is calculated as weighted sum of exposure in different intervals of past time before five years of the age at calculation. These intervals are 5-14 y, 15-24y, and 25+y past the calculation age. The respective exposures w_{5-14}, w_{15-24}, and w_{25+} , are weighed by corresponding weighing fractions, θ_{5-14} (=1), θ_{15-24}, and θ_{25+}. Because of the latency period, the exposure in the last 5 y is not considered in calculation of risk. γ_z is the parameter which accounts for the effect of rate of exposure (exposure duration for same exposure). The effect of a particular level of exposure increases with decreasing exposure rate. The parameter φ_{age} accounts for the observed decrease in the ERR value with increase in age.

The model helps to understand the risk to an individual exposed to radon or thoron. The overall risk due to exposure will be dependent on the background risk of lung cancer which in turn depends on other factors like lifestyle, ethnicity, age etc. The background risk is known to be considerably higher in case of smokers; hence the risk due to thoron and its decay products exposure will also be more for them. According to the model, for a single exposure the risk of lung cancer decreases with time since exposure. Calculation of ERR for individuals of different age exposed to an equilibrium equivalent thoron concentration of 10 Bq m^{-3} for a period of 1 year (8000 hours), at different times after exposure was done using the EAD model. The results for the same are shown graphically in Figure 5.9.

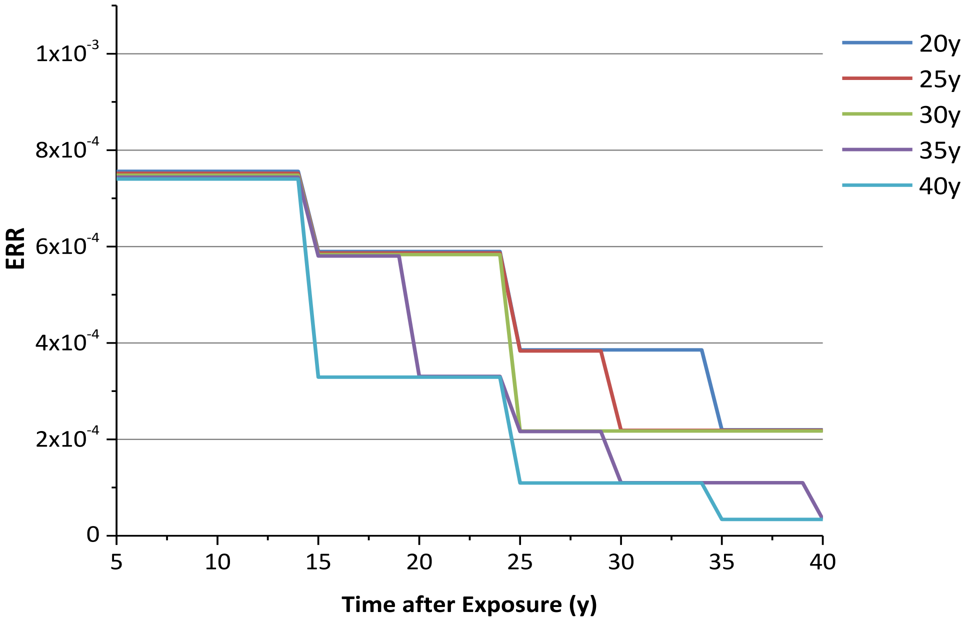

Figure 5.9: Plot of excess relative risk at different time intervals from the exposure to 8×10^4 Bq m^{-3} h, for different age at exposure

5.7. Summary

The work done towards study of radiation dosimetry with respect to exposure to thoron and its decay products is presented in this chapter. The primary pathway for exposure to thoron and its decay products being inhalation, the ICRP HRT model was used to study thoron dose. The deposition pattern for thoron decay products in the respiratory tract was estimated using ICRP lung deposition model followed by calculation of number of radioactive transformations in the respiratory tract using the ICRP 130 HRT model and dosimetry model. The thoron dose conversion factor for Indian worker was calculated by modifying the lung deposition model using suitable scaling factor derived on the basis of physical and physiological parameters reported in literature for Indian adult male. The calculation showed that the dose to Indian worker was higher by 10 to 20 per cent as compared to ICRP standard worker. A software program was written to implement the calculations. The results for study of effect of thoron decay product properties like activity size distribution and unattached fraction on thoron dose conversion factor was presented. The significance of radiation dose due to thoron gas itself was discussed. The general variation of thoron risk following exposure was discussed for different ages of individual using a typical risk model for radon exposure.

Chapter 6

CONCLUDING REMARKS OF THE THESIS

6.1. Summary and Conclusions

In context of the imminent plan of India to take up thorium based reactors for generation of nuclear power based electricity and the large number of facilities that will be required to cater to thorium fuel cycle, the study of thoron risk in these facilities achieves considerable significance. Thoron emission, which is generally not a major radiological concern in normal environments, will however, be an important issue in case of thorium handling facilities because of the extremely high thoron emission potential of the materials handled. Much of the research previously done in case of thoron is for normal residential environments considering thoron emission from natural earthen materials. The work presented in this thesis was taken up considering the need to have the readiness to deal with thoron issue in occupational environments of thorium processing facilities. In order to address it, a conceptual framework was developed which divided the issue into three components: 1) Source term estimation, 2) Thoron and decay product behaviour in occupational environment, and 3) Dose calculation. The thesis has also been written and presented along these lines.

The materials handled in the thorium fuel cycle facilities and the processes to which they are submitted are very different from the natural materials, on which most of the prior research was focussed. The two main areas in case of thorium fuel processing, where thoron emission can take place were identified as porous material handling and bubbling of air through thorium bearing liquid on the basis of careful analysis and observations in the existing nuclear fuel facilities. In porous materials thoron can come out from a deeper layer of source under the surface by diffusion through pores. Hence a diffusion based model for thoron emission from a porous material was developed and validated for thorium powders and monazite rich sands. The model can be applied to calculate thoron emission from sources with different geometries using the surface area available for emission with thoron mass emanation rate and diffusion length as input parameters. Simple setups were developed to measure these parameters in-situ. The general range for value of these parameters was also discussed to help in choosing suitable values in cases where actual measurement is not possible. The effect of various parameters like moisture content and heating on thoron emission was also discussed to account for changes in thoron emission in situations like drying of wet filtered precipitates or subjecting of thorium powders to processes like calcination.

An important basic property which determines the thoron emission potential for a material is its emanation coefficient. It was studied in detail for case of simple grain structures which can be observed for materials like sand. Geometry based thoron emanation models were developed for the shapes of cylinder, octahedron and parallelepiped, which can be applied to grain sizes where edge effect is negligible. The models have a high utility value in explaining the dependence of emanation coefficient on grain size for many materials. Emanation coefficient for powders having structures of the form ‘aggregate of granulates’ was also discussed and challenges this complex geometry presents for any generalisation of emanation behaviour were brought out.

For thoron emission from liquids, laboratory scale measurements were carried out to measure the liquid to air thoron transfer factor. The measured values were compared with the predictions of ‘single bubble thoron transfer model’. Though the range of bubble residence time and bubble size was small, the measurements are of importance because such data has been obtained for the first time in case of thoron. The measured values of transfer factor were comparable to those predicted by the model. This showed that the model could be used to estimate the thoron transfer factor.

The work done towards thoron source term estimation is a novel contribution which now provides a substantive idea of thoron emission in thorium processing facilities and equips with the required theoretical models and measurement tools to predict thoron source term, which is a prerequisite for any strategy to deal with radiological risk due to thoron and its decay products.

The next component in the framework to address the thoron problem is Behaviour of thoron and its decay products in the occupational environment. Due to its short half-life, thoron demonstrates unique non-uniform concentration profiles. A model for thoron concentration distribution was derived assuming diffusive transport in air and a simplified geometry of point source. Though the model over simplifies the actual thoron behaviour, it is very helpful to understand the general nature of thoron concentration variation around the source. An understanding of this is necessary especially in case of workers working with high thorium content sources, where moving closer to the source by some distance can increase the exposure to thoron gas considerably.

The major component of thoron dose is however delivered by the decay products. The properties of thoron decay products are governed by the environmental aerosols, the ventilation rate and room dimensions. These properties are very different in case of thorium processing facilities because of the forced ventilation, formation of aerosols from industrial processes and higher turbulence in air. A decay product model was developed for predicting properties in occupational environment which used parameters such as aerosol size averaged attachment rates and deposition velocities, room dimensions and ventilation rate as input parameters. Simple working relations between aerosol size distribution and average attachment rate and deposition velocity was provided for use in the thorium facilities. The model was validated for occupational environment through comprehensive multi-parametric measurements in a thorium processing facility. The model was also validated for dwellings environment through measurements in twenty-five houses in two different parts of India. A new method for thoron dose estimation in houses emerged as an outcome of this work.

The application of this model for study of thoron decay products in a typical thorium facility helped to obtain an insight of how the various factors acting in presence of each other influenced the decay products' properties. The aerosol generation rate is higher in occupational environments as compared to houses, but the removal rate is also higher because of forced ventilation which results in the aerosol number concentration which is comparable to normal living environment. However, the size characteristics of aerosols are purely governed by the processes taking place in the facility and hence not only are they different from normal environments but there is a considerable difference even amongst the different types of facilities, as evident from the size characteristics data for the different facilities published in literature. The developed model can be used with information on thoron source term, ventilation and characteristics of environmental aerosols to predict the properties of thoron decay products which are very important for use in estimation of radiation dose due to thoron.

The last component of the framework to address the radiological risk due to thoron and its decay products is determination of radiation dose. Inhalation is the main pathway for exposure to thoron for personnel working in thorium processing facilities. The dose is hence dependent on the amount of inhaled radioactivity, the activity size distribution of radioactive decay products and physiological parameters for the exposed individual. The latest ICRP human respiratory tract model and dosimetric model was used to calculate the dose delivered to human respiratory tract, which constitutes almost the entire dose due to thoron and its decay products. A program was written in Wolfram Mathematica to implement the model and to work with the various parameters of the model. Due to the difference in body structure of a typical Indian adult male and ICRP standard worker based on Caucasian male body, the dose coefficients for the standard Indian worker were expected to be different from the ICRP dose coefficients. Hence the lung deposition model was modified by using scaling factors based on body structure of Indian adult male obtained from literature. The values of dose conversion factor for Indian worker were higher than the corresponding ICRP dose conversion factor by 10-20 per cent for different sizes of thoron decay products. The thoron dose conversion factor values were calculated over a wide range of size for attached decay products. The effect of change in unattached fraction of decay products on the dose was also discussed.

The analysis for thoron dose dependence on different factors showed that it is quite sensitive to the size distribution of the thoron decay products. The breathing rate was also an important parameter affecting the dose as it decided the amount of inhaled radioactivity for same exposure. Hence it is necessary to take into account the type of physical activity, an occupational worker will be involved in, before estimating the dose. In case of labour intensive work, the dose will be much more for exposure to same airborne radioactivity for same time.

The variation of risk following exposure to thoron decay product at different ages was discussed using BEIR-VI model for radon risk. It should however be noted that the dosimetric approach for radon and thoron dose and risk estimation has always overestimated the risk actually obtained from epidemiology. The choice of methodology for dose estimation for radiological protection purpose is a topic of intense research and debate in current time. However, the work done on dose estimation greatly contributes to the understanding of how different parameters influence the thoron dose received by an individual working in a thorium facility.

To sum up, the work presented in this dissertation is an important original contribution to the area of thoron dose and risk estimation for thorium fuel cycle facilities. It provides necessary tools for estimation of risk in upcoming facilities catering to thorium based reactors proposed to be built in India. It provides new information and models for thoron emission from materials handled in thorium fuel cycle, the concentration and properties of thoron and decay products in the occupational environments and thoron dose estimation. These equip us to make predictions for thoron right from its source term to its concentration in workplaces and finally to the radiation dose. This information is crucial for planning the radiation protection measures and systems at the stage of designing of facilities. It is also useful in dealing with the radiological risk due to thoron and its decay products in present facilities in a better way.

6.2. Future Scope

Though an attempt was made to treat all the issues of importance for thoron risk estimation in thorium fuel cycle with great detail, some remain open to further investigation and more detailed study. An experimental study was carried out to measure thoron transfer factor for bubbling in liquid but the same can be expanded to cover a wider range of bubble rise time and bubble size. The effect of heating on thoron emission from powers was addressed only through theoretical treatment. The same can also be studied experimentally for different sets of thorium powders, but will require advanced measurement setups. In case of thoron decay product behaviour in occupational environment greater information is required for predicting the effect of ventilation on turbulence in air and hence the deposition velocities for aerosols. This can be achieved through a combination of experimental investigation along with tools like computational fluid dynamics (CFD). The thoron gas concentration profiles can also be better predicted by use of more realistic source geometries and use of CFD. How the presence of various structures like process equipment present in a room can affect the turbulence in air and deposition of decay products and aerosols in general on its surfaces is another interesting area which demands attention.

The Room model for thoron and its decay products assumes that unattached ^{212}Pb has a homogeneous distribution. Though this is a good and justified simplification, in reality the concentration of unattached ^{212}Pb is greater close to the thoron source because the freshly originated ^{212}Pb is unattached and it takes some time to attach to aerosol particles. How this affects the dose distribution in the room can also be studied in greater detail.

In case of dose estimation, only dose to the human respiratory tract was estimated in the present study. However, the accuracy can be increased by calculating the dose to all other organs to account for whatever minor contribution they make. The present estimation of thoron risk is carried out by comparing their radiological potency through dosimetric calculation and then proportionately mapping the radon risk. But it is always desirable to have direct estimate of thoron risk by identifying populations like nuclear workers with exposure to thoron and tapping them for thoron epidemiology. The thorium processing facilities can provide opportunity for such study.

In the end, it is hoped that the work done and the various insights obtained through this study will stimulate further field studies and theoretical modeling to address the radiological issue of thoron in thorium fuel cycle facilities. This will have an immense practical value for radiation protection of the large number of occupational persons who will be involved in the thorium processing facilities.

REFERENCES

[1] "Properties and behaviour of radon and thoron and their decay products in the air," J. Porstendörfer, *J. Aerosol Sci.*, **1994**, *vol.* 25, *no.* 2, 219–263.

[2] *Sources and Effects of Ionizing Radiation: UNSCEAR 2000 Report to the General Assembly with Scientific Annexes*, UNSCEAR, **2000**. New York: United Nations.

[3] *Effects of Ionizing Radiation: UNSCEAR 2006 Report to the General Assembly with Scientific Annexes, Volume II Scientific AnnexesC, D and E*, UNSCEAR, **2009**. New York: United Nations Publication.

[4] *Who Handbook on Indoor Radon - A Public Health Perspective*, WHO, **2009**. Geneva: World Health Organization.

[5] "Contribution of Thoron and Progeny Towards Inhalation Dose in a Thorium Abundant Beach Environment," A. K. Visnuprasad, G. Jaikrishnan, B. K. Sahoo, C. E. Pereira, P. J. Jojo, L. Level, B. Atomic, R. Physics, A. Division, B. Atomic, and P. New, *Radiat. Prot. Dosimetry*, **2017**, *vol.* 178, *no.* January, 405–413.

[6] "Measurements of radon and thoron concentrations in high radiation background area using pin-hole dosimeter," R. C. Ramola, B. S. Rautela, G. S. Gusain, G. Prasad, S. K. Sahoo, and S. Tokonami, *Radiat. Meas.*, **2013**, *vol.* 53–54, 71–73.

[7] "Environmental 220Rn: A review," F. Steinhäusler, *Environ. Int.*, **1997**, *vol.* 22, *no.* SUPPL. 1.

[8] "Energy from thorium — An Indian perspective," U. Kannan and P. D. Krishnani, *Sadhana*, **2013**, *vol.* 38, *no.* 5, 817–837.

[9] "Utilisation of thorium in reactors," K. Anantharaman, V. Shivakumar, and D.

Saha, *J. Nucl. Mater.*, **2008**, *vol.* 383, *no.* 1–2, 119–121.

[10] "Role of thorium in the Indian nuclear power programme," P. K. Vijayan, V. Shivakumar, S. Basu, and R. K. Sinha, *Prog. Nucl. Energy*, **2017**, *vol.* 101, 43–52.

[11] "The Indian perspective on thorium fuel cycles," K. Balakrishnan, S. Majumdar, A. Ramanujam, and A. Kakodkar, *Thorium fuel Util. Options trends*, **2002**, 257.

[12] "Design and development of the AHWR—the Indian thorium fuelled innovative nuclear reactor," R. K. Sinha and A. Kakodkar, *Nucl. Eng. Des.*, **2006**, *vol.* 236, *no.* 7–8, 683–700.

[13] "Conceptual design of Indian molten salt breeder reactor," P. K. Vijayan, A. Basak, I. V. Dulera, K. K. Vaze, S. Basu, and R. K. Sinha, *Pramana - J. Phys.*, **2015**, *vol.* 85, *no.* 3, 539–554.

[14] "ICRP Publication 115 Lung Cancer Risk from Radon and Progeny and Statement on Radon," M. Tirmarche, J. D. Harrison, D. Laurier, F. Paquet, E. Blanchardon, J. W. Marsh, and Others, *Ann. ICRP*, **2010**, *vol.* 40, *no.* 1, 1–64.

[15] *Health Effects of Exposure to Radon: BEIR VI*, National Research Council, **1999**, *vol.* 6. Washington, D.C.

[16] *Sources, Effects and Risks of Ionizing Radiation, United Nations Scientific Committee on the Effects of Atomic Radiation (UNSCEAR) 2016 Report: Report to the General Assembly, with Scientific Annexes*, UNSCEAR, **2017**. New York: United Nations Publication.

[17] "Progress in Nuclear Energy The evolution of the Indian nuclear power programme," S. Banerjee and H. P. Gupta, *Prog. Nucl. Energy*, **2017**, *vol.* 101, 4–18.

[18] "Processing of Indian monazite for the recovery of thorium and uranium values," T. K. Mukherjee, , *Characterisation and quality control of nuclear fuels,* **2004**, C. Ganguly and R. N. Jayaraj, Eds. New Delhi: Allied Publishers Pvt Ltd.

[19] "Monazite, the Basic Raw Material for Rare Earths Beneficiation from Beach Sands," V. S. Bashir, *Mater. Sci. Forum,* **1988**, *vol.* 30, 33–44.

[20] "Assessment of Radiological Safety for Irradiated Thorium Fuel Handling Operations," P. Srinivasan, P. C. Gupta, D. N. Sharma, H. S. Kushwaha, R. Safety, S. Division, E. Group, and B. Atomic, in *IAEA 12th International Congress of the International Radiation Protection Association (IRPA-12),* **2008**.

[21] "Estimation of dose rates on the PHWR irradiated thorium oxide bundles based on BARC updated nuclear data," P. Srinivasan, S. Ganesan, D. N. Sharma, and H. S. Kushwaha, in *DAE-BRNS National Workshop on Nuclear Data for Advanced Nuclear Systems, Nuclear Databases and Applications, NWND-2006,* **2006**.

[22] "Burn-up determination of irradiated thoria samples by isotope dilution-thermal ionisation mass spectrometry," S. K. Aggarwal, P. G. Jaison, V. M. Telmore, R. V Shah, V. L. Sant, K. Sasibhushan, A. R. Parab, and D. Alamelu, **2010**.

[23] "Radon Emanation Mechanism from Finely Ground Rocks," P. Kruger and K. Satomi, **1982**, Stanford University.

[24] "Initial sintering stage of thoria powder investigated by emanation thermal analysis," **1982**, *vol.* 17, 1269–1276.

[25] "Modeling and Measurement of Radon and Thoron Emission from Naturally Occurring Radioactive Materials Modeling and Measurement of Radon and Thoron," B. K. Sahoo, **2013**, Homi Bhabha National Institute.

[26] “Radon and thoron exhalation from the ground,” K. Megumi and T. Mamuro, *J. Geophys. Res.*, **1973**, *vol.* 78, *no.* 11, 1804–1808.

[27] “Influence of soil environmental parameters on thoron exhalation rate,” M. Hosoda, S. Tokonami, A. Sorimachi, T. Ishikawa, S. K. Sahoo, M. Furukawa, Y. Shiroma, Y. Yasuoka, M. Janik, N. Kavasi, and others, *Radiat. Prot. Dosimetry*, **2010**, *vol.* 141, *no.* 4, 420–423.

[28] “The flux of radon and thoron from Australian soils,” S. D. Schery, S. Whittlestone, K. P. Hart, and S. E. Hill, *J. Geophys. Res. Atmos.*, **1989**, *vol.* 94, *no.* D6, 8567–8576.

[29] “Distributions of Indoor Radon and Thoron,” E. Centre and Zhuo, *Radiat. Prot. Dosimetry*, **2001**, *vol.* 93, *no.* 4, 357–368.

[30] “Spatial distribution of thoron and radon concentrations in the indoor air of a traditional Japanese wooden house.,” M. Doi, K. Fujimoto, S. Kobayashi, and H. Yonehara, *Health Phys.*, **1994**, *vol.* 66, *no.* 1, 43–49.

[31] “Thoron, radon and air ions spatial distribution in indoor air,” P. Kolarž, J. Vaupotič, I. Kobal, P. Ujić, Z. Stojanovska, and Z. S. Žunić, *J. Environ. Radioact.*, **2017**, *vol.* 173, 70–74.

[32] “Characteristic of thoron (220 Rn) in environment,” M. Hosoda, H. Kudo, K. Iwaoka, R. Yamada, and T. Suzuki, **2017**, *vol.* 120, *no.* October 2016, 7–10.

[33] “A theoretical approach to indoor radon and thoron distribution,” V. Urosevic, D. Nikezic, and S. Vulovic, *J. Environ. Radioact.*, **2008**, *vol.* 99, *no.* 12, 1829–1833.

[34] “Physical parameters and dose factors of the radon and thoron decay products.,” J. Porstendörfer, J. Porstendo, V. Dankelmann, A. Reineking, and J.

Porstendörfer, *Radiat. Prot. Dosimetry,* **2001**, *vol.* 94, *no.* 4, 365–373.

[35] "Specific properties of a model of thoron and its decay products in indoor atmospheres," O. Meisenberg and J. Tschiersch, *Nukleonika,* **2010**, *vol.* 55, *no.* 4, 463–469.

[36] "ICRP Publication 32 Limits for Inhalation of Radon Daughters by Workers," ICRP, *Ann. ICRP,* **1981**, *vol.* 6, *no.* 1.

[37] "The New ICRP Model for the Respiratory Tract," M. R. Bailey, , **1994**, *Radiat Prot Dosimetry, vol.* 53. 107–114.

[38] *Protection Against Radon-222 at Home and at Work. ICRP Publication 65,* ICRP, **1993**, *vol.* 23, *no.* 2. Pergamon Press.

[39] "Sources-to-Effects Assessment for Radon in Homes and Workplaces," A. E. UNSCEAR, *United Nations, New York,* **2006**.

[40] "ICRP Publication 137: Occupational Intakes of Radionuclides: Part 3.," F. Paquet, M. R. Bailey, R. W. Leggett, J. Lipsztein, J. Marsh, T. P. Fell, T. Smith, D. Nosske, K. F. Eckerman, V. Berkovski, and others, *Ann. ICRP*, **2017**, *vol.* 46, *no.* 3–4, 1–486.

[41] "Building materials as a source of indoor radon," E. Stranden, , *Radon and its decay products in indoor air,* **1988**, W. W. Nazaroff and A. V Nero, Eds. New York: John Wiley & Sons NY, 1–608.

[42] "Radon transport from soil to air," W. W. Nazaroff, *Rev. Geophys.,* **1992**, *vol.* 30, *no.* 2, 137–160.

[43] "Emanation and exhalation of radon and thoron gases from soil particles," K. Megumi and T. Mamuro, *J. Geophys. Res.*, **1974**, *vol.* 79, *no.* 23, 3357–3360.

[44] *Measurement and calculation of radon releases from NORM residues:*

Technical Report Series No 474, Y. Ishimori, K. Lange, P. Martin, Y. S. Mayya, and M. Phaneuf, **2013**. Vienna: IAEA Publications.

[45] “A combined analysis of North American case-control studies of residential radon and lung cancer,” D. Krewski, J. H. Lubin, J. M. Zielinski, M. Alavanja, V. S. Catalan, R. William Field, J. B. Klotz, E. G. Létourneau, C. F. Lynch, J. L. Lyon, and others, *J. Toxicol. Environ. Heal. Part A*, **2006**, *vol.* 69, *no.* 7–8, 533–597.

[46] “Radon in homes and risk of lung cancer: collaborative analysis of individual data from 13 European case-control studies.,” S. Darby, D. Hill, A. Auvinen, J. M. Barros-Dios, H. Baysson, F. Bochicchio, H. Deo, R. Falk, F. Forastiere, M. Hakama, I. Heid, L. Kreienbrock, M. Kreuzer, F. Lagarde, I. Mäkeläinen, C. Muirhead, W. Oberaigner, G. Pershagen, A. Ruano-Ravina, E. Ruosteenoja, A. S. Rosario, M. Tirmarche, L. Tomásek, E. Whitley, H.-E. Wichmann, and R. Doll, *BMJ*, **2005**, *vol.* 330, *no.* 7485, 223.

[47] “Risk of lung cancer and residential radon in China: Pooled results of two studies,” J. H. Lubin, Z. Y. Wang, J. D. Boice, Z. Y. Xu, W. J. Blot, L. De Wang, and R. A. Kleinerman, *Int. J. Cancer*, **2004**, *vol.* 109, *no.* 1, 132–137.

[48] “Risk of lung cancer associated with residential radon exposure in south-west England: a case-control study.,” S. Darby, E. Whitley, P. Silcocks, B. Thakrar, M. Green, P. Lomas, J. Miles, G. Reeves, T. Fearn, and R. Doll, *Br. J. Cancer*, **1998**, *vol.* 78, *no.* 3, 394–408.

[49] “An overview of thoron and its progeny in the indoor environment,” J. Mclaughlin, *Radiat. Prot. Dosimetry*, **2010**, *vol.* 141, *no.* 4, 316–321.

[50] “Thoron: Its metrology, health effects and implications for radon epidemiology:

A summary of roundtable discussions," S. Akiba, S. Tokonami, F. Bochicchio, J. McLaughlin, L. Tommasino, and N. Harley, *Radiat. Prot. Dosimetry*, **2010**, *vol.* 141, *no.* 4, 477–481.

[51] "Characteristics of thoron and thoron progeny in Canadian homes," J. Chen, D. Moir, A. Sorimachi, and S. Tokonami, *Radiat. Environ. Biophys.*, **2011**, *vol.* 50, *no.* 1, 85–89.

[52] "Increased indoor thoron concentrations and implication to inhalation dosimetry," J. Tschiersch, W. B. Li, and O. Meisenberg, *Radiat. Prot. Dosimetry*, **2007**, *vol.* 127, *no.* 1–4, 73–78.

[53] "Modeling seasonal variation in indoor radon concentrations.," D. Krewski, R. Mallick, J. M. Zielinski, and E. G. Létourneau, *J. Expo. Anal. Environ. Epidemiol.*, **2005**, *vol.* 15, *no.* 3, 234–43.

[54] "Lung cancer in French and Czech uranium miners: radon-associated risk at low exposure rates and modifying effects of time since exposure and age at exposure," L. Tomasek, A. Rogel, M. Tirmarche, N. Mitton, and D. Laurier, *Radiat. Res.*, **2008**, *vol.* 169, *no.* 2, 125–137.

[55] "Unattached fraction and size distribution of aerosol-attached radon and thoron daughters in realistic living atmospheres and their influence on radiation dose," A. Reineking, G. Butterweck, J. Kesten, and J. Porstendörfer, , *Indoor radon and lung cancer: Reality or Myth? Part 1*, **1992**, F. T. Cross, Ed. Colombus, Ohio: Battelle Press.

[56] "Development of online thoron monitor for thoron and its flux measurements in HBRA," J. J. Gaware, B. K. Sahoo, S. D. Kanse, B. K. Sapra, and Y. S. Mayya, in *Proceedings of the seventh international conference on high levels of natural*

radiation and radon areas: abstracts, **2010**.

[57] "Powder sandwich technique: A novel method for determining the thoron emanation potential of powders bearing high224Ra content," S. D. Kanse, B. K. Sahoo, B. K. Sapra, J. J. Gaware, and Y. S. Mayya, *Radiat. Meas.*, **2013**, *vol.* 48, *no.* 1, 82–87.

[58] "A new pin-hole discriminated222Rn/220Rn passive measurement device with single entry face," B. K. Sahoo, B. K. Sapra, S. D. Kanse, J. J. Gaware, and Y. S. Mayya, *Radiat. Meas.*, **2013**, *vol.* 58, 52–60.

[59] "Improvements in the spark counting technique for damage track neutron dosemeters," W. G. Cross and L. Tommasino, **1972**.

[60] "Study of a deposition-based direct thoron progeny sensor (DTPS) technique for estimating equilibrium equivalent thoron concentration (EETC) in indoor environment," R. Mishra and Y. S. Mayya, *Radiat. Meas.*, **2008**, *vol.* 43, *no.* 8, 1408–1416.

[61] "Measurement of 220Rn/222Rn progeny deposition velocities on surfaces and their comparison with theoretical models," R. Mishra, Y. S. Mayya, and H. S. Kushwaha, *J. Aerosol Sci.*, **2009**, *vol.* 40, *no.* 1, 1–15.

[62] "Development of an integrated sampler based on direct 222Rn/220Rn progeny sensors in flow-mode for estimating unattached/attached progeny concentration," R. Mishra, B. K. Sapra, and Y. S. Mayya, *Nucl. Instruments Methods Phys. Res. Sect. B Beam Interact. with Mater. Atoms*, **2009**, *vol.* 267, *no.* 21–22, 3574–3579.

[63] *Aerosol technology: properties, behavior, and measurement of airborne particles*, W. C. Hinds, **1999**. John Wiley & Sons.

[64] "Factors controlling the emanation of radon and thoron in soils of the eastern

U.S.A.," D. J. Greeman and A. W. Rose, *Chem. Geol.*, **1996**, *vol.* 129, *no.* 1–2, 1–14.

[65] "Emanating power of Rn from a powdery radiation source," T. Iimoto, T. Nagai, N. Sugiura, and T. Kosako, *Int. Congr. Ser.*, **2005**, *vol.* 1276, 303–304.

[66] "Standardization and difficulties of the thoron exhalation rate measurements using an accumulation chamber," P. Ujić, I. Čeliković, A. Kandić, and Z. Žunić, *Radiat. Meas.*, **2008**, *vol.* 43, *no.* 8, 1396–1401.

[67] "Estimation of radon emanation factor in Indian building materials," B. K. Sahoo, D. Nathwani, K. P. Eappen, T. V. Ramachandran, J. J. Gaware, and Y. S. Mayya, *Radiat. Meas.*, **2007**, *vol.* 42, *no.* 8, 1422–1425.

[68] "An assessment of in situ radon exhalation measurements, and the relation between free and bound exhalation rates," F. J. Aldenkamp, R. J. De Meijer, L. W. Put, and P. Stoop, *Radiat. Prot. Dosimetry*, **1992**, *vol.* 45, *no.* 1–4, 449–453.

[69] "Two dimensional diffusion theory of trace gas emission into soil chambers for flux measurements," B. K. Sahoo and Y. S. Mayya, *Agric. For. Meteorol.*, **2010**, *vol.* 150, *no.* 9, 1211–1224.

[70] "A study of thoron exhalation from monazite-rich beach sands of High Background Radiation Areas of Kerala and Odisha, India," S. D. Kanse, B. K. Sahoo, J. J. Gaware, R. Prajith, and B. K. Sapra, *Environ. Earth Sci.*, **2016**, *vol.* 75, *no.* 23, 1–10.

[71] "Theory of radon exhalation into accumulators placed at the soil-atmosphere interface," Y. S. Mayya, *Radiat. Prot. Dosimetry*, **2004**, *vol.* 111, *no.* 3, 305–318.

[72] "Natural radioactivity and radiation exposure in the high background area at

Chhatrapur beach placer deposit of Orissa, India," A. K. Mohanty, D. Sengupta, S. K. Das, S. K. Saha, and K. V. Van, *J. Environ. Radioact.*, **2004**, *vol.* 75, *no.* 1, 15–33.

[73] *Fabrication of thorium fuel elements*, L. R. Weissert and G. Schileo, **1968**. American Nuclear Society.

[74] "Thermal decomposition of oxalates of lanthanum and thorium in vacuum.," O. K. Srivastava, A. R. Murthy, and Vasudeva, *J. Indian Inst. Sci.*, **1965**, *vol.* 47, *no.* 3, 87.

[75] "Thorium--Preparation and Properties," J. F. Smith, O. N. Carlson, D. T. Peterson, and T. E. Scott, *Iowa State Univ. Press. Ames. 1975, 385 p*, **1975**.

[76] "Thorium oxide: Calcination, compaction and sintering," P. Balakrishna, B. P. Varma, T. S. Krishnan, T. R. R. Mohan, and P. Ramakrishnan, *J. Nucl. Mater.*, **1988**, *vol.* 160, *no.* 1, 88–94.

[77] "Study of the Changes in Composition of Ammonium Diuranate with Progress of Precipitation, and Study of the Properties of Ammonium Diuranate and its Subsequent Products Produced from both Uranyl Nitrate and Uranyl Fluoride Solutions," S. Manna, R. Kumar, S. K. Satpati, S. B. Roy, and J. B. Joshi, *Nucl. Eng. Technol.*, **2017**, *vol.* 49, *no.* 3, 541–548.

[78] "Geochemical studies of monazite sands of Chhatrapur beach placer deposit of Orissa, India by PIXE and EDXRF method," A. K. Mohanty, S. K. Das, V. Vijayan, D. Sengupta, and S. K. Saha, *Nucl. Instruments Methods Phys. Res. Sect. B Beam Interact. with Mater. Atoms*, **2003**, *vol.* 211, *no.* 1, 145–154.

[79] "A review of the studies of high background areas of the SW coast of India," C. M. Sunta, in *Proceedings of the international conference on high levels of*

natural radiation, Ramsar, IAEA, **1993**, 71–86.

[80] "Processing of monazite at the rare earths Division, Udyogamandal," N. S. Narajanan, S. Thulasidoss, T. V Ramachandran, T. V Swaminathan, and K. R. Prasad, in *Materials Science Forum*, **1988**, *vol.* 30, 45–56.

[81] "Radiation dose due to radon and thoron progeny inhalation in high-level natural radiation areas of Radiation dose due to radon and thoron progeny inhalation in high-level natural radiation areas of Kerala , India," Y. Omori, S. Tokonami, and S. K. Sahoo, *J. Radiol. Prot.*, **2017**, *vol.* 37, *no.* 1, 1–16.

[82] "Inhalation exposures due to radon and thoron (222 Rn and 220 Rn): Do they differ in high and normal background radiation areas in India ?," R. Mishra, B. K. Sapra, R. Prajith, R. P. Rout, S. Jalaluddin, and Y. S. Mayya, *J. Environ. Radioact.*, **2015**, *vol.* 147, 125–129.

[83] "Recoil-emanation theory applied to radon release from mineral grains," T. M. Semkow, *Geochim. Cosmochim. Acta*, **1990**, *vol.* 54, *no.* 2, 425–440.

[84] "Die bestimmung von komgrOssen und von diffusionskonstanten aus dem emaniervermdgen (Die theorie der emaniermcthode).," S. Flugge and K. E. Zimens, *Zeitschrift Phys. Chem.*, **1939**, *vol.* B42, 179–220.

[85] "Theoretical estimation of radon emanation coefficients for uo2particles deposited on surfaces of uranium-bearing wastes," T. Sasaki, Y. Gunji, and T. Okuda, *J. Nucl. Sci. Technol.*, **2007**, *vol.* 44, *no.* 5, 774–778.

[86] "SRIM--The stopping and range of ions in matter (2010)," J. F. Ziegler, M. D. Ziegler, and J. P. Biersack, *Nucl. Instruments Methods Phys. Res. Sect. B Beam Interact. with Mater. Atoms*, **2010**, *vol.* 268, *no.* 11–12, 1818–1823.

[87] "Theory of emanation thermal analysis. I. Mathematical model for inert gas

release from porous solids," J. Kříẑ and V. Balek, *Thermochim. Acta*, **1983**, *vol.* 71, *no.* 1–2, 175–185.

[88] "Theory of emanation thermal analysis. X. Characterization of morphology changes during hydration of cementitious binders," V. Balek and I. N. Beckman, *J. Therm. Anal. Calorim.*, **2002**, *vol.* 67, *no.* 1, 37–47.

[89] *The Preparation and Calcination of Ammonium Uranates - A Literature Survey : Report AAEC/TM476*, J. L. Woolfrey, **1968**. Australian Atomic Energy Commission Research Establishment Lucas Heights.

[90] "Effect of ammonium nitrate on precipitation of Ammonium Di-Uranate (ADU) and its characteristics," S. Paik, S. Biswas, S. Bhattacharya, and S. B. Roy, *J. Nucl. Mater.*, **2013**, *vol.* 440, *no.* 1–3, 34–38.

[91] "Physical properties of thorium oxalate powders and their influence on the thermal decomposition," E. Oktay and A. Yayli, *J. Nucl. Mater.*, **2001**, *vol.* 288, *no.* 1, 76–82.

[92] "The Use of Radioactive Inert Gases in the Study of Solids," G. M. Zhabrova and M. D. Shibanova, *Russ. Chem. Rev.*, **1967**, *vol.* 36, *no.* 8, 592–602.

[93] "Mathematical modeling of radon emanation," T. Sasaki, Y. Gunji, and T. Okuda, *J. Nucl. Sci. Technol.*, **2004**, *vol.* 41, *no.* 2, 142–151.

[94] "Theoretical calculation of radon emanation fraction," J. M. Stajic and D. Nikezic, *Nucl. Instruments Methods Phys. Res. Sect. B Beam Interact. with Mater. Atoms*, **2014**, *vol.* 336, 19–25.

[95] "A comprehensive review of radon emanation measurements for mineral, rock, soil, mill tailing and fly ash," A. Sakoda, Y. Ishimori, and K. Yamaoka, *Appl. Radiat. Isot.*, **2011**, *vol.* 69, *no.* 10, 1422–1435.

[96] “Effect of Soil Moisture Content on Radon and Thoron Exhalation,” M. Hosoda, M. Shimo, M. Sugino, M. Furukawa, and M. Fukushi, *J. Nucl. Sci. Technol.*, **2007**, *vol.* 44, *no.* 4, 664–672.

[97] “Influence of soil environmental parameters on thoron exhalation rate,” M. Hosoda, S. Tokonami, A. Sorimachi, T. Ishikawa, S. K. Sahoo, M. Furukawa, Y. Shiroma, Y. Yasuoka, M. Janik, N. Kavasi, S. Uchida, and M. Shimo, *Radiat. Prot. Dosimetry*, **2010**, *vol.* 141, *no.* 4, 420–423.

[98] “Radon exhalation studies in an Indian uranium tailings pile,” B. K. Sahoo, Y. S. Mayya, B. K. Sapra, J. J. Gaware, K. S. Banerjee, and H. S. Kushwaha, *Radiat. Meas.*, **2010**, *vol.* 45, *no.* 2, 237–241.

[99] “Radon Emanation And Transport In Porous Media,” V. Rogers and K. Nielson, *Symp. Radon Radon Reduct. Technol.*, **1988**.

[100] “Radon Emanation in Partially Saturated Porous Media,” P. M. Adler and F. Perrier, *Transp. Porous Media*, **2009**, *vol.* 78, *no.* 2, 149–159.

[101] “Thorium Fuel Cycle and Associated Radiological Issues,” R. M. Tripathi, S. D. Kanse, P. Srinivasan, R. G. Purohit, P. K. Sarkar, Y. S. Mayya, V. D. Puranik, D. N. Sharma, and A. K. Ghosh, , **2012**. .

[102] “ImageJ,” W. S. Rasband, , **1997**. Bethesda, MD.

[103] “Shotcut,” D. Dennedy, , **2015**. Meltytech, LLC.

[104] “Thoron in indoor air: Modeling for a better exposure estimate,” O. Meisenberg and J. Tschiersch, *Indoor Air*, **2011**, *vol.* 21, *no.* 3, 240–252.

[105] “Room model with three modal distributions of attached 220Rn progeny and dose conversion factor,” D. Nikezić and N. Stevanovic, *Radiat. Prot. Dosimetry*, **2007**, *vol.* 123, *no.* 1, 95–102.

[106] "Behaviour of Radon Daughter Products in Indoor Air," J. Porstendörfer, , **1984**, *Radiation Protection Dosimetry, vol.* 7*, no.* 1–4. 107–113.

[107] *Sources and effects of ionizing radiation UNSCEAR 1993 report to the General Assembly,* UNSCEAR, **1993**. New York: United Nations Publication.

[108] "Thoron gas concentration and aerosol characteristics of thoron decay products," A. Reineking, G. Butterweck, J. Kesten, and J. Porstendörfer, *Radiat. Prot. Dosimetry,* **1992**, *vol.* 45, *no.* 1–4, 353–356.

[109] "ICRP Publicaton 66: Human Respiratory Tract Model for Radiological Protection," W. J. Bair, M. R. Bailey, F. T. Cross, R. G. Cuddihy, P. Gehr, W. Stahlhofen, A. C. James, J. R. Johnson, R. Masse, and M. Roy, *Ann. ICRP*, **1994**, *vol.* 24*, no.* 1–3.

[110] "Relationship between deposition and attachment rates in Jacobi room model," N. Stevanovic, V. M. Markovic, and D. Nikezic, *J. Environ. Radioact.,* **2010**, *vol.* 101*, no.* 5, 349–352.

[111] *Aspects of travel and deposition of aerosol and vapour clouds,* A. C. Chamberlain, **1953**. Atomic Energy Research Establishment, Harwell, Berks,(England).

[112] "The mechanics of aerosols," N. A. Fuchs, R. E. Daisley, M. Fuchs, C. N. Davies, and M. E. Straumanis, *Phys. Today*, **1965**, *vol.* 18, *no.* 4, 73.

[113] "Modeling indoor particle deposition from trubulent flow onto smooth sufaces," A. C. K. Lai and W. W. Nazaroff*, J. Aerosol Sci.,* **2000**, *vol.* 31, *no.* 4, 463–476.

[114] "The influence of environmental factors on the deposition velocity of thoron progeny," H. Li, L. Zhang, and Q. Guo, *Radiat. Prot. Dosimetry,* **2012**, *vol.* 152, *no.* 1–3, 84–88.

[115] *Radiation Protection and NORM Residue Management in the Production of Rare Earths from Thorium Containing Minerals: IAEA Safety Report Series No. 68*, IAEA, **2011**. Vienna: IAEA Publications.

[116] "Effects of Ionizing Radiation," UNSCEAR, *Rep. to Gen. Assem.*, **2006**, 116.

[117] "ICRP Publication 130: Occupational intakes of radionuclides: Part 1," F. Paquet, G. Etherington, M. R. Bailey, R. W. Leggett, J. Lipsztein, W. Bolch, K. F. Eckerman, J. D. Harrison, and ICRP, *Ann. ICRP*, **2015**, *vol.* 44, *no.* 2, 5–188.

[118] "ICRP Publication 133: The ICRP computational framework for internal dose assessment for reference adults: specific absorbed fractions," W. E. Bolch, D. Jokisch, M. Zankl, K. F. Eckerman, T. Fell, R. Manger, A. Endo, J. Hunt, K. P. Kim, and N. Petoussi-Henss, *Ann. ICRP*, **2016**, *vol.* 45, *no.* 2, 5–73.

[119] "Age and sex dependent inhalation doses to members of the public from indoor thoron progeny," L. Bi, W. B. Li, J. Tschiersch, and J. L. Li, *J. Radiol. Prot.*, **2010**, *vol.* 30, *no.* 4, 639–658.

[120] "ICRP dose coefficients: computational development and current status," W. E. Bolch, N. Petoussi-Henss, F. Paquet, and J. Harrison, *Ann. ICRP*, **2015**, *vol.* 45, 156–177.

[121] *Physical, Anatomical, Physiological and Metabolic data for reference Indian man-a proposal: BARC-1994/E/043*, H. S. Dang, D. D. Jaiswal, M. Parameswaran, and S. Krishnamony, **1994**. Bhabha Atomic Research Centre.

[122] "Compilation of anatomical, physiological and metabolic characteristics for a Reference Asian Man-IAEA-TECDOC-1005," H. Kawamura, G. Tanaka, K. Shiraishi, Y. Honda, M. Nishimuta, T. Koyanagi, J. Wang, C. Soegiarto, P. Akhter, and Griffith, *J. Radiat. Res.*, **1998**, *vol.* 39, 350.

[123] "Studies of the anatomical, physiological and metabolic characteristics of the Indian population for setting up a Reference Man," S. Dang, H.S., Jaiswal, D.D. Parameswaran, M., Krishnamony, , *Anatomical, physiological and metabolic characteristics for a Reference Asian Man Volume 2: Country reports (1998): 47.*, **1998**, IAEA Publications.

[124] "ICRP Publication 107. Nuclear decay data for dosimetric calculations.," K. Eckerman and A. Endo, *Ann. ICRP*, **2008**, *vol.* 38, *no.* 3, 7–96.

[125] "Assessment of AMAD and MMAD for airborne particulate matter in the beach mineral separation plants-Modification of ALI and DAC," P. P. Haridasan, P. Pillai, and A. C. Paul, **1999**.

[126] "Characterisation of radioactivity carrying aerosol in a mineral sand processing plant," C. Jeffries and L. Morawska, **1998**.

[127] "Uranium Aerosol Activity Size Distributions at a Nuclear Fuel Fabrication Plant," E. Hansson, H. B. L. L. Pettersson, and M. Eriksson, *Health Phys.*, **2020**, *vol.* 119, *no.* 3, 327.

[128] "Aerosol size distribution in a uranium processing and fuel fabrication facility," K. V. Prasad, A. Y. Balbudhe, G. K. Srivastava, R. M. Tripathi, and V. D. Puranik, *Radiat. Prot. Dosimetry*, **2010**, *vol.* 140, *no.* 4, 357–361.

[129] "Size distribution of aerosol particles produced during mining and processing uranium ore," H. Mala, L. Tomasek, P. Rulik, V. Beckova, and J. Hulka, *J. Environ. Radioact.*, **2016**, *vol.* 157, 97–101.

APPENDIX A

Mathematica Code for the decay product model

```
*(*Input Parameters*)
*
*CThnAv=7680; (*Average thoron gas concentration Bq/m3*)(*= S/(V*lam)*)
*
*LRoom=10; (*Length of room in meters*)
*WRoom=6; (*Width of room in meters*)
*HRoom=4; (*Height of room in meters*)
*
*Vent=4;(* Ventilation rate /h*)
*LamVent= Vent/3600 ; (* /s*)
*
*LamPb212= 1.82*10.^-5; (*Decay constant of Pb-212 /s *)
*LamBi212=1.92*10.^-4; (*Decay constant of Bi-212 /s *)
*
*SurfaceV=2*HRoom*(LRoom+WRoom);
*SurfaceUp=LRoom*WRoom;
*SurfaceDn=LRoom*WRoom;
*VolumeRoom=LRoom*WRoom*HRoom;
*VdUnatt=0.0001; (*Deposition velocity for Unattached fraction m/s*)
*
*Nc=10^9; (*Aerosol Particle concentration No/m3  *)
*
*ust=3*10.^-2; (* u star value for the environment m/s *)
*
*(*Aerosol Parameters for the 2 modes*)
*
*CMD1=0.45;(*Value in um*)
*F1=0.92;(*Fraction of particles in mode m *)
*sigma1=1.5;
*
*CMD2=1.45;(*Value in um*)
*F2=0.08;(*Fraction of particles in mode m *)
*sigma2=2.5;
*(*sigma2=1+1.5*(1-((100*CMD2^1.5+1)^-1));*)
*
```

```
(*****************************************************************************************************************)
```

(*Module for calculation of attachment rate and deposition rate for 2 modes of aerosols. *)

```
(* Calculation of attachment rate for the modes 1 and 2 of aerosol*)

(*Mode1*)

D0=6.8*10.^-6; (*Diffusion Coefficient of particle m2/s*)
v0=1.72*10.^2; (* mean thermal velocity m/s*)
l0=4.9*10.^-8; (* mean free path of unattached decay product m*)
AttCoeff=(2*Pi*D0*d)/((8*D0/(d*v0))+d/(d+2*l0)); (* beta in units m3/s *)

NoConDist1=(F1*Nc*(Exp[-((Log[d]-Log[CMD1*10.^-6])^2)/(2*(Log[sigma1]^2))])/ (((2*Pi)^0.5)*d*Log[sigma1]) ); (* dZ/dd /m3*)
(*Number size concentration distribution as a function of diameter d in m, But AMAD in um *)
NIntegrate[NoConDist1, {d, 10.^-9,10.^-4}, MaxRecursion->50];

LamAtt1= NIntegrate[AttCoeff*NoConDist1, {d, 10.^-9,10.^-4}, MaxRecursion->50]; (* Attachment Rate in /s*)

Nattp1=AttCoeff*NoConDist1/LamAtt1;(*Activity size distribution of attached Tn DP for the mode*) (*Porstendorfer Equation*)
(*Plot[Nattp1,{d, 10.^-8,10.^-4}, PlotRange□Full] *)
NIntegrate[Nattp1, {d, 10.^-9,10.^-4}, MaxRecursion->50];
Print["Attachment coefficient for mode 1 =", LamAtt1];

(*Mode2*)

D0=6.8*10.^-6; (*Diffusion Coefficient of particle m2/s*)
v0=1.72*10.^2; (* mean thermal velocity m/s*)
l0=4.9*10.^-8; (* mean free path of unattached decay product m*)
AttCoeff=(2*Pi*D0*d)/((8*D0/(d*v0))+d/(d+2*l0)); (* beta in units m3/s *)

NoConDist2=(F2*Nc*(Exp[-((Log[d]-Log[CMD2*10.^-6])^2)/(2*(Log[sigma2]^2))])/ (((2*Pi)^0.5)*d*Log[sigma2]) ); (* dZ/dd /m3*)
```

```
(*Number size concentration distribution as a function of diameter d in m, But AMAD in um *)
NIntegrate[NoConDist2, {d, 10.^-9,10.^-4}, MaxRecursion->50];


LamAtt2= NIntegrate[AttCoeff*NoConDist2, {d, 10.^-9,10.^-4}, MaxRecursion->50];(* Attachment Rate in /s*)

Nattp2=AttCoeff*NoConDist2/LamAtt2;(*Activity size distribution of attached Tn DP for the mode*) (*Porstendorfer Equation*)
(*Plot[Nattp2,{d, 10.^-8,10.^-4}, PlotRange□Full] *)
NIntegrate[Nattp2, {d, 10.^-9,10.^-4}, MaxRecursion->50];
Print["Attachment coefficient for mode 2 =", LamAtt2];
```

(*Module for calculation of deposition velocity and deposition rate for 2 modes of aerosols. *)

```

(*Deposition rate for unattached aerosols. *)
LamDepUnatt=        VdUnatt*(SurfaceV+SurfaceUp+SurfaceDn)/(VolumeRoom)(* Deposition rate for unattached progeny /s*)

(* The deposition velocity for mode 1 *)

AMAD1=1.4526*CMD1^0.9757;
K=1.38*10.^-23;  (*Boltzmann const*)
T=293;
mfp=0.066*10.^-6;  (*mean free path in air for unattached particles m*)
Eta=1.81*10.^-5;(*d=10.^-8*)
Cc=1+(mfp/d)*(2.34+1.05*Exp[-0.39*(d/mfp)]);
B=Cc/(3*3.141*Eta*d);
(*mobility*)
Df=K*T*B;
(*Calculation of Schimdt no.*)
vis=1.6*10.^-5;    (*kinematic viscosity of air in m2/s*)
Sc=vis/Df;
rd=d*ust/(2*vis);
(*Calculation of a and b and integration*)
p=10.92*Sc^(-1/3);
q=Sc^-1;
```

```
a=(0.5*Log[((p+4.3)^3)/(q+0.0609)])+(1.73*ArcTan[(8.6-p)/(1.73*p)]);
b=(0.5*Log[((p+rd)^3)/(q+(7.669*(10^-4)*(rd^3)))])+(1.73*ArcTan[(2*rd-p)/(1.73*p)]);
int=39+(3.64*(Sc^(2/3))*(a-b));
(*calculation of gravitational settling velocity*)
g=9.8;
density=1000  ;     (*density in kg/m3*)
vts=(density*d^2*g*Cc)/(18*Eta);
(*Calculation of dep velocities*)
Vdv=ust/int;
Vdu=vts/(1-Exp[-vts*int/ust]);
Vdd=vts/(Exp[vts*int/ust]-1);

VduAv1=NIntegrate[Vdu*Nattp1,{d,0,10.^-4}, MaxRecursion->100]/NIntegrate[Nattp1,{d,0,10.^-4}, MaxRecursion->100];
VdvAv1=NIntegrate[Vdv*Nattp1,{d,0,10.^-4}, MaxRecursion->100]/NIntegrate[Nattp1,{d,0,10.^-4}, MaxRecursion->100];
VddAv1=NIntegrate[Vdd*Nattp1,{d,0,10.^-4}, MaxRecursion->100]/NIntegrate[Nattp1,{d,0,10.^-4}, MaxRecursion->100];

 (* The deposition rate for mode 1  /s *)
LamDepAtt1= (VdvAv1*SurfaceV+VduAv1*SurfaceUp+VddAv1*SurfaceDn)/VolumeRoom;

Print["CMD","   ","AMAD","   ","LamAtt","   ","LamDepAtt","   ","VduAv","   ", "VdvAv","   ", "VddAv"]
Print["Unattached","   ","-","   ","-","   ","=",LamDepUnatt,"   ",0.0001,"   ",0.0001,"   ",0.0001]
Print[CMD1*10^3,"   ",AMAD1*10^3,"   ","=",LamAtt1,"   ","=",LamDepAtt1,"   ","=",VduAv1,"   ", "=",VdvAv1,"   ", "=",VddAv1]
(*Will print CMD and AMAD in nm *)

(* The deposition velocity for mode 2 *)
AMAD2=1.4526*CMD2^0.9757;
K=1.38*10.^-23;  (*Boltzmann const*)
T=293;
mfp=0.066*10.^-6;  (*mean free path in air for unattached particles m*)
Eta=1.81*10.^-5;
(*d=10.^-8*)
Cc=1+(mfp/d)*(2.34+1.05*Exp[-0.39*(d/mfp)]);
```

```
B=Cc/(3*3.141*Eta*d); (*mobility*)
Df=K*T*B;
(*Calculation of Schimdt no.*)
vis=1.6*10.^-5;    (*kinematic viscosity of air in m2/s*)
Sc=vis/Df;
rd=d*ust/(2*vis);
(*Calculation of a and b and integration*)
p=10.92*Sc^(-1/3);
q=Sc^-1;
a=(0.5*Log[((p+4.3)^3)/(q+0.0609)])+(1.73*ArcTan[(8.6-p)/(1.73*p)]);
b=(0.5*Log[((p+rd)^3)/(q+(7.669*(10^-4)*(rd^3)))])+(1.73*ArcTan[(2*rd-
p)/(1.73*p)]);
int=39+(3.64*(Sc^(2/3))*(a-b));
(*calculation of gravitational settling velocity*)
g=9.8;
density=1000  ;      (*density in kg/m3*)
vts=(density*d^2*g*Cc)/(18*Eta);
(*Calculation of dep velocities*)
Vdv=ust/int;
Vdu=vts/(1-Exp[-vts*int/ust]);
Vdd=vts/(Exp[vts*int/ust]-1);

VduAv2=NIntegrate[Vdu*Nattp2,{d,0,10.^-4}, MaxRecursion-
>100]/NIntegrate[Nattp2,{d,0,10.^-4}, MaxRecursion->100];
VdvAv2=NIntegrate[Vdv*Nattp2,{d,0,10.^-4}, MaxRecursion-
>100]/NIntegrate[Nattp2,{d,0,10.^-4}, MaxRecursion->100];
VddAv2=NIntegrate[Vdd*Nattp2,{d,0,10.^-4}, MaxRecursion-
>100]/NIntegrate[Nattp2,{d,0,10.^-4}, MaxRecursion->100];

(* The deposition rate for mode 2  /s *)
LamDepAtt2=
(VdvAv2*SurfaceV+VduAv2*SurfaceUp+VddAv2*SurfaceDn)/VolumeRoom;

Print[CMD2*10^3,"     ",AMAD2*10^3,"     ","=",LamAtt2,"     ","=",LamDepAtt2,"
","=",VduAv2,"     ", "=",VdvAv2,"    ", "=",VddAv2] (*Will print CMD and AMAD
in nm*)
```

(*Module for calculation of Concentration of attached and unattached decay product concentrations*)

```
(* Calculation of concentration of unattached 212Pb*)
LamAtt=LamAtt1+LamAtt2; (* Sum of LamAtt1 for all modes *)

CPb212Unatt=(CThnAv*LamPb212)/(LamPb212+LamVent+LamAtt+LamDepUnatt);(* Concentration of Unattached Pb-212 Bq/m3 *)

Print["Conc. of Unttached Pb212 = ", CPb212Unatt]

(* Calculation of concentration of attached 212Pb for  a mode. Can be for multiple modes by indexing for m  *)

CPb212Att1=(CPb212Unatt*LamAtt1)/(LamPb212+LamVent+LamDepAtt1);(* Concentration of Attached Pb-212 in mode 1 Bq/m3 *)
CPb212Att      2=(CPb212Unatt*LamAtt2)/(LamPb212+LamVent+LamDepAtt2);(* Concentration of Attached Pb-212 in mode 2 Bq/m3 *)

CPb212Att=CPb212Att1+CPb212Att2; (* Sum of CPbAttm for all modes *)
Print["Conc. of Attached Pb212 = ", CPb212Att]

CPb212Tot=CPb212Att+CPb212Unatt;
Print["Total Conc. of Pb212 = ", CPb212Tot]

(* Calculation of concentration of unattached 212Bi*)

CBi212Unatt=(CPb212Unatt*LamBi212)/(LamBi212+LamVent+LamAtt+LamDepUnatt);(* Concentration of Unattached Pb-212 Bq/m3 *)

Print["Conc. of Unattached Bi212 = ", CBi212Unatt]

(* Calculation of concentration of attached 212Bi for  a mode. Can be for multiple modes by indexing for m  *)

CBi212Att1=(CPb212Att1*LamBi212+LamAtt1*CBi212Unatt)/(LamBi212+LamVent+LamDepAtt1);(* Concentration of Attached Bi-212 in mode 1 Bq/m3 *)
CBi212Att2=(CPb212Att2*LamBi212+LamAtt2*CBi212Unatt)/(LamBi212+LamVent+LamDepAtt2);(* Concentration of Attached Bi-212 in mode 2 Bq/m3 *)
```

```
CBi212Att=CBi212Att1+CBi212Att2; (* Sum of CBiAttm for all modes *)
Print["Conc. of Attached Bi212 = ", CBi212Att]

CBi212Tot=CBi212Att+CBi212Unatt;
Print["Total Conc. of Bi212 = ", CBi212Tot]

BiPbRatio=CBi212Tot/CPb212Tot;
Print["Ratio of Bi212 to Pb212 = ",BiPbRatio]

(* Calculation of EETC of thoron decay products*)

EETC= 0.913*(CPb212Att+CPb212Unatt)+0.087*(CBi212Att+CBi212Unatt);
Print["EETC for thoron decay products = ",EETC]

EETCAtt=0.913*CPb212Att+0.087*CBi212Att;
Print["EETC for attached thoron decay products = ",EETCAtt]
EETCUnatt=0.913*CPb212Unatt+0.087*CBi212Unatt;
Print["EETC for unattached thoron decay products = ",EETCUnatt]

(* Calculation of Unattached fraction*)
fPb212=CPb212Unatt/(CPb212Unatt+CPb212Att) ;(* Unattached fraction of Pb-212*)
fBi212=CBi212Unatt/(CBi212Unatt+CBi212Att);(* Unattached fraction of Bi-212*)
fTot=0.913*fPb212+0.087*fBi212 ;(*Total unattached fraction of thoron decay products*)

Print["Unattached fraction for thoron decay products = ",fTot]
Print["AMAD","    ","CPb","    ","CBi"]
Print["Unattached","    ","=",CPb212Unatt,"    ","=",CBi212Unatt]
Print[AMAD1*10^3,"    ","=",CPb212Att1,"    ","=",CBi212Att1]
Print[AMAD2*10^3,"    ","=",CPb212Att2,"    ","=",CBi212Att2]
```

APPENDIX B

Mathematica Code for Calculation of Human respiratory tract dose

```
Calculation of Inhalation Dose for Thoron

Input Parameters

Texp=1.;    (*Exposure time in h*)
CTnDP=1;    (*Concentration of thoron DP Bq/m3 EETC*)

BR=1; (*Breathing Rate m3/h*)

(*Deposition fraction for different regions of HRTM obtained by Lung deposition
code*)
(*(*For diameter =  100 nm*)
DFET1=0.0418;
DFET2=0.0225;
DFBB=0.0073;
DFbb=0.0471;
DFAI=0.2073;*)
DFET1=0.0310;
DFET2=0.0327;
DFBB=0.0116;
DFbb=0.0776;
DFAI=0.2828;

Input Parameters
(*Calculation of Inhaled activity *)

TnDPIn=CTnDP*Texp*BR; (*Total intake of thoron DP Bq EET *)
InPb=0.91*TnDPIn; (*Intake of Lead Bq*)
InBi=0.09*TnDPIn; (*Intake of Bismuth Bq*)

(* The symbol' in compartment names of ICRP 130 is replaced by d eg BB' with BBd
*)

(*Partition of Inhaled Lead activity in the 11 compartments - for standard assumption
of Nose breather by ICRP 130*)
```

```
CPbET1=(InPb*DFET1*1);
CPbET2d=(InPb*DFET2*0.998);
CPbETseq=(InPb*DFET2*0.002);
CPbLNET=0;
CPbBBd=(InPb*DFBB*0.998);
CPbBBseq=(InPb*DFBB*0.002);
CPbbbd=(InPb*DFbb*0.998);
CPbbbseq=(InPb*DFbb*0.002);
CPbALV=(InPb*DFAI*1);
CPbINT=0;
CPbLNTH=0;

(*Partition of Inhaled Bismuth activity in the 11 compartments - for standard
assumption of Nose breather by ICRP 130*)
CBiET1=(InBi*DFET1*1);
CBiET2d=(InBi*DFET2*0.998);
CBiETseq=(InBi*DFET2*0.002);
CBiLNET=0;
CBiBBd=(InBi*DFBB*0.998);
CBiBBseq=(InBi*DFBB*0.002);
CBibbd=(InBi*DFbb*0.998);
CBibbseq=(InBi*DFbb*0.002);
CBiALV=(InBi*DFAI*1);
CBiINT=0;
CBiLNTH=0;

Print["Pb: ",CPbET1," ",CPbET2d," ",CPbETseq," ",CPbLNET," ",CPbBBd,"
",CPbBBseq," ",CPbLNTH," ",CPbbbd," ",CPbbbseq," ",CPbALV," ",CPbINT]
Print["Bi: ",CBiET1," ",CBiET2d," ",CBiETseq," ",CBiLNET," ",CBiBBd,"
",CBiBBseq," ",CBiLNTH," ",CBibbd," ",CBibbseq," ",CBiALV," ",CBiINT]

Pb:  0.02821    0.0296975    0.000059514    0    0.0105349    0.000021112    0
0.0704748    0.000141232    0.257348    0
Bi:  0.00279    0.00293711    5.886*10^-6    0    0.00104191    2.088*10^-6    0
0.00697003    0.000013968    0.025452    0
(*Calculations for Activity Remaining in HRT Compartments*)

LamPb=1.569; (*Lamda radioactive decay for Pb-212 /d*)
LamBi=16.359; (*Lamda radioactive decay for Bi-212 /d*)
LamPo=2*10^11; (*Lamda radioactive decay for Po-212 /d*)
```

```
LamTl=326.87; (*Lamda radioactive decay for Tl-208 /d*)

(*Total activity loss rate by transport for all compartments /d *)
mET1Out=0.6;
mET1ET2d=1.5;
mET1=mET1ET2d+mET1Out;
mET2d=100;
mETseq=0.001;
mBBd=10;
mBBseq=0.001;
mbbd=0.2;
mbbseq=0.001;
mALVINT=0.001;
mALVbbd=0.002;
mALV=mALVINT+mALVbbd;
mINT=0.00003;

(*Activity clearance by absorption into blood *)

(*Calculation of activity of Lead in each compartment *)

(*ICRP 137 value for Lead as progeny of radon*)
frPb=0.1;
srPb=100; (* /d *)
ssPb=1.7; (* /d *)
fbPb=0.5;
sbPb=1.7;(* /d *)
spPb=(frPb*((1-fbPb)*srPb)+(frPb*srPb*fbPb))+((1-frPb)*(1-
fbPb)*ssPb)+(fbPb*ssPb*sbPb);   (* Total blood absorption rate /d *)

qPbALV=DSolveValue[{qALV'[t]==-
(spPb+LamPb+mALV)*qALV[t],qALV[0]==CPbALV},qALV[t],t];
qPbINT = DSolveValue[{qINT'[t]==(mALVINT*qPbALV)-
(spPb+LamPb+mINT)*qINT[t],qINT[0]==CPbINT},qINT[t],t];
qPbbbd=DSolveValue[{qbbd'[t]==(mALVbbd*qPbALV)-
(spPb+LamPb+mbbd)*qbbd[t],qbbd[0]==CPbbbd},qbbd[t],t];
qPbbbseq=DSolveValue[{qbbseq'[t]==-
(spPb+LamPb+mbbseq)*qbbseq[t],qbbseq[0]==CPbbbseq},qbbseq[t],t];
qPbBBd=DSolveValue[{qBBd'[t]==(mbbd*qPbbbd)-
(spPb+LamPb+mBBd)*qBBd[t],qBBd[0]==CPbBBd},qBBd[t],t];
```

```
qPbBBseq=DSolveValue[{qBBseq'[t]==-
(spPb+LamPb+mBBseq)*qBBseq[t],qBBseq[0]==CPbBBseq},qBBseq[t],t];
qPbLNTH=DSolveValue[{qLNTH'[t]==((mINT*qPbINT)+(mbbseq*qPbbbseq)+(
mBBseq*qPbBBseq))-(spPb+LamPb)*qLNTH[t],qLNTH[0]==0},qLNTH[t],t];
qPbET2d= DSolveValue[{qET2d'[t]==(mBBd*qPbBBd)-
(LamPb+mET2d)*qET2d[t],qET2d[0]==CPbET2d},qET2d[t],t];
qPbETseq=DSolveValue[{qETseq'[t]==-
(spPb+LamPb+mETseq)*qETseq[t],qETseq[0]==CPbETseq},qETseq[t],t];
qPbLNET=DSolveValue[{qLNET'[t]==(mETseq*CPbETseq)-
(spPb+LamPb)*qLNET[t],qLNET[0]==0},qLNET[t],t];
qPbET1=DSolveValue[{qET1'[t]==-
(LamPb+mET1)*qET1[t],qET1[0]==CPbET1},qET1[t],t];


(*Calculation of activity of Bismuth in each compartment *)

(*ICRP 137 value for Bismuth as progeny of radon*)
frBi=1;
srBi=1;     (* /d *)
ssBi=0;    (* /d *)
fbBi=0;
sbBi=0;(* /d *)
spBi=(frBi*((1-fbBi)*srBi)+(frBi*srBi*fbBi))+((1-frBi)*(1-
fbBi)*ssBi)+(fbBi*ssBi*sbBi);   (* Total blood absorption rate /d *)

qBiALV=DSolveValue[{pALV'[t]==(LamBi*qPbALV)-
(spBi+LamBi+mALV)*pALV[t],pALV[0]==CBiALV},pALV[t],t];
qBiINT = DSolveValue[{pINT'[t]==(LamBi*qPbINT)+(mALVINT*qBiALV)-
(spBi+LamBi+mINT)*pINT[t],pINT[0]==CBiINT},pINT[t],t];
qBibbd=DSolveValue[{pbbd'[t]==(LamBi*qPbbbd)+(mALVbbd*qBiALV)-
(spBi+LamBi+mbbd)*pbbd[t],pbbd[0]==CBibbd},pbbd[t],t];
qBibbseq=DSolveValue[{pbbseq'[t]==(LamBi*qPbbbseq)-
(spBi+LamBi+mbbseq)*pbbseq[t],pbbseq[0]==CBibbseq},pbbseq[t],t];
qBiBBd=DSolveValue[{pBBd'[t]==(LamBi*qPbBBd)+(mbbd*qBibbd)-
(spBi+LamBi+mBBd)*pBBd[t],pBBd[0]==CBiBBd},pBBd[t],t];
qBiBBseq=DSolveValue[{pBBseq'[t]==(LamBi*qPbBBseq)-
(spBi+LamBi+mBBseq)*pBBseq[t],pBBseq[0]==CBiBBseq},pBBseq[t],t];
qBiLNTH=DSolveValue[{pLNTH'[t]==(LamBi*qPbLNTH)+((mINT*qBiINT)+(m
bbseq*qBibbseq)+(mBBseq*qBiBBseq))-
(spBi+LamBi)*pLNTH[t],pLNTH[0]==0},pLNTH[t],t];
```

```
qBiET2d= DSolveValue[{pET2d'[t]==(LamBi*qPbET2d)+(mBBd*qBiBBd)-
(LamBi+mET2d)*pET2d[t],pET2d[0]==CBiET2d},pET2d[t],t];
qBiETseq=DSolveValue[{pETseq'[t]==(LamBi*qPbETseq)-
(spBi+LamBi+mETseq)*pETseq[t],pETseq[0]==CBiETseq},pETseq[t],t];
qBiLNET=DSolveValue[{pLNET'[t]==(LamBi*qPbLNET)+(mETseq*qBiETseq)-
(spBi+LamBi)*pLNET[t],pLNET[0]==0},pLNET[t],t];
qBiET1=DSolveValue[{pET1'[t]==(LamBi*qPbET1)-
(LamBi+mET1)*pET1[t],pET1[0]==CBiET1},pET1[t],t];


(*Calculation of activity of Polonium in each compartment *)

(*ICRP 137 value for Polonium as progeny of radon*)
frPo=1;
srPo=3;   (* /d *)
ssPo=0;   (* /d *)
fbPo=0;
sbPo=0;   (* /d *)
spPo=(frPo*((1-fbPo)*srPo)+(frPo*srPo*fbPo))+((1-frPo)*(1-
fbPo)*ssPo)+(fbPo*ssPo*sbPo);   (* Total blood absorption rate /d *)

qPoALV=DSolveValue[{rALV'[t]==(LamPo*0.64*qBiALV)-
(srPo+LamPo+mALV)*rALV[t],rALV[0]==0},rALV[t],t];
qPoINT =
DSolveValue[{rINT'[t]==(LamPo*0.64*qBiINT)+(mALVINT*qPoALV)-
(srPo+LamPo+mINT)*rINT[t],rINT[0]==0},rINT[t],t];
qPobbd=DSolveValue[{rbbd'[t]==(LamPo*0.64*qBibbd)+(mALVbbd*qPoALV)-
(srPo+LamPo+mbbd)*rbbd[t],rbbd[0]==0},rbbd[t],t];
qPobbseq=DSolveValue[{rbbseq'[t]==(LamPo*0.64*qBibbseq)-
(srPo+LamPo+mbbseq)*rbbseq[t],rbbseq[0]==0},rbbseq[t],t];
qPoBBd=DSolveValue[{rBBd'[t]==(LamPo*0.64*qBiBBd)+(mbbd*qPobbd)-
(srPo+LamPo+mBBd)*rBBd[t],rBBd[0]==0},rBBd[t],t];
qPoBBseq=DSolveValue[{rBBseq'[t]==(LamPo*0.64*qBiBBseq)-
(srPo+LamPo+mBBseq)*rBBseq[t],rBBseq[0]==0},rBBseq[t],t];
qPoLNTH=0.64*qBiLNTH;(*DSolveValue[{rLNTH'[t]□(LamPo*0.36*qBiLNTH)
+((mINT*qPoINT)+(mbbseq*qPobbseq)+(mBBseq*qPoBBseq))-
(srPo+LamPo)*rLNTH[t],rLNTH[0]□0},rLNTH[t],t]*)
qPoET2d= DSolveValue[{rET2d'[t]==(LamPo*0.64*qBiET2d)+(mBBd*qPoBBd)-
(LamPo+mET2d)*rET2d[t],rET2d[0]==0},rET2d[t],t];
qPoETseq=DSolveValue[{rETseq'[t]==(LamPo*0.64*qBiETseq)-
(srPo+LamPo+mETseq)*rETseq[t],rETseq[0]==0},rETseq[t],t];
```

```
qPoLNET=DSolveValue[{rLNET'[t]==(LamPo*0.64*qBiLNET)+(mETseq*qPoET
seq)-(srPo+LamPo)*rLNET[t],rLNET[0]==0},rLNET[t],t];
qPoET1=DSolveValue[{rET1'[t]==(LamPo*0.64*qBiET1)-
(LamPo+mET1)*rET1[t],rET1[0]==0},rET1[t],t];

(*Calculation of activity of Thallium in each compartment *)

(*ICRP 137 value for Thallium as progeny of radon*)
frTl=1;
srTl=3;    (* /d *)
ssTl=0;    (* /d *)
fbTl=0;
sbTl=0;    (* /d *)
spTl=(frTl*((1-fbTl)*srTl)+(frTl*srTl*fbTl))+((1-frTl)*(1-
fbTl)*ssTl)+(fbTl*ssTl*sbTl);   (* Total blood absorption rate /d *)

qTlALV=DSolveValue[{rALV'[t]==(LamTl*0.36*qBiALV)-
(srTl+LamTl+mALV)*rALV[t],rALV[0]==0},rALV[t],t];
qTlINT = DSolveValue[{rINT'[t]==(LamTl*0.36*qBiINT)+(mALVINT*qTlALV)-
(srTl+LamTl+mINT)*rINT[t],rINT[0]==0},rINT[t],t];
qTlbbd=DSolveValue[{rbbd'[t]==(LamTl*0.36*qBibbd)+(mALVbbd*qTlALV)-
(srTl+LamTl+mbbd)*rbbd[t],rbbd[0]==0},rbbd[t],t];
qTlbbseq=DSolveValue[{rbbseq'[t]==(LamTl*0.36*qBibbseq)-
(srTl+LamTl+mbbseq)*rbbseq[t],rbbseq[0]==0},rbbseq[t],t];
qTlBBd=DSolveValue[{rBBd'[t]==(LamTl*0.36*qBiBBd)+(mbbd*qTlbbd)-
(srTl+LamTl+mBBd)*rBBd[t],rBBd[0]==0},rBBd[t],t];
qTlBBseq=DSolveValue[{rBBseq'[t]==(LamTl*0.36*qBiBBseq)-
(srTl+LamTl+mBBseq)*rBBseq[t],rBBseq[0]==0},rBBseq[t],t];
qTlLNTH=DSolveValue[{rLNTH'[t]==(LamTl*0.36*qBiLNTH)+((mINT*qTlINT)
+(mbbseq*qTlbbseq)+(mBBseq*qTlBBseq))-
(srTl+LamTl)*rLNTH[t],rLNTH[0]==0},rLNTH[t],t];
qTlET2d=    DSolveValue[{rET2d'[t]==(LamTl*0.36*qBiET2d)+(mBBd*qTlBBd)-
(LamTl+mET2d)*rET2d[t],rET2d[0]==0},rET2d[t],t];
qTlETseq=DSolveValue[{rETseq'[t]==(LamTl*0.36*qBiETseq)-
(srTl+LamTl+mETseq)*rETseq[t],rETseq[0]==0},rETseq[t],t];
qTlLNET=DSolveValue[{rLNET'[t]==(LamTl*0.36*qBiLNET)+(mETseq*qTlETs
eq)-(srTl+LamTl)*rLNET[t],rLNET[0]==0},rLNET[t],t];
qTlET1=DSolveValue[{rET1'[t]==(LamTl*0.36*qBiET1)-
(LamTl+mET1)*rET1[t],rET1[0]==0},rET1[t],t];

Plot[qPbALV,{t,0,0.5}];
```

```
Plot[qPbET1,{t,0,0.5}];

Plot[qBiALV,{t,0,0.5}];
Plot[qBiET1,{t,0,0.5}];

Plot[qPoALV,{t,0,0.5}];
Plot[qPoLNTH,{t,0,0.5}];

Plot[qTlALV,{t,0,0.5}]
Plot[qTlLNTH,{t,0,0.5}];
(*Calculation of nuclear transformations of Lead in 50 y*)

APbALV=86400*Integrate[qPbALV,{t,0,18250}];(* 50 years=18250 days
*)(*Factor 86400 s/d is used to match units *)
APbINT=86400*Integrate[qPbINT,{t,0,18250}];
APbbbd=86400*Integrate[qPbbbd,{t,0,18250}];
APbbbseq=86400*Integrate[qPbbbseq,{t,0,18250}];
APbBBd=86400*Integrate[qPbBBd,{t,0,18250}];
APbBBseq=86400*Integrate[qPbBBseq,{t,0,18250}];
APbLNTH=86400*Integrate[qPbLNTH,{t,0,18250}];
APbET2d=86400*Integrate[qPbET2d,{t,0,18250}];
APbETseq=86400*Integrate[qPbETseq,{t,0,18250}];
APbLNET=86400*Integrate[qPbLNET,{t,0,18250}];
APbET1=86400*Integrate[qPbET1,{t,0,18250}];

(*Calculation of nuclear transformations of Bismuth in 50 y*)
ABiALV=86400*Integrate[qBiALV,{t,0,18250}];
ABiINT=86400*Integrate[qBiINT,{t,0,18250}];
ABibbd=86400*Integrate[qBibbd,{t,0,18250}];
ABibbseq=86400*Integrate[qBibbseq,{t,0,18250}];
ABiBBd=86400*Integrate[qBiBBd,{t,0,18250}];
ABiBBseq=86400*Integrate[qBiBBseq,{t,0,18250}];
ABiLNTH=86400*Integrate[qBiLNTH,{t,0,18250}];
ABiET2d=86400*Integrate[qBiET2d,{t,0,18250}];
ABiETseq=86400*Integrate[qBiETseq,{t,0,18250}];
ABiLNET=86400*Integrate[qBiLNET,{t,0,18250}];
ABiET1=86400*Integrate[qBiET1,{t,0,18250}];

(*Calculation of nuclear transformations of Polonium in 50 y*)
APoALV=86400*Integrate[qPoALV,{t,0,18250}];
```

```
APoINT=86400*Integrate[qPoINT,{t,0,18250}];
APobbd=86400*Integrate[qPobbd,{t,0,18250}];
APobbseq=86400*Integrate[qPobbseq,{t,0,18250}];
APoBBd=86400*Integrate[qPoBBd,{t,0,18250}];
APoBBseq=86400*Integrate[qPoBBseq,{t,0,18250}];
APoLNTH=86400*Integrate[qPoLNTH,{t,0,18250}];
APoET2d=86400*Integrate[qPoET2d,{t,0,18250}];
APoETseq=86400*Integrate[qPoETseq,{t,0,18250}];
APoLNET=86400*Integrate[qPoLNET,{t,0,18250}];
APoET1=86400*Integrate[qPoET1,{t,0,18250}];

(*Calculation of nuclear transformations of Thallium in 50 y*)
ATlALV=86400*Integrate[qTlALV,{t,0,18250}];
ATlINT=86400*Integrate[qTlINT,{t,0,18250}];
ATlbbd=86400*Integrate[qTlbbd,{t,0,18250}];
ATlbbseq=86400*Integrate[qTlbbseq,{t,0,18250}];
ATlBBd=86400*Integrate[qTlBBd,{t,0,18250}];
ATlBBseq=86400*Integrate[qTlBBseq,{t,0,18250}];
ATlLNTH=86400*Integrate[qTlLNTH,{t,0,18250}];
ATlET2d=86400*Integrate[qTlET2d,{t,0,18250}];
ATlETseq=86400*Integrate[qTlETseq,{t,0,18250}];
ATlLNET=86400*Integrate[qTlLNET,{t,0,18250}];
ATlET1=86400*Integrate[qTlET1,{t,0,18250}];

Print["Pb: ",APbET1," ",APbET2d," ",APbETseq," ",APbLNET," ",APbBBd," ",APbBBseq," ",APbLNTH," ",APbbbd," ",APbbbseq," ",APbALV," ",APbINT]
Print["Bi: ",ABiET1," ",ABiET2d," ",ABiETseq," ",ABiLNET," ",ABiBBd," ",ABiBBseq," ",ABiLNTH," ",ABibbd," ",ABibbseq," ",ABiALV," ",ABiINT]
Print["Po: ",APoET1," ",APoET2d," ",APoETseq," ",APoLNET," ",APoBBd," ",APoBBseq," ",APoLNTH," ",APobbd," ",APobbseq," ",APoALV," ",APoINT]
Print["Tl: ",ATlET1," ",ATlET2d," ",ATlETseq," ",ATlLNET," ",ATlBBd," ",ATlBBseq," ",ATlLNTH," ",ATlbbd," ",ATlbbseq," ",ATlALV," ",ATlINT]



(*Calculation of Committed Equivalent dose coefficient in different target regions*)
```

```
TargetRegions={{1,"Adrenals"},{2,"UBWall"},{3,"BoneSur"},{4,"Brain"},{5,"Bre
asts"},{6,"StWall"},{7,"SIWall"},{8,"ULIWall"},{9,"LLIWall"},{10,"Kidneys"},{
11,"Liver"},{12,"ET1bas"},{13,"ET2bas"},{14,"LNET"},{15,"BBibas"},{16,"BBis
ec"},{17,"bbesec"},{18,"AI"},{19,"LNTh"},{20,"Muscle"},{21,"Ovaries"},{22,"Pa
ncreas"},{23,"RMarrow"},{24,"Skin"},{25,"Spleen"},{26,"Testes"},{27,"Thymus"
},{28,"Thyroid"},{29,"GBWall"},{30,"HtWall"},{31,"Uterus"}};

SourceRegions={{1,"AI"},{2,"bbegel"},{3,"bbesol"},{4,"bbeseq"},{5,"BBigel"},{
6,"BBisol"},{7,"BBiseq
"},{8,"ET2sur"},{9,"ET1sur"},{10,"ET2seq"},{11,"LNTh"},{12,"LNET"},{13,"St
Cont"},{14,"SICont
"},{15,"Blood"},{16,"ULICont"},{17,"LLICont"},{18,"UBCont"},{19,"TBoneS"},
{20,"CBoneS"},{21,"Other
"},{22,"Liver"},{23,"Kidneys"},{24,"TBoneV"},{25,"CBoneV"},{26,"Spleen"},{2
7,"RMarrow"}};

c=1; (* Since SEE values used are in Sv/nt *)
WT={{0.00923},{0.00923},{0.00923},{9.23*10^-
6},{0.00922},{0.000738},{0.000738},{0.00923},{0.00923},{0.00923},{0.00923},
{0.00923},{0.00923},{0.00923},{0.12},{0.12},{0.06},{0.06},{0.02},{0.02},{0.04}
,{0.04},{0.12},{0.08},{0.08},{0.04},{0.04},{0.04},{0.01},{0.01},{0.01}}
(*WTAdrenals=9.23*10^-03
WTSIWall=9.23*10^-03
WTKidneys=9.23*10^-03
WTET1bas=9.23*10^-06
WTET2bas=9.22*10^-03
WTLNET=7.38*10^-04
WTLNTh=7.38*10^-04
WTMuscle=9.23*10^-03
WTPancreas=9.23*10^-03
WTSpleen=9.23*10^-03
WTGBWall=9.23*10^-03
WTHtWall=9.23*10^-03
WTUterus=9.23*10^-03
WTThymus=9.23*10^-03
WTBreasts=1.20*10^-01
WTStWall=1.20*10^-01
WTULIWall=6.00*10^-02
WTLLIWall=6.00*10^-02
WTBBibas=2.00*10^-02
WTBBisec=2.00*10^-02
```

```
WTbbesec=4.00*10^-02
WTAI=4.00*10^-02
WTRMarrow=1.20*10^-01
WTOvaries=8.00*10^-02
WTTestes=8.00*10^-02
WTUBWall=4.00*10^-02
WTLiver=4.00*10^-02
WTThyroid=4.00*10^-02
WTBoneSur=1.00*10^-02
WTBrain=1.00*10^-02
WTSkin=1.00*10^-02*)

(*Calculation of Committed Equivalent dose due to Lead*)

(* Total disintegrations in various Source regions*)
APbAI= APbALV+APbINT;
APbbbegel=APbbbd*(2/6);
APbbbesol=APbbbd*(4/6);
APbbbeseq= APbbbseq;
APbBBigel=APbBBd*(5/11);
APbBBisol=APbBBd*(6/11);
APbBBiseq=APbBBseq;
APbET2sur=APbET2d;
APbET1sur=APbET2d;
APbET2seq=APbETseq;
APbLNTh=APbLNTH;
APbLNET=APbLNET;
APbStCont=0;
APbSICont=0;
APbBlood=0;
APbULICont=0;
APbLLICont=0;
APbUBCont=0;
APbTBoneS=0;
APbCBoneS=0;
APbOther=0;
APbLiver=0;
APbKidneys=0;
APbTBoneV=0;
APbCBoneV=0;
```

```
APbSpleen=0;
APbRMarrow=0;

APb={{APbAI },{APbbbegel },{APbbbesol },{APbbbeseq },{APbBBigel
},{APbBBisol },{APbBBiseq },{APbET2sur },{APbET1sur },{APbET2seq
},{APbLNTh },{APbLNET },{APbStCont },{APbSICont },{APbBlood
},{APbULICont },{APbLLICont },{APbUBCont },{APbTBoneS },{APbCBoneS
},{APbOther },{APbLiver },{APbKidneys },{APbTBoneV },{APbCBoneV
},{APbSpleen },{APbRMarrow }}; (*Matrix form of total disintegrations*)

MatrixForm[APb];

(*SEE values for Pb-212 obtained from SEECAL with 27 source regions and 31 target
regions*)

MatrixForm[PbSEEAdult];
Dimensions[APb];
Dimensions[PbSEEAdult];
HTPb=c*(PbSEEAdult.APb);
HTPb//MatrixForm;

HTPbAdrenals=HTPb[[1,1]];
HTPbUBWall=HTPb[[2,1]];
HTPbBoneSur=HTPb[[3,1]];
HTPbBrain=HTPb[[4,1]];
HTPbBreasts=HTPb[[5,1]];
HTPbStWall=HTPb[[6,1]];
HTPbSIWall=HTPb[[7,1]];
HTPbULIWall=HTPb[[8,1]];
HTPbLLIWall=HTPb[[9,1]];
HTPbKidneys=HTPb[[10,1]];
HTPbLiver=HTPb[[11,1]];
HTPbET1bas=HTPb[[12,1]];
HTPbET2bas=HTPb[[13,1]];
HTPbLNET=HTPb[[14,1]];
HTPbBBibas=HTPb[[15,1]];
HTPbBBisec=HTPb[[16,1]];
HTPbbbesec=HTPb[[17,1]];
HTPbAI=HTPb[[18,1]];
HTPbLNTh=HTPb[[19,1]];
```

```
HTPbMuscle=HTPb[[20,1]];
HTPbOvaries=HTPb[[21,1]];
HTPbPancreas=HTPb[[22,1]];
HTPbRMarrow=HTPb[[23,1]];
HTPbSkin=HTPb[[24,1]];
HTPbSpleen=HTPb[[25,1]];
HTPbTestes=HTPb[[26,1]];
HTPbThymus=HTPb[[27,1]];
HTPbThyroid=HTPb[[28,1]];
HTPbGBWall=HTPb[[29,1]];
HTPbHtWall=HTPb[[30,1]];
HTPbUterus=HTPb[[31,1]];

CDPb=HTPb*WT *10.^9(*Committed dose to different organs*)

EDPb=Total[CDPb](*Committed Effective Dose due to lead disintegrations in HRT*)

(*Calculation of Committed Equivalent dose due to Bismuth*)

(* Total disintegrations in various Source regions*)
ABiAI= ABiALV+ABiINT;
ABibbegel=ABibbd*(2/6);
ABibbesol=ABibbd*(4/6);
ABibbeseq= ABibbseq;
ABiBBigel=ABiBBd*(5/11);
ABiBBisol=ABiBBd*(6/11);
ABiBBiseq=ABiBBseq;
ABiET2sur=ABiET2d;
ABiET1sur=ABiET2d;
ABiET2seq=ABiETseq;
ABiLNTh=ABiLNTH;
ABiLNET=ABiLNET;
ABiStCont=0;
ABiSICont=0;
ABiBlood=0;
ABiULICont=0;
ABiLLICont=0;
ABiUBCont=0;
ABiTBoneS=0;
```

```
ABiCBoneS=0;
ABiOther=0;
ABiLiver=0;
ABiKidneys=0;
ABiTBoneV=0;
ABiCBoneV=0;
ABiSpleen=0;
ABiRMarrow=0;

ABi={{ABiAI },{ABibbegel },{ABibbesol },{ABibbeseq },{ABiBBigel },{ABiBBisol },{ABiBBiseq },{ABiET2sur },{ABiET1sur },{ABiET2seq },{ABiLNTh },{ABiLNET },{ABiStCont },{ABiSICont },{ABiBlood },{ABiULICont },{ABiLLICont },{ABiUBCont },{ABiTBoneS },{ABiCBoneS },{ABiOther },{ABiLiver },{ABiKidneys },{ABiTBoneV },{ABiCBoneV },{ABiSpleen },{ABiRMarrow }} (*Matrix form of total disintegrations*)

MatrixForm[ABi];
(*SEE values for Bi-212 obtained from SEECAL with 27 source regions and 31 target regions*)

MatrixForm[BiSEEAdult];
Dimensions[ABi];
Dimensions[BiSEEAdult];
HTBi=c*(BiSEEAdult.ABi);
HTBi//MatrixForm;

HTBiAdrenals=HTBi[[1,1]];
HTBiUBWall=HTBi[[2,1]];
HTBiBoneSur=HTBi[[3,1]];
HTBiBrain=HTBi[[4,1]];
HTBiBreasts=HTBi[[5,1]];
HTBiStWall=HTBi[[6,1]];
HTBiSIWall=HTBi[[7,1]];
HTBiULIWall=HTBi[[8,1]];
HTBiLLIWall=HTBi[[9,1]];
HTBiKidneys=HTBi[[10,1]];
HTBiLiver=HTBi[[11,1]];
HTBiET1bas=HTBi[[12,1]];
HTBiET2bas=HTBi[[13,1]];
HTBiLNET=HTBi[[14,1]];
```

```
HTBiBBibas=HTBi[[15,1]];
HTBiBBisec=HTBi[[16,1]];
HTBibbesec=HTBi[[17,1]];
HTBiAI=HTBi[[18,1]];
HTBiLNTh=HTBi[[19,1]];
HTBiMuscle=HTBi[[20,1]];
HTBiOvaries=HTBi[[21,1]];
HTBiPancreas=HTBi[[22,1]];
HTBiRMarrow=HTBi[[23,1]];
HTBiSkin=HTBi[[24,1]];
HTBiSpleen=HTBi[[25,1]];
HTBiTestes=HTBi[[26,1]];
HTBiThymus=HTBi[[27,1]];
HTBiThyroid=HTBi[[28,1]];
HTBiGBWall=HTBi[[29,1]];
HTBiHtWall=HTBi[[30,1]];
HTBiUterus=HTBi[[31,1]];

CDBi=HTBi*WT *10.^9(*Committed dose to different organs*)

EDBi=Total[CDBi](*Committed Effective Dose due to Bismuth disintegrations in HRT*)

(*Calculation of Committed Equivalent dose due to Polonium*)

(* Total disintegrations in various Source regions*)
APoAI= APoALV+APoINT;
APobbegel=APobbd*(2/6);
APobbesol=APobbd*(4/6);
APobbeseq= APobbseq;
APoBBigel=APoBBd*(5/11);
APoBBisol=APoBBd*(6/11);
APoBBiseq=APoBBseq;
APoET2sur=APoET2d;
APoET1sur=APoET2d;
APoET2seq=APoETseq;
APoLNTh=APoLNTH;
APoLNET=APoLNET;
APoStCont=0;
APoSICont=0;
```

```
APoBlood=0;
APoULICont=0;
APoLLICont=0;
APoUBCont=0;
APoTBoneS=0;
APoCBoneS=0;
APoOther=0;
APoLiver=0;
APoKidneys=0;
APoTBoneV=0;
APoCBoneV=0;
APoSpleen=0;
APoRMarrow=0;

APo={{APoAI },{APobbegel },{APobbesol },{APobbeseq },{APoBBigel
},{APoBBisol },{APoBBiseq },{APoET2sur },{APoET1sur },{APoET2seq
},{APoLNTh },{APoLNET },{APoStCont },{APoSICont },{APoBlood
},{APoULICont },{APoLLICont },{APoUBCont },{APoTBoneS },{APoCBoneS
},{APoOther },{APoLiver },{APoKidneys },{APoTBoneV },{APoCBoneV
},{APoSpleen },{APoRMarrow }}; (*Matrix form of total disintegrations*)

MatrixForm[APo];
(*SEE values for Po-212 obtained from SEECAL with 27 source regions and 31 target
regions*)

MatrixForm[PoSEEAdult];
Dimensions[APo];
Dimensions[PoSEEAdult];
HTPo=c*(PoSEEAdult.APo);
HTPo//MatrixForm;

HTPoAdrenals=HTPo[[1,1]];
HTPoUBWall=HTPo[[2,1]];
HTPoBoneSur=HTPo[[3,1]];
HTPoBrain=HTPo[[4,1]];
HTPoBreasts=HTPo[[5,1]];
HTPoStWall=HTPo[[6,1]];
HTPoSIWall=HTPo[[7,1]];
HTPoULIWall=HTPo[[8,1]];
HTPoLLIWall=HTPo[[9,1]];
```

```
HTPoKidneys=HTPo[[10,1]];
HTPoLiver=HTPo[[11,1]];
HTPoET1bas=HTPo[[12,1]];
HTPoET2bas=HTPo[[13,1]];
HTPoLNET=HTPo[[14,1]];
HTPoBBibas=HTPo[[15,1]];
HTPoBBisec=HTPo[[16,1]];
HTPobbesec=HTPo[[17,1]];
HTPoAI=HTPo[[18,1]];
HTPoLNTh=HTPo[[19,1]];
HTPoMuscle=HTPo[[20,1]];
HTPoOvaries=HTPo[[21,1]];
HTPoPancreas=HTPo[[22,1]];
HTPoRMarrow=HTPo[[23,1]];
HTPoSkin=HTPo[[24,1]];
HTPoSpleen=HTPo[[25,1]];
HTPoTestes=HTPo[[26,1]];
HTPoThymus=HTPo[[27,1]];
HTPoThyroid=HTPo[[28,1]];
HTPoGBWall=HTPo[[29,1]];
HTPoHtWall=HTPo[[30,1]];
HTPoUterus=HTPo[[31,1]];

CDPo=HTPo*WT *10.^9(*Committed dose to different organs*)

EDPo=Total[CDPo](*Committed Effective Dose due to lead disintegrations in HRT*)
(*Calculation of Committed Equivalent dose due to Thallium*)

(* Total disintegrations in various Source regions*)
ATlAI= ATlALV+ATlINT;
ATlbbegel=ATlbbd*(2/6);
ATlbbesol=ATlbbd*(4/6);
ATlbbeseq= ATlbbseq;
ATlBBigel=ATlBBd*(5/11);
ATlBBisol=ATlBBd*(6/11);
ATlBBiseq=ATlBBseq;
ATlET2sur=ATlET2d;
ATlET1sur=ATlET2d;
ATlET2seq=ATlETseq;
```

```
ATlLNTh=ATlLNTH;
ATlLNET=ATlLNET;
ATlStCont=0;
ATlSICont=0;
ATlBlood=0;
ATlULICont=0;
ATlLLICont=0;
ATlUBCont=0;
ATlTBoneS=0;
ATlCBoneS=0;
ATlOther=0;
ATlLiver=0;
ATlKidneys=0;
ATlTBoneV=0;
ATlCBoneV=0;
ATlSpleen=0;
ATlRMarrow=0;

ATl={{ATlAI },{ATlbbegel },{ATlbbesol },{ATlbbeseq },{ATlBBigel },{ATlBBisol },{ATlBBiseq },{ATlET2sur },{ATlET1sur },{ATlET2seq },{ATlLNTh },{ATlLNET },{ATlStCont },{ATlSICont },{ATlBlood },{ATlULICont },{ATlLLICont },{ATlUBCont },{ATlTBoneS },{ATlCBoneS },{ATlOther },{ATlLiver },{ATlKidneys },{ATlTBoneV },{ATlCBoneV },{ATlSpleen },{ATlRMarrow }}; (*Matrix form of total disintegrations*)

MatrixForm[ATl];

(*SEE values for Tl-212 obtained from SEECAL with 27 source regions and 31 target regions*)

MatrixForm[TlSEEAdult];
Dimensions[ATl];
Dimensions[TlSEEAdult];
HTTl=c*(TlSEEAdult.ATl);
HTTl//MatrixForm;

HTTlAdrenals=HTTl[[1,1]];
HTTlUBWall=HTTl[[2,1]];
HTTlBoneSur=HTTl[[3,1]];
HTTlBrain=HTTl[[4,1]];
```

```
HTTlBreasts=HTTl[[5,1]];
HTTlStWall=HTTl[[6,1]];
HTTlSIWall=HTTl[[7,1]];
HTTlULIWall=HTTl[[8,1]];
HTTlLLIWall=HTTl[[9,1]];
HTTlKidneys=HTTl[[10,1]];
HTTlLiver=HTTl[[11,1]];
HTTlET1bas=HTTl[[12,1]];
HTTlET2bas=HTTl[[13,1]];
HTTlLNET=HTTl[[14,1]];
HTTlBBibas=HTTl[[15,1]];
HTTlBBisec=HTTl[[16,1]];
HTTlbbesec=HTTl[[17,1]];
HTTlAI=HTTl[[18,1]];
HTTlLNTh=HTTl[[19,1]];
HTTlMuscle=HTTl[[20,1]];
HTTlOvaries=HTTl[[21,1]];
HTTlPancreas=HTTl[[22,1]];
HTTlRMarrow=HTTl[[23,1]];
HTTlSkin=HTTl[[24,1]];
HTTlSpleen=HTTl[[25,1]];
HTTlTestes=HTTl[[26,1]];
HTTlThymus=HTTl[[27,1]];
HTTlThyroid=HTTl[[28,1]];
HTTlGBWall=HTTl[[29,1]];
HTTlHtWall=HTTl[[30,1]];
HTTlUterus=HTTl[[31,1]];

CDTl=HTTl*WT *10.^9(*Committed dose to different organs*)

EDTl=Total[CDTl](*Committed Effective Dose due to lead disintegrations in HRT*)
```